Dissertation zur Erlangung des Doktorgrades

der Fakultät für Chemie und Pharmazie

der Ludwig-Maximilians-Universität München

Targeting the endolysosomal system of cancer cells by inhibition of V-ATPase and TPC function

Lina Sophie Schneider

aus

Freising, Deutschland

2015

Erklärung

Diese Dissertation wurde im Sinne von § 7 der Promotionsordnung vom 28. November 2011 von Frau Prof. Dr. Angelika M. Vollmar betreut.

Eidesstattliche Versicherung

Diese Dissertation wurde eigenständig und ohne unerlaubte Hilfe erarbeitet.

München, den 28. Oktober 2015

_____

(Lina Sophie Schneider)

Dissertation eingereicht am 03.11.2015

1.Gutachterin Prof. Dr. Angelika M. Vollmar

2.Gutachter Prof. Dr. Christian Wahl-Schott

Mündliche Prüfung am 02.12.2015

Meinen Eltern und meiner Schwester

1 Table of contents

2 Abbreviations

2-OG	2-oxoglutarate
3-AP	3-aminopyridine-2-carboxaldehyde thiosemicarbazone
ADP	adenosine diphosphate
AIF	apoptosis-inducing factor
AML	acute myeloid leukemia
Arch	archazolid
ATM	ataxia telangiectasia mutated
ATP	adenosine triphosphate
Bax	Bcl-2-associated X protein
Bcl-2	B-cell lymphoma 2
Bcl-xL	B-cell lymphoma extra large
Bid	BH3-interacting domain death agonist
BNIP3	Bcl-2/adenovirus E1B 19kDa interacting protein 3
CAIX	carbonic anhydrase IX
Caspase	cysteine-dependent aspartate-specific protease
CDK1	cyclin-dependent kinase 1
CO	control
CREB	cyclic AMP response element-binding
DBZ	dibenzazepine
dCTP	deoxycytidine triphosphate
DFO	deferoxamine
DMSO	dimethyl sulfoxide

DMT1	divalent metal transporter 1
dNTP	deoxyribonucleotide triphosphate
Doxo	doxorubicin
DSB	double-strand break
DTT	dithiothreitol
ECM	extracellular matrix
EDTA	ethylenediaminetetraacetic acid
EEA1	early endosome antigen 1
EGF	epidermal growth factor
EGFR	epidermal growth factor receptor
EGTA	ethylene glycol tetraacetic acid
ErbB2	human epidermal growth factor receptor 2
EV	empty vector
FACS	fluorescence-activated cell sorting
FAK	focal adhesion kinase
FCS	fetal calf serum
FeCit	iron citrate
Glut1	glucose transporter 1
GSI	γ-secretase inhibitor
HEPES	4-(2-hydroxyethyl)-1-piperazineethanesulfonic acid
Hes1	hairy and enhancer of split 1
Hey1/2	hairy and enhancer of split related with YRPW motif 1/2
HIF1α	hypoxia-inducible factor 1α

HRP	horseradish peroxidase
IAP1/2	inhibitor of apoptosis 1/2
IGFBP3	insulin-like growth factor-binding protein 3
LAMP1/3	lysosomal-associated membrane protein 1/3
LDL	low density lipoprotein
LDLR	low density lipoprotein receptor
LMP	lysosomal membrane permeabilization
MCT	monocarboxylate transporter
MDM2	mouse double minute 2
MDS	myelodysplastic syndrome
MEF	mouse embryonic fibroblasts
MES	2-(N-morpholino)ethanesulfonic acid
MSA	methanesulfonic acid
mTOR	mammalian target of rapamycin
mTORC1	mammalian target of rapamycin complex 1
NAADP	nicotinic acid adenine dinucleotide phosphate
NADP	nicotinamide adenine dinucleotide phosphate
Ned-19	*trans*-Ned-19
NHE1	Na^+/H^+ exchanger 1
NICD	notch intracellular domain
NRARP	notch-regulated ankyrin repeat protein
NT	non-targeting
OXPHOS	oxidative phosphorylation

PARP	poly ADP ribose polymerase
PBMC	peripheral blood mononuclear cell
PBS	phosphate-buffered saline
PDGFRβ	platelet-derived growth factor receptor β
PDX	patient-derived xenograft
PFA	paraformaldehyde
PHD	prolyl hydroxylase
PI	propidium iodide
$PI(3,5)P_2$	phosphatidylinositol 3,5-bisphosphate
PMSF	phenylmethylsulfonyl fluoride
Rb	retinoblastoma
RNR	ribonucleotide reductase
SD	standard deviation
SEM	standard error of the mean
T-ALL	T-cell acute lymphoblastic leukemia
Tet	tetrandrine
Tf	transferrin
TfR	transferrin receptor
TIGAR	TP53-induced glycolysis and apoptosis regulator
TPC	two-pore channel
TRP	transient receptor potential
TRPML1	transient receptor potential mucolipin 1
V-ATPase	vacuolar-type ATPase

VEGF	vascular endothelial growth factor
VHL	von Hippel-Lindau
XIAP	X-linked inhibitor of apoptosis
γH2AX	phosphorylation of the H2AX histone

3 Manuscripts

This thesis is based on following manuscripts, which are referred to in the text by their roman numerals (I-IV):

I. **Lina S. Schneider**, Karin von Schwarzenberg, Thorsten Lehr, Melanie Ulrich, Rebekka Kubisch-Dohmen, Johanna Liebl, Dirk Menche and Angelika M. Vollmar
Vacuolar-ATPase inhibition blocks iron metabolism to mediate therapeutic effects in breast cancer
2015, **Cancer Research**, 75(14):2863–2874

II. Siwei Zhang, **Lina S. Schneider**, Binje Vick, Michaela Grunert, Irmela Jeremias, Dirk Menche, Rolf Müller, Angelika M. Vollmar and Johanna Liebl
Anti-leukemic effects of the V-ATPase inhibitor Archazolid A
2015, accepted for publication in **Oncotarget**

III. **Lina S. Schneider**, Melanie Ulrich, Thorsten Lehr, Dirk Menche, Rolf Müller, Angelika M. Vollmar and Karin von Schwarzenberg
MDM2 antagonist nutlin-3a sensitizes tumors to V-ATPase inhibition
Submitted

IV. **Lina S. Schneider***, Christian Grimm*, Yu-Kai Chao, Anna Watermann, Melanie Ulrich, Doris Mayr, Christian Wahl-Schott, Martin Biel* and Angelika M. Vollmar*
Two-pore channel function is crucial for migration of invasive cancer cells
*These authors contributed equally to this work
Submitted

4 Summary

Fighting cancer is one of the big challenges of this century. The success of today's anti-cancer agents is limited by a variety of resistance mechanisms against the majority of chemotherapeutics. Moreover, it is dependent on the existence of metastasis. Overcoming these restraints by addressing new targets and by developing new treatment strategies is therefore highly appreciated.

In recent years, targeting the endolysosomal machinery in cancer cells has come into focus as a promising anti-tumor approach. Preserving the balance between endocytic internalization and recycling of extracellular material, receptors, ligands and plasma membrane proteins is substantially required to control cellular processes such as signal transduction, nutrient uptake, cell adhesion and migration. Hence, disturbing endocytosis might be a promising strategy to interfere with pro-survival mechanisms, especially in fast proliferating and high metabolic active cancer cells.

To this end, we here addressed two endolysosomal proteins to unveil their roles in cancer cells: the vacuolar-type ATPases (V-ATPases) and two-pore channels (TPCs). The V-ATPase is a multisubunit proton pump located in the membranes of endosomes and lysosomes, which actively transports protons into the lumen. Inhibition of these pumps was shown to induce apoptosis in different cancer cells before, however the precise mechanism stayed unclear. To investigate this matter, we used the myxobacterial V-ATPase inhibitor archazolid. Our first study (**manuscript I, Cancer Research**, 75(14):2863–2874) confirmed a strong cell death induction in the breast cancer cell lines MCF7 and MDA-MB-231 and showed induction of the hypoxia-inducible factor 1α (HIF1α) after archazolid treatment. Considering that HIF1α gets not only stabilized under hypoxia but also under iron depletion has led to experiments with excessive iron citrate in the cell culture medium which showed a complete abolishment of HIF1α stabilization and diminished cell death induction. The lack of cytosolic iron after archazolid treatment could be attributed to disturbed transferrin (Tf)/transferrin receptor (TfR) recycling. As a consequence, the iron depletion led to S-phase cell cycle arrest, double-strand breaks and the induction of the tumor suppressor p53. Moreover, this study showed *in vivo* efficacy of archazolid in a 4T1 mouse model, however it was not successful in abrogating tumor growth completely.

In a second study (**manuscript II, Oncotarget**), archazolid's apoptosis-inducing capabilities were confirmed in leukemic cell lines and in patient derived xenograft (PDX) leukemic cells. Mechanistically, V-ATPase inhibition reduced the expression level of the anti-apoptotic

protein survivin, contributing to archazolid-induced cell death since overexpression significantly diminished the amount of dead cells. In respect to the underlying mechanism, this study ties in with the above reported findings of manuscript I that archazolid led to S-phase arrest by interfering with the iron metabolism in leukemic cells. Since survivin expression strongly depends on cell cycle, these results suggest that archazolid decreased survivin at the protein level by inducing S-phase arrest.

As above mentioned, manuscript I unveiled only a moderate reduction of tumor burden *in vivo* for archazolid in breast cancer cells. Thus, we intended to improve this by a rational combination approach. Since manuscript I further showed that archazolid treatment led to p53 stabilization in p53 wild type tumor cells, combination treatment within the p53 pathway seemed promising. To this end, combination of archazolid with the small molecule p53 activator nutlin-3a (**manuscript III**) in different p53 wild type tumor cells resulted in synergistic cell death induction. Remarkably, these findings were recapitulated in a U87MG (U87) wild type p53 xenograft model as combination was more efficient in reducing tumor growth compared to single dose treatment. On a molecular level we found reduced glycolysis, since TP53-induced glycolysis and apoptosis regulator (TIGAR) mRNA levels were elevated and glucose uptake and glucose transporter 1 (Glut1) protein levels were diminished. Moreover, pro-apoptotic pathways including insulin-like growth factor-binding protein 3 (IGFBP3) and Bcl-2-associated X protein (Bax) were activated by the combination treatment.

In a different approach we addressed the endolysosomal system of cancer cells by targeting TPCs (**manuscript IV**). TPCs are recently identified nicotinic acid adenine dinucleotide phosphate (NAADP)- and phosphatidylinositol 3,5-bisphosphate ($PI(3,5)P_2$)-sensitive Ca^{2+}-permeable outward channels located in the membrane of endosomes and lysosomes. Their impact on cancer has not yet been studied. For that reason, silencing of TPC1 and TPC2 mRNA levels with siRNA significantly reduced adhesion, migration through pores and directed migration of T24 cancer cells. Pharmacological inhibition of TPCs by either *trans*-Ned-19 (Ned-19) or tetrandrine was efficient in diminishing migration through pores in T24, HUH7 and 4T1 cells. Mechanistic studies revealed that β1-integrin trafficking is disturbed after Ned-19 treatment leading to accumulation in early endosome antigen 1 (EEA1)-positive vesicles. This is suggested to be due to alterations in Ca^{2+} signaling since acidification of vesicles was not affected. As a consequence, invasive cancer cells were no longer able to form leading edges, which is substantially required for adequate migration. Finally, tetrandrine showed anti-metastatic efficacy in a 4T1-Luc dissemination assay *in vivo*, altogether suggesting a role for TPCs in cancer cell migration.

Taken together, targeting the endolysosomal system either by TPC or V-ATPase inhibition can apparently both impair adequate endocytic trafficking of receptors or signaling molecules as seen for TfR (**manuscript I**) and β1-integrin (**manuscript IV**). As a result, this triggers the induction of apoptosis in cancer cells or reduces their invasive phenotype (Figure 1). One might speculate that there could be a link between V-ATPases and TPCs, most notably because the positive inward currents of V-ATPase could be balanced by an outward flux through TPCs. Thus, this work unveils new insights into the role of V-ATPases and TPCs in tumors und renders them highly attractive new targets to combat this disease.

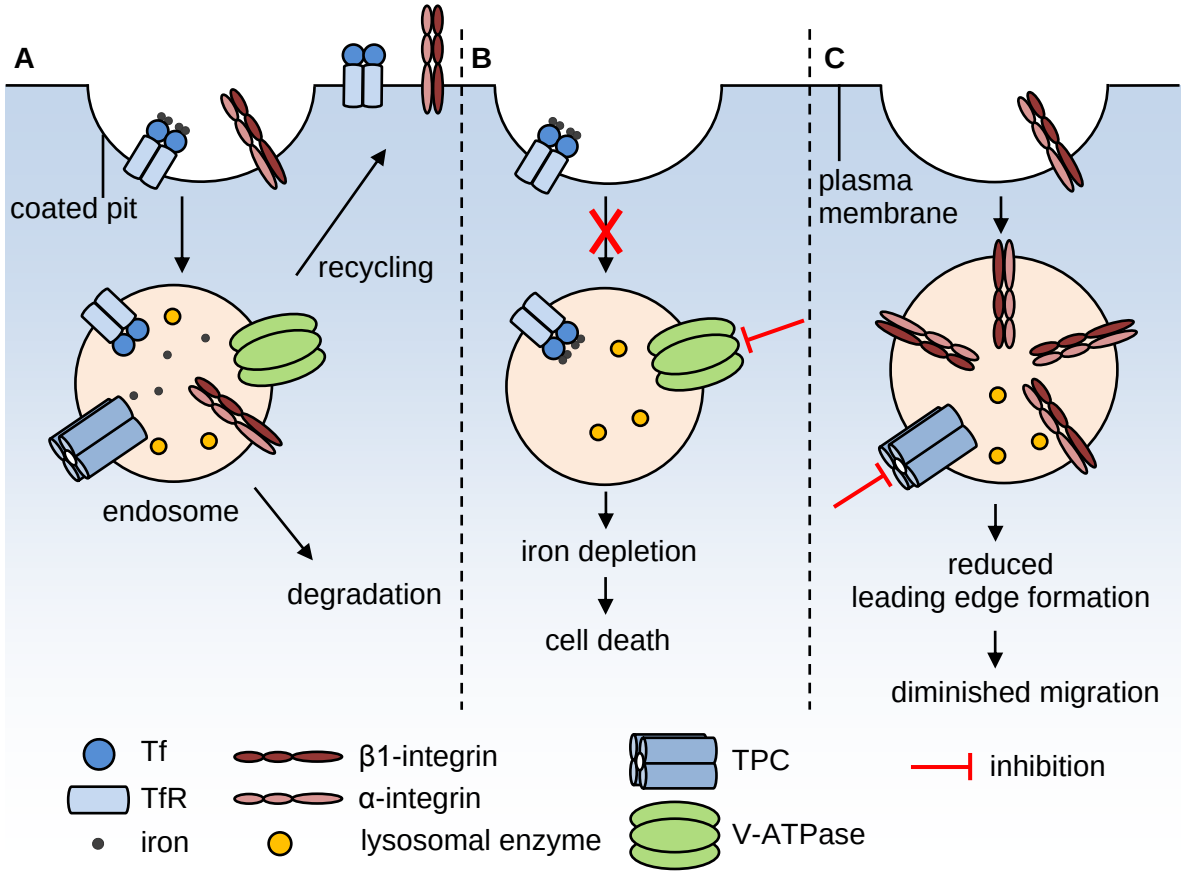

Figure 1 Proposed influence of V-ATPase and TPC inhibition on endocytosis pathways. A shows simplified endocytic trafficking of TfR and integrins under normal conditions. **B** displays disturbed internalization of TfR after V-ATPase inhibition leading to iron depletion in the cell. **C** depicts halted β1-integrin trafficking after inhibition of TPC function resulting in accumulation of β1-integrin in enlarged vesicles.

In conclusion, we here provide evidence that hitting highly metabolic active and invasive cancer cells through interfering with endocytosis is effective in disturbing pro-survival processes. The success of this strategy might be explained by the fact that malignant cells have to accomplish a high turnover of signaling molecules and nutrients to enable fast proliferation and migration. Moreover, targeting a complex and essential machinery like the endocytic trafficking system might allow to elude escape mechanisms and is therefore an innovative anti-tumor approach.

5 Introduction

5.1 Cancer and current treatment strategies

Cancer remains a leading cause of death worldwide. Hence, treating this disease is one of the big challenges of this century, particularly because the burden is thought to increase in the future (1). Nonetheless, due to improvements in treatment and earlier diagnosis the survival rate for certain cancers has improved over the past 30 years. For example, the overall 5-year relative survival rate for female breast cancer patients has increased from 74.8% between 1975 and 1977 to 90.3% between 2003 and 2009. However, it drops to 24.3% for patients with distant-stage breast cancer. The clinical treatment of cancers mainly implicates, dependent on the type and stage of the tumor, surgery, radiation and pharmacological therapy (2). As the development of tumors involves in most cancers four to seven independent mutations, pharmacological targeting of only one pathway is in many cases insufficient to combat this disease. Therefore, a change to multi-target therapeutics has occurred in recent years (3). Moreover, the success of today's anti-cancer drugs is challenged by resistance mechanisms against a variety of chemotherapeutics (4). Thus, there is still an urgent need to find new targets and treatment strategies to fight cancer, especially for invasive malignancies homing to distant sites.

5.2 Targeting the endolysosomal system of cancer cells

The uptake of extracellular material, lipids, ligands and plasma membrane proteins into the cell is processed by endocytosis and is essential for fundamental cellular processes such as signal transduction (5). Endocytosed cargos are subsequently delivered to early endosomes, where the first sorting takes place. Here, distinct components, like house-keeping receptors, are recycled to the plasma membrane whereas others are trafficked to late endosomes for additional sorting or to lysosomes for degradation (6). There are several ways how endocytosis can occur for example in a clathrin-dependent or -independent manner. Prominent clathrin-dependent cargo proteins are the transferrin receptor (TfR) and the low density lipoprotein receptor (LDLR) (5). TfR for instance binds its ligand ferrotransferrin at the cell surface and is subsequently transported in clathrin-coated vesicles after recognition by adaptor proteins. After internalization of Tf/TfR, iron dissociates from the receptor-ligand complex and enters the cytosol whereas the complex gets recycled to the cell surface (7, 8) (Figure 2). Clathrin-independent endocytosis appears in various forms and needs to be further studied (5). Interestingly, some proteins can follow more than one internalization route as it

has been shown for integrin heterodimers, which are a family of adhesion molecules mediating the interaction between a cell and the extracellular matrix (ECM) (9). Preserving the balance between endocytic internalization and recycling is substantially required to control cellular processes such as signal transduction, nutrient uptake, cell polarity, cell adhesion and migration (5).

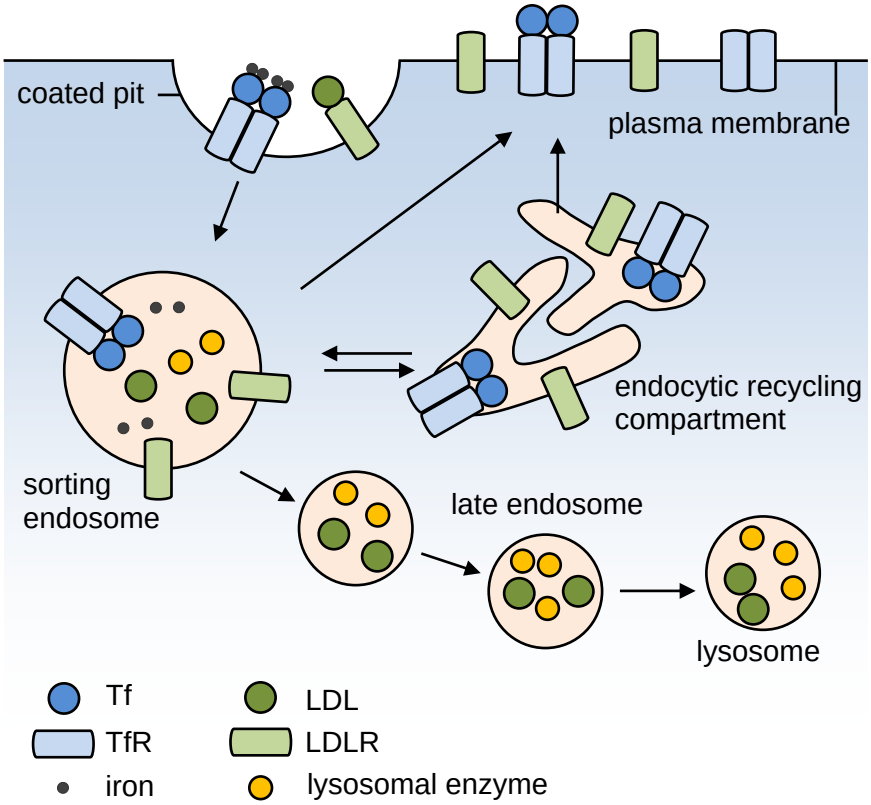

Figure 2 Endocytic trafficking pathways. The scheme depicts the transport of endocytic cargos upon internalization exemplified by trafficking of Tf/TfR and LDL/LDLR. After uptake in clathrin-coated pits, cargos are delivered to sorting endosomes and can be returned directly or recycled to the surface as shown for Tf/TfR or transported to early and late endosomes and finally to lysosomes for degradation as illustrated for LDL. Scheme designed and modified according to the model of Maxfield and MacGraw (10).

To function as the cellular sorting and degrading network, the endolysosomal system establishes a pH gradient from 6.2 in early endosomes to 4.6 in lysosomes which allows for high activity of degrading enzymes and for receptor-ligand processing. The luminal acidic milieu is maintained by vacuolar-type ATPases (V-ATPases) which actively pump protons across the endolysosomal membrane generating a positive inside membrane potential. As this would quickly build a self-limiting electrochemical gradient, the flux of other ions is required (6). Hence, despite V-ATPases, diverse other ion channels are thought to function in the endolysosomal system of cells including Cl^- antiporters, K^+/H^+ exchangers, Na^+/H^+ exchangers or Ca^{2+}/H^+ exchangers and Ca^{2+} channels (6, 11). Despite the mucolipins, which

represent members of the transient receptor potential (TRP) superfamily of Ca^{2+} channels, the two-pore channel (TPC) family has recently been identified as endolysosomal Ca^{2+} channels (6) (Figure 3).

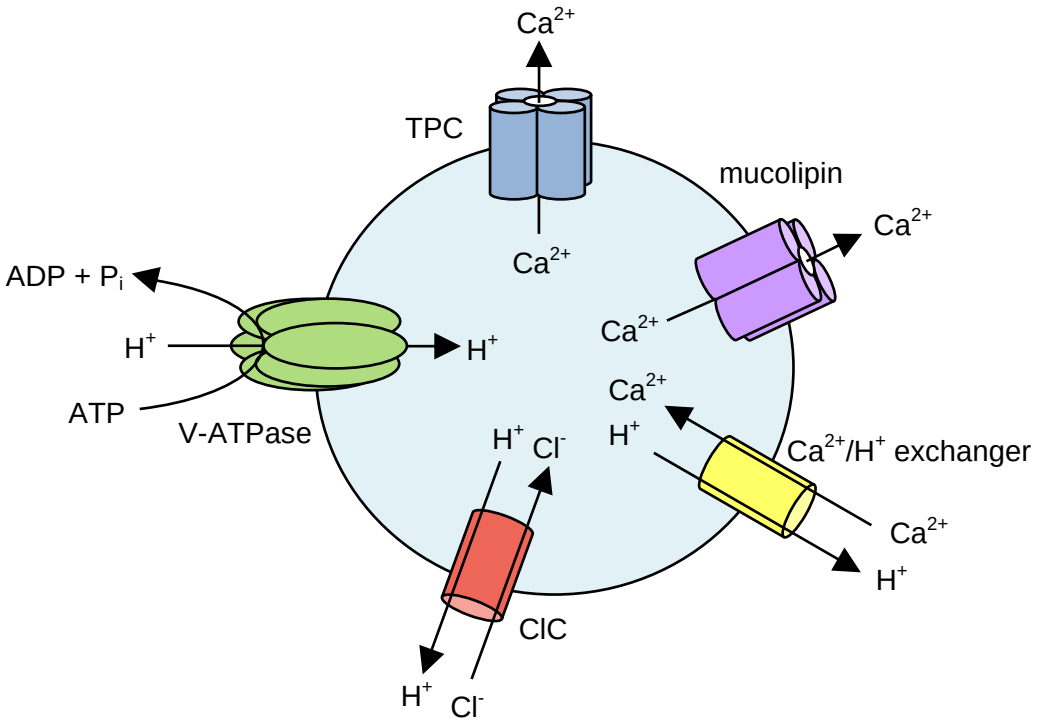

Figure 3 Overview of the main ionic influx and outflux mechanisms of an acidic organelle. Depicted is the V-ATPase, which pumps protons across the membrane into the lumen upon ATP hydrolysis, two families of voltage gated Ca^{2+} releasing channels: TPCs and the mucolipins, which are members of the TRP superfamily, the postulated Ca^{2+}/H^+ exchanger and a Cl^-/H^+ antiporter (ClC, Cl^- channel). TPCs and mucolipins may additionally function as release channels for other cations (6, 11-13).

In search for new promising cancer targets lysosomes came in focus. In the acidic milieu of these organelles hydrolases, such as cathepsins, are highly active in breaking down nucleic acids, proteins or lipids. Interestingly, after lysosomal membrane permeabilization (LMP) cathepsins can still function at cytosolic pH. Hence, recently it has been hypothesized that lysosomal cell death through LMP could be implicated in cancer and might therefore be an interesting target (14). However, secreted cathepsins in the extracellular space are of oncogenic character, suggesting the inhibition of this process as another promising anti-cancer strategy (15). Moreover, targeting the lysosomal pH by blocking V-ATPase in diverse cancer cell lines showed strong anti-tumor activity (16). Taken together, first studies revealed that addressing the endolysosomal machinery might be a very promising anti-cancer strategy. Nevertheless, further research is needed especially because the implication of other

endomembrane-associated proteins such as the TPCs has not yet been investigated in this context.

5.2.1 The vacuolar-type ATPase

As mentioned above, V-ATPases are proton pumps located in the membranes of endosomes and lysosomes of cells. In cancer cells they are additionally expressed at the plasma membrane (17), presumably to facilitate invasion of surrounding tissue by acidifying the microenvironment (18). The V-ATPase is a multisubunit enzyme organized into two functional domains: the cytosolic V_1 and the membrane integral V_0. The V_1 complex is composed of eight different subunits and provides the energy for proton transport as it comprises three catalytic binding sites for the hydrolysis of ATP to ADP and a free phosphate. The V_0 domain is required for proton translocation upon energy release and consists of the subunits a, c, d and e. In yeast, there are three possible isoforms for c: c, c´ and c´´. Mammalian V_0 is lacking c´ but has an additional glycoprotein named Ac45. The released energy through ATP cleavage results in a conformational change in the catalytic A subunits effecting a rotational movement of the central shaft subunits D and F of V_1, and d and the c-ring of V_0. Protons enter the lumen through the interaction of two proton conducting half channels in subunit a and an acidic amino acid side chain, located in each of the c subunits (19) (Figure 4).

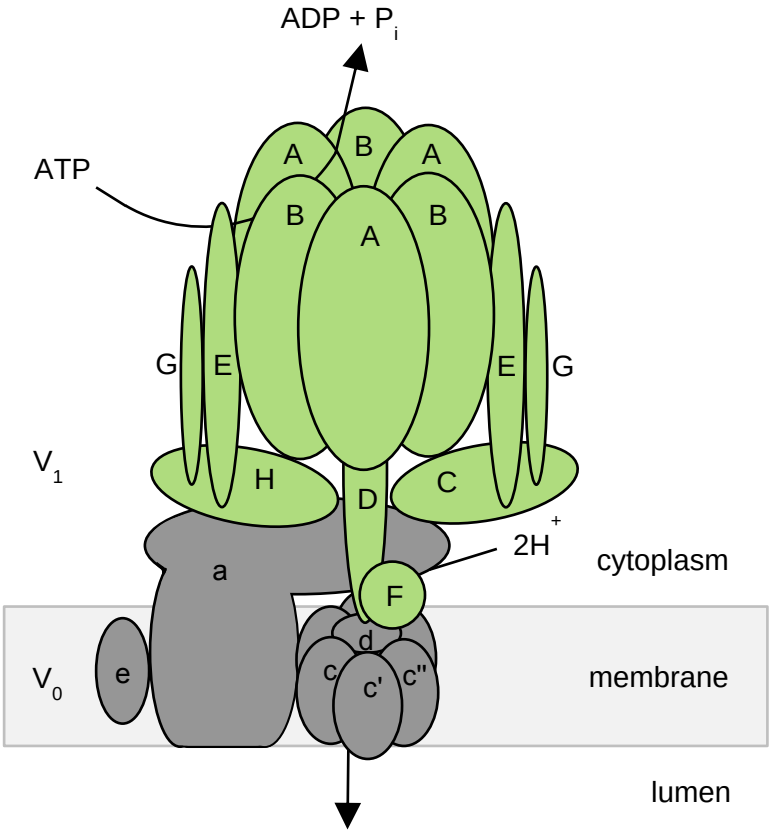

Figure 4 Structure and function of the V-ATPase in yeast. The V-ATPase is composed of two major complexes V_1 and V_0: $V_1$is extended to the cytoplasm and consists of eight subunits (A-H). The V_0 complex is located within the membrane with its six different subunits (a, d, e and c, c`, c``). A conformational change of the subunit A, which is driven by ATP hydrolysis, results in the rotational movement of the central shaft subunits D and F of V_1 and d and the c-ring of V_0. Subunit a of V_0 provides two proton conducting half channels. Protons can enter the first channel and bind to an amino acid side chain of one of the c subunits of V_0. Rotation of the c-ring of V_0 translocates the proton to the second channel finally releasing it to the lumen. Illustrated according to the model of Jefferies et al. (19) and Inoue et al. (20).

Due to its indispensable role in the endocytic pathway, V-ATPases are associated with a variety of normal cellular processes such as membrane and intracellular trafficking, degradation of macromolecules and acidification of secretory vesicles, which drives the transport of neurotransmitters like glutamate. Moreover, V-ATPase functions in diseases as it is implicated for instance in the endocytic entry of viruses into the cell (21). Interestingly, in the last decade evidence is increasing that V-ATPases might play a pivotal role in cancer cells. Reports show that human invasive pancreatic tumors overexpress V-ATPase (22) and it has been hypothesized that plasma membrane located V-ATPases are implicated in gaining an invasive phenotype in cancer cells (23). Pharmacological V-ATPase inhibition showed cell death induction in different cancer cell lines (24-26) and was less effective in non-tumor cells (16, 27). Although the cytotoxic effects of V-ATPase inhibitors have extensively been

studied, the precise mechanism still awaits molecular explanation. Researchers have hypothesized that inhibition of macroautophagy (24) or the release of proteases after lysosomal dysfunction might play a role (25). In another approach, inhibition of V-ATPase was efficient in reducing migration of invasive cancer cells *in vitro* and *in vivo*. This work further unveiled effects on receptor recycling after block of V-ATPase function since epidermal growth factor receptor (EGFR) internalization was delayed (28). A contribution of V-ATPase to receptor trafficking was also observed in another study (29).

A lot of the recent knowledge about V-ATPases has been gained by using pharmacological V-ATPase inhibitors. The oldest members, bafilomycin and concanamycin, have already been identified in the early 1980s (30). They are plecomacrolides and inhibit V-ATPase function by binding to subunit c of V_0 with a minor contribution of subunit a to the binding site. A novel very interesting player in this field is the myxobacteria-derived archazolid. It is produced by *Archangium gephyra* and *Cystobacter violaceus* and the main structural features are a macrocyclic lactone ring with a thiazole side chain (Figure 5). Archazolid interacts with subunit c of V_0 as it competes with concanamycin for its binding site (30). However, archazolid's binding site is located within the equatorial region of the V_0 rotor subunit c and not at the interface of two adjacent c subunits as it is for plecomacrolides (31). First studies revealed anti-cancer activity for archazolid (16, 28, 32), suggesting further research to elucidate a potential implication in cancer therapy.

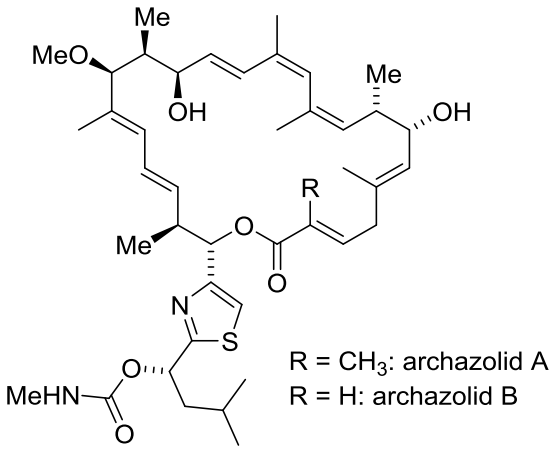

Figure 5 Structure of archazolid A and archazolid B. Chemical structure adapted from Roethle et al. (33)

5.2.2 Two-pore channels

The very first evidence for the existence of a vacuolar located ATPase was given in 1962 and this was confirmed by diverse studies until the early 1980s (34). The identification of endolysosomal TPCs happened much later. There was emerging evidence at the beginning of this century that nicotinic acid adenine dinucleotide phosphate (NAADP) is a Ca^{2+} mobilizing messenger and that it addresses stores separate from the endoplasmic reticulum in acidic organelles. However, the precise target was unclear. NAADP displays a high structural similarity to nicotinamide adenine dinucleotide phosphate (NADP) despite the carboxyl group at position 3 of the pyridine (35). Recently, TPCs have been identified as the long-sought endolysosomal NAADP-dependent Ca^{2+} release channels (36-38). TPCs are assigned to the superfamily of voltage-gated ion channels. Their postulated structure implicates a two-fold symmetry with six putative transmembrane α-helices each (36, 39). It has been suggested that TPC channels form homo- and heterodimers (40) (Figure 6). Up to now there are three TPC genes identified in sea urchins and most vertebrates: TPC1, TPC2 and TPC3, however TPC3 is not present in most primates (36).

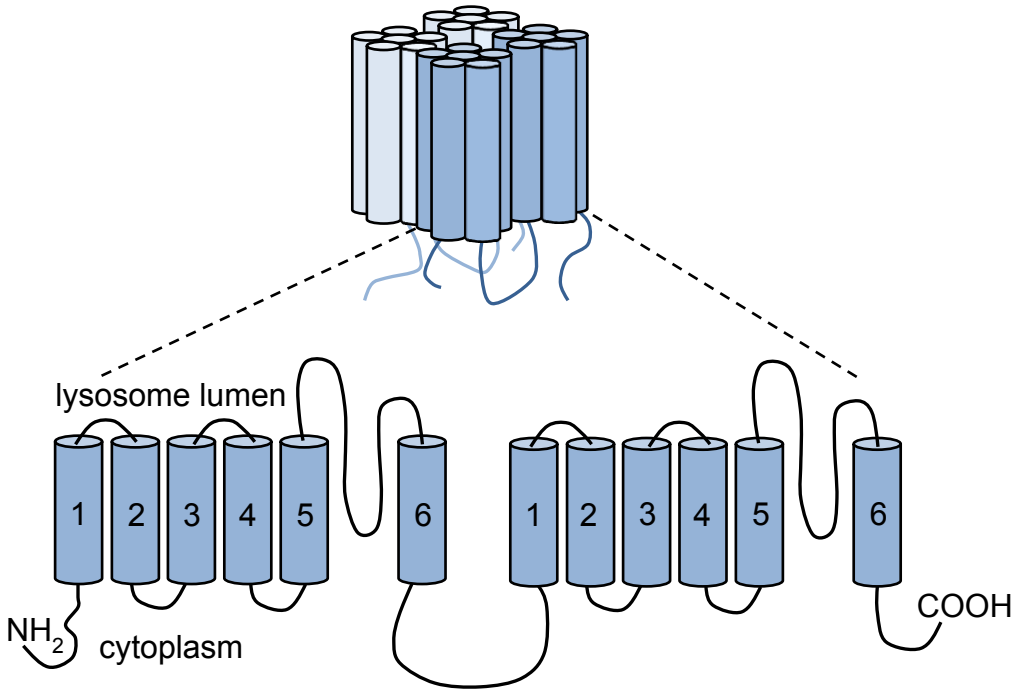

Figure 6 Membrane topology of TPCs. Depicted is the predicted transmembrane organization of TPCs with two putative pore-forming repeats containing six transmembrane segments and an intervening pore-loop between segment 5 and 6. Upper panel shows the postulated composition of the native TPC channel consisting of two TPC monomers forming a dimer. Illustrated according to Zhu et al. (12).

Diverse studies revealed that TPC1 and TPC2 are located in the endolysosomal system of cells with TPC1 expressed in endosomes and lysosomes whereas TPC2 can predominantly be found in lysosomes (36-38, 40, 41). Although most researchers claimed that activation of TPCs is triggered by NAADP (36-38, 42-44), it has also been suggested that phosphatidylinositol 3,5-bisphosphate ($PI(3,5)P_2$) is implicated (43, 45). Independent experiments hypothesized TPCs as Ca^{2+} channels, suggesting them responsible for Ca^{2+} release from endolysosomal stores (36, 38, 42, 44), albeit conductance for Na^+ was also discussed (45).

Given the fact that TPCs are located in endosomes and lysosomes, it does not come as a surprise that they function in the endocytic pathway. Reports show that overexpression of TPC2 inhibits autophagosomal-lysosomal fusion (46) and that they are crucially involved in the regulation of endolysosomal trafficking. Thus, TPC2 deficient mouse embryonic fibroblasts showed accumulation of EGF/EGFR and LDL in intracellular vesicles (47) and delayed platelet-derived growth factor receptor β (PDGFRβ) degradation (48). Moreover, cholera toxin, which is under normal conditions trafficked to the Golgi, was halted in endolysosomes after overexpression of TPCs (41). Disturbed TPC function retained Ebola virus trafficking, which prevented host cell infection (49). Despite effects on endocytic trafficking, TPCs were recently connected to lysosomal control of nutrient recycling. It was hypothesized that TPCs form a lysosomal ATP-sensitive Na^+ channel complex which is associated with and regulated by the mammalian target of rapamycin (mTOR). Under starvation mTOR delocates from the complex resulting in release of Na^+ and other ions from lysosomes (50). Interestingly, V-ATPase was also identified as a component of the mTOR pathway. It has been postulated that V-ATPase is crucial for amino acid signaling to mTOR complex 1 (51). Given the fact that TPCs and V-ATPases are both implicated in endocytic trafficking and mTOR signaling, one might speculate that there could be a link between these two proteins, most notably because the positive inward currents of V-ATPase could be balanced by an outward flux through TPCs.

To target the TPC pathway pharmacologically the NAADP antagonist Ned-19 was used in different studies (46, 49, 52). Ned-19 was identified as a noncompetitive antagonist of NAADP by virtual screening, with the *trans* form more potent than the *cis* form regarding Ca^{2+} release (53). In addition, lately, the bis-benzylisoquinoline alkaloid tetrandrine was reported to block TPC-mediated currents elicited by NAADP and $PI(3,5)P_2$ (49), however it

might act on other Ca^{2+} channels as well (54). Tetrandrine can be purified form the root of *Stephania tetrandra* and has been used in traditional chinese medicine for instance against hypertension (54) (Figure 7).

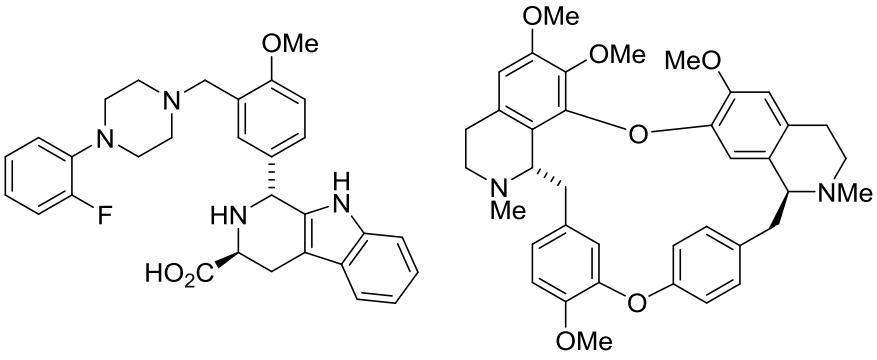

trans-Ned-19 tetrandrine

Figure 7 Structure of *trans*-Ned-19 and tetrandrine. Chemical structure of *trans*-Ned-19 adapted from Naylor et al. (53). Chemical structure of tetrandrine adapted from Inubushi et al. (55).

Although in some studies cancer cell lines were used as a cellular system to investigate TPC function, its implication in cancer progression, cancer cell migration and formation of metastasis has not been studied up to now. Therefore, it would be highly interesting to investigate this matter to elucidate a potential role in cancer treatment.

5.3 Overcoming the hallmarks of cancer

The development of a normal cell into a malignant cancer cell requires in most cases four to seven mutations (3). These mutations allow cancer cells to behave different to normal cells. For cancer therapy it is highly appreciated to find treatment strategies which mainly target malignant cells to reduce side effects. To achieve this, it seems promising to address the altered behavior of cancer cells.

In 2000, Hannahan and Weinberg defined the hallmarks of cancer describing the gained abilities of malignant cells. One is to evade apoptosis (56). Apoptosis, the programmed and controlled cell death, occurs during development or aging but is also a defense mechanism for instance when cells are damaged by noxious agents. Morphologically, apoptosis starts with cell shrinkage and chromatin condensation which is followed by plasma membrane blebbing and subsequent separation of cell fragments into apoptotic bodies. Degradation of these bodies occurs finally by phagocytosis through macrophages. Induction of apoptosis can be triggered by a variety of signals. Mechanistically, there are two main apoptotic pathways: the

intrinsic and the extrinsic. The intrinsic pathway is for example stimulated by radiation, toxins or hypoxia. These stimuli cause mitochondrial changes effecting an opening of the mitochondrial permeability pore and release of pro-apoptotic proteins such as cytochrome c. These processes are regulated by members of the B-cell lymphoma 2 (Bcl-2) family such as Bcl-2 or Bcl-2-associated X protein (Bax). The release of pro-apoptotic proteins from mitochondria triggers the formation of the apoptosome and activation of caspase-9. The extrinsic pathway is activated by the binding of a death ligand such as Fas ligand to its receptor which results in formation of the death inducing signaling complex, finally activating caspase-8. Both pathways converge in the activation of caspase-3 which initiates the degradation of the chromosomal DNA (57). Cancer cells are often resistant to apoptosis and self-sufficient in growth signals, another gained ability (56), which enables uncontrolled and fast proliferation. Overcoming these hallmarks of cancer by pharmacological induction of apoptosis is therefore a viable strategy for cancer therapy, albeit its contribution to treatment success was questioned. Therefore, investigating non-apoptotic types of cell death might be an alternative anti-cancer approach (58).

Despite evading apoptosis, cancer cells gained the ability to migrate and invade which allows for pulling themselves forward into new tissues to build metastasis (56). The formation of growth at secondary sites starts with the acquisition of an invasive phenotype of the primary tumor. Then, some tumor cells detach and intravasate to enter hematogenous circulation which is followed by extravasation into the new tissue. There, the tumor cell adapts to the foreign site and initiates proliferation. Since as much as 90% of cancer-related mortality is due to metastasis, new strategies to improve the treatment of invasive cancers remain of interest to develop (59).

In order to enable fast proliferation and migration, cancer cells have to be highly metabolic active. Therefore, malignant cells established an altered turnover of signaling molecules (60) and a rapid uptake of nutrients which allows tumor imaging in the clinic (61). Thus, derailed endocytosis was described as an emerging multifaceted hallmark of these cells (60). In turn, targeting the endocytic machinery pharmacologically might be a highly promising strategy to selectively hit cancer cells. Moreover, addressing this tumor-essential process could be an innovative approach to elude escape mechanisms.

6 Aim of the study

Cancer remains one of the leading causes of death worldwide. The success of today's anti-cancer drugs is challenged by a variety of resistance mechanisms against the most chemotherapeutics and by the occurrence of metastasis. Thus, new targets and treatment strategies are urgently needed. Previous work of our group revealed targeting the endolysosomal vacuolar-type ATPase as a promising future anti-cancer approach as it induces apoptosis in cancer cells. However, the precise mode of action still awaits molecular explanation.

Hence, the aim of this study was to elucidate this matter and to extend the previous data for *in vivo* efficacy including rational combination therapy. Moreover, the question was addressed whether targeting the endolysosomal system by inhibition of two-pore channels might be a new and viable approach for the treatment of invasive tumor cells.

7 Short summary of manuscripts

7.1 Vacuolar-ATPase inhibition blocks iron metabolism to mediate therapeutic effects in breast cancer

Lina S. Schneider, Karin von Schwarzenberg, Thorsten Lehr, Melanie Ulrich, Rebekka Kubisch-Dohmen, Johanna Liebl, Dirk Menche and Angelika M. Vollmar
2015, **Cancer Research**, 75(14):2863–2874

Within the last decade evidence is increasing that the vacuolar-type ATPase (V-ATPase), a heteromultimeric proton pump, plays a vital role in the survival of tumor cells. However, the precise mode of action still awaits molecular explanation. To investigate V-ATPase mediated cytotoxicity we used the myxobacteria-derived compound archazolid, a highly potent V-ATPase inhibitor. While V-ATPase inhibitors showed anti-tumoral potential in diverse cancer cell lines, *in vivo* data are limited up to now. Our study showed for the first time reduced tumor growth in a 4T1 mammary mouse model. With regard to the molecular mechanisms of V-ATPase-related cell death, we found that archazolid stabilizes the hypoxia-inducible factor 1α (HIF1α) protein in the two breast cancer cell lines MCF7 and MDA-MB-231. As HIF1α has many target genes involved in glycolysis, we could detect elevated levels of the hexokinase II protein as well as of other glycolytic gene products such as aldolase c. Further experiments unveiled that the HIF1α stabilization is due to iron depletion in the cytosol since an excess of iron citrate in the medium abolished it completely. Moreover, the lack of iron is partially responsible for the induction of cell death after V-ATPase inhibition and could be associated with disrupted transferrin/transferrin receptor internalization upon V-ATPase inhibition. As a consequence, activity of the iron dependent enzyme ribonucleotide reductase is diminished leading to S-phase block and double-strand breaks. Additionally, in p53 wild type MCF7 cells protein levels of the tumor suppressor p53 were elevated after archazolid treatment, which contributed to the induced cell death since pifithrin-α diminished significantly the amount of dead cells. These findings eventually connect V-ATPase inhibition to fundamental cellular processes such as DNA synthesis and DNA repair. Hence, our study reveals a novel mode of action for V-ATPase-induced cell death in tumor cells and proposes V-ATPase inhibition as a promising and viable strategy for breast cancer therapy.

7.2 Anti-leukemic effects of the V-ATPase inhibitor Archazolid A

Siwei Zhang, **Lina S. Schneider**, Binje Vick, Michaela Grunert, Irmela Jeremias, Dirk Menche, Rolf Müller, Angelika M. Vollmar and Johanna Liebl

2015, accepted for publication in **Oncotarget**

The V-ATPase inhibitor archazolid showed promising anti-tumor effects in different cancer cell lines as for example demonstrated in manuscript I. Since new treatment strategies for patients suffering from T-cell acute lymphoblastic leukemia (T-ALL) are urgently needed, we elucidated archazolid's potential as an anti-leukemic drug. Indeed, V-ATPase inhibition triggered induction of apoptosis in leukemic cell lines which could be shown by flow cytometry analysis, cleavage of caspase-3, caspase-9 and poly ADP ribose polymerase (PARP). Along this line, archazolid treatment in patient derived xenograft (PDX) leukemic cells, but not in non-tumor primary human peripheral blood mononuclear cells, resulted in induction of cell death. Mechanistically, by inhibiting lysosomal acidification, archazolid reduced activation of the notch pathway as the expression of notch1 intracellular domain (NICD) and of the downstream target c-myc were diminished. However, NICD overexpression was not able to rescue archazolid-mediated cell death, suggesting further studies regarding the underlying mechanisms. In fact, V-ATPase inhibition by archazolid decreased the expression level of the anti-apoptotic protein survivin. Remarkably, its overexpression significantly diminished the amount of dead cells during V-ATPase inhibition providing evidence for its implication in archazolid-induced cell death. Regarding the underlying mechanism, this work ties in with our previous findings of manuscript I that archazolid led to S-phase cell cycle arrest by interfering with the iron metabolism in leukemic cells. Thus, this study renders V-ATPases as potential new targets for the treatment of T-ALL.

Declaration of contribution: I contributed to this work of Dr. Siwei Zhang and Dr. Johanna Liebl by conducting a set of experiments including FACS and western blot analysis of PDX leukemic cells, cell cycle analysis of Jurkat cells and PCR analysis of Jurkat cell samples. I was partially involved in the design of the study since the investigated underlying mechanism is associated with my earlier work (manuscript I).

7.3 MDM2 antagonist nutlin-3a sensitizes tumors to V-ATPase inhibition

Lina S. Schneider, Melanie Ulrich, Thorsten Lehr, Dirk Menche, Rolf Müller, Angelika M. Vollmar and Karin von Schwarzenberg

Submitted

The anti-cancer potential of the V-ATPase inhibitor archazolid has been proven in distinct *in vitro* studies, however *in vivo* data are rare. Manuscript I showed first promising *in vivo* efficacy of archazolid in a 4T1 mouse model, albeit tumor growth was not abrogated completely. To improve this matter, we searched for a rational and innovative combination strategy. As tumors often carry several mutations, using multiple drugs targeting different proteins seems therefore more beneficial for cancer treatment. Since our recent study (manuscript I) unveiled that inhibition of V-ATPase caused the induction of p53 protein levels in cancer cells, we considered a combination strategy within the p53 pathway. In fact, in this study we found that combining archazolid with the p53 activator, nutlin-3a, induces synergistically cell death in different p53 wild type tumor cell lines, but not in p53 mutated cells, as shown by flow cytometry analysis. Investigating the underlying mechanism, we could detect reduced glycolysis as TP53-induced glycolysis and apoptosis regulator (TIGAR) mRNA levels were elevated and glucose uptake, glucose transporter 1 (Glut1) protein levels and ATP levels were decreased by the combination. Moreover, treatment of archazolid and nutlin-3a activated pro-apoptotic pathways involving the induction of insulin-like growth factor-binding protein 3 (IGFBP3) and active Bcl-2-associated X protein (Bax) and the cleavage of caspase-9 and PARP. Finally, combination treatment was more efficient in reducing tumor growth compared to single dose treatment in a p53 wild type U87MG glioblastoma xenograft. Especially the success of archazolid and nutlin-3a *in vivo* suggests this combination as a potential new therapeutic option for p53 wild type carcinomas.

7.4 Two-pore channel function is crucial for migration of invasive cancer cells

Lina S. Schneider*, Christian Grimm*, Yu-Kai Chao, Anna Watermann, Melanie Ulrich, Doris Mayr, Christian Wahl-Schott, Martin Biel* and Angelika M. Vollmar*
*These authors contributed equally to this work
Submitted

The most cancer-related deaths are caused by metastasis. Spread of single tumor cells to anatomically distant sites requires the ability to migrate and invade. Disrupting these processes is therefore thought to be a promising strategy for the treatment of invasive carcinomas. As targeting the endocytic system by V-ATPase inhibition was effective in reducing cancer cell migration before, we here investigated the impact of endolysosomal two-pore channels (TPCs) in this context. TPCs are recently identified nicotinic acid adenine dinucleotide phosphate (NAADP)- and phosphatidylinositol 3,5-bisphosphate ($PI(3,5)P_2$)-sensitive Ca^{2+}-permeable ion channels located in the membrane of endosomes and lysosomes. Their implication in cancer cell progression and migration has not been studied up to now. To this end, siRNA silencing of TPC1 and TPC2 mRNA levels in T24 cancer cells resulted in reduced adhesion, migration through pores and directed migration. Along this line, pharmacological inhibition of TPC function through Ned-19 and tetrandrine inhibited migration through pores in T24, HUH7 and 4T1 cancer cells. Mechanistically, we found that disturbing TPC function affected β1-integrin trafficking, causing accumulation in early endosome antigen 1 (EEA1)-positive vesicles. This is suggested to result from alterations in Ca^{2+} signaling since acidification of vesicles was not inhibited. Finally, *trans*-Ned-19-treated cells showed insufficient formation of leading edges, which is crucial for adequate migration. Remarkably, these effects were recapitulated in a mouse model of tumor dissemination showing significantly reduced lung metastasis of 4T1-Luc cells after tetrandrine treatment. Thus, this study identified TPCs as new and interesting candidates to address in the treatment of invasive cancer cells. Once more, targeting the endolysosomal system of cancer cells seems to be a promising anti-cancer approach.

8 References

1. Torre LA, Bray F, Siegel RL, Ferlay J, Lortet-Tieulent J, Jemal A (2015) Global cancer statistics, 2012. *CA Cancer J Clin* 65(2):87–108.
2. DeSantis CE, Lin CC, Mariotto AB, Siegel RL, Stein KD, Kramer JL, Alteri R, Robbins AS, Jemal A (2014) Cancer treatment and survivorship statistics, 2014. *CA Cancer J Clin* 64(4):252–271.
3. Zimmermann GR, Lehár J, Keith CT (2007) Multi-target therapeutics: when the whole is greater than the sum of the parts. *Drug Discov Today* 12(1-2):34–42.
4. Holohan C, Van Schaeybroeck S, Longley DB, Johnston PG (2013) Cancer drug resistance: an evolving paradigm. *Nat Rev Cancer* 13(10):714–726.
5. Grant BD, Donaldson JG (2009) Pathways and mechanisms of endocytic recycling. *Nat Rev Mol Cell Biol* 10(9):597–608.
6. Scott CC, Gruenberg J (2011) Ion flux and the function of endosomes and lysosomes: pH is just the start. *Bioessays* 33(2):103–110.
7. Le Roy C, Wrana JL (2005) Clathrin- and non-clathrin-mediated endocytic regulation of cell signalling. *Nat Rev Mol Cell Biol* 6(2):112–126.
8. Dautry-Varsat A, Ciechanover A, Lodish HF (1983) pH and the recycling of transferrin during receptor-mediated endocytosis. *Proc Natl Acad Sci U S A* 80(8):2258–2262.
9. Caswell PT, Vadrevu S, Norman JC (2009) Integrins: masters and slaves of endocytic transport. *Nat Rev Mol Cell Biol* 10(12):843–853.
10. Maxfield FR, McGraw TE (2004) Endocytic recycling. *Nat Rev Mol Cell Biol* 5(2):121–132.
11. Christensen KA, Myers JT, Swanson JA (2002) pH-dependent regulation of lysosomal calcium in macrophages. *J Cell Sci* 115(Pt 3):599–607.
12. Zhu MX, Ma J, Parrington J, Calcraft PJ, Galione A, Evans AM (2009) Calcium signaling via two-pore channels: local or global, that is the question. *Am J Physiol Cell Physiol* 298(3):C430–C441.
13. Grimm C, Hassan S, Wahl-Schott C, Biel M (2012) Role of TRPML and Two-Pore Channels in Endolysosomal Cation Homeostasis. *J Pharmacol Exp Ther* 342(2):236-244.
14. Gyparaki M-T, Papavassiliou AG (2014) Lysosome: the cell's ‘suicidal bag’ as a promising cancer target. *Trends Mol Med* 20(5):239–241.

15. Kroemer G, Jäättelä M (2005) Lysosomes and autophagy in cell death control. *Nat Rev Cancer* 5(11):886–897.
16. von Schwarzenberg K, Wiedmann RM, Oak P, Schulz S, Zischka H, Wanner G, Efferth T, Trauner D, Vollmar AM (2012) Mode of Cell Death Induction by Pharmacological Vacuolar H+-ATPase (V-ATPase) Inhibition. *J Biol Chem* 288(2):1385–1396.
17. Martinez-Zaguilan R, Lynch RM, Martinez GM, Gillies RJ (1993) Vacuolar-type H(+)-ATPases are functionally expressed in plasma membranes of human tumor cells. *Am J Physiol* 265(4 Pt 1):C1015–1029.
18. Pérez-Sayáns M, Somoza-Martín JM, Barros-Angueira F, Rey JMG, García-García A (2009) V-ATPase inhibitors and implication in cancer treatment. *Cancer Treat Rev* 35(8):707–713.
19. Jefferies KC, Cipriano DJ, Forgac M (2008) Function, structure and regulation of the vacuolar (H+)-ATPases. *Arch Biochem Biophys* 476(1):33–42.
20. Inoue T, Wilkens S, Forgac M (2003) Subunit structure, function, and arrangement in the yeast and coated vesicle V-ATPases. *J Bioenerg Biomembr* 35(4):291–299.
21. Hinton A, Bond S, Forgac M (2007) V-ATPase functions in normal and disease processes. *Pflugers Arch* 457(3):589–598.
22. Ohta T, Numata M, Yagishita H, Futagami F, Tsukioka Y, Kitagawa H, Kayahara M, Nagakawa T, Miyazaki I, Yamamoto M, Iseki S, Ohkuma S (1996) Expression of 16 kDa proteolipid of vacuolar-type H(+)-ATPase in human pancreatic cancer. *Br J Cancer* 73(12):1511–1517.
23. Sennoune SR (2004) Vacuolar H+-ATPase in human breast cancer cells with distinct metastatic potential: distribution and functional activity. *Am J Physiol Cell Physiol* 286(6):C1443–C1452.
24. Wu YC, Wu WK, Li Y, Yu L, Li ZJ, Wong CC, Li HT, Sung JJ, Cho CH (2009) Inhibition of macroautophagy by bafilomycin A1 lowers proliferation and induces apoptosis in colon cancer cells. *Biochem Biophys Res Commun* 382(2):451–456.
25. Nakashima S, Hiraku Y, Tada-Oikawa S, Hishita T, Gabazza EC, Tamaki S, Imoto I, Adachi Y, Kawanishi S (2003) Vacuolar H+-ATPase inhibitor induces apoptosis via lysosomal dysfunction in the human gastric cancer cell line MKN-1. *J Biochem* 134(3):359–364.
26. Ohta T, Arakawa H, Futagami F, Fushida S, Kitagawa H, Kayahara M, Nagakawa T, Miwa K, Kurashima K, Numata M, Kitamura Y, Terada T, Ohkuma S (1998)

Bafilomycin A1 induces apoptosis in the human pancreatic cancer cell line Capan-1. *J Pathol* 185(3):324–330.

27. Morimura T, Fujita K, Akita M, Nagashima M, Satomi A (2008) The proton pump inhibitor inhibits cell growth and induces apoptosis in human hepatoblastoma. *Pediatr Surg Int* 24(10):1087–1094.
28. Wiedmann RM, von Schwarzenberg K, Palamidessi A, Schreiner L, Kubisch R, Liebl J, Schempp C, Trauner D, Vereb G, Zahler S, Wagner E, Muller R, Scita G, Vollmar AM (2012) The V-ATPase-Inhibitor Archazolid Abrogates Tumor Metastasis via Inhibition of Endocytic Activation of the Rho-GTPase Rac1. *Cancer Res* 72(22):5976–5987.
29. Kozik P, Hodson NA, Sahlender DA, Simecek N, Soromani C, Wu J, Collinson LM, Robinson MS (2012) A human genome-wide screen for regulators of clathrin-coated vesicle formation reveals an unexpected role for the V-ATPase. *Nat Cell Biol* 15(1):50–60.
30. Huss M, Wieczorek H (2009) Inhibitors of V-ATPases: old and new players. *J Exp Biol* 212(3):341–346.
31. Bockelmann S, Menche D, Rudolph S, Bender T, Grond S, von Zezschwitz P, Muench SP, Wieczorek H, Huss M (2010) Archazolid A Binds to the Equatorial Region of the c-Ring of the Vacuolar H+-ATPase. *J Biol Chem* 285(49):38304–38314.
32. von Schwarzenberg K, Lajtos T, Simon L, Müller R, Vereb G, Vollmar AM (2014) V-ATPase inhibition overcomes trastuzumab resistance in breast cancer. *Mol Oncol* 8(1):9–19.
33. Roethle PA, Chen IT, Trauner D (2007) Total Synthesis of (−)-Archazolid B. *J Am Chem Soc* 129(29):8960–8961.
34. Beyenbach KW, Wieczorek H (2006) The V-type H+ ATPase: molecular structure and function, physiological roles and regulation. *J Exp Biol* 209(Pt 4):577–589.
35. Galione A (2010) NAADP Receptors. *Cold Spring Harb Perspect Biol* 3(1):a004036–a004036.
36. Calcraft PJ, Ruas M, Pan Z, Cheng X, Arredouani A, Hao X, Tang J, Rietdorf K, Teboul L, Chuang K-T, Lin P, Xiao R, Wang C, Zhu Y, Lin Y, Wyatt CN, Parrington J, Ma J, Evans AM, Galione A, Zhu MX (2009) NAADP mobilizes calcium from acidic organelles through two-pore channels. *Nature* 459(7246):596–600.

37. Brailoiu E, Churamani D, Cai X, Schrlau MG, Brailoiu GC, Gao X, Hooper R, Boulware MJ, Dun NJ, Marchant JS, Patel S (2009) Essential requirement for two-pore channel 1 in NAADP-mediated calcium signaling. *J Cell Biol* 186(2):201–209.

38. Zong X, Schieder M, Cuny H, Fenske S, Gruner C, Rötzer K, Griesbeck O, Harz H, Biel M, Wahl-Schott C (2009) The two-pore channel TPCN2 mediates NAADP-dependent Ca2+-release from lysosomal stores. *Pflugers Arch* 458(5):891–899.

39. Ishibashi K, Suzuki M, Imai M (2000) Molecular Cloning of a Novel Form (Two-Repeat) Protein Related to Voltage-Gated Sodium and Calcium Channels. *Biochem Biophys Res Commun* 270(2):370–376.

40. Rietdorf K, Funnell TM, Ruas M, Heinemann J, Parrington J, Galione A (2011) Two-pore Channels Form Homo- and Heterodimers. *J Biol Chem* 286(43):37058–37062.

41. Ruas M, Rietdorf K, Arredouani A, Davis LC, Lloyd-Evans E, Koegel H, Funnell TM, Morgan AJ, Ward JA, Watanabe K, Cheng X, Churchill GC, Zhu MX, Platt FM, Wessel GM, Parrington J, Galione A (2010) Purified TPC Isoforms Form NAADP Receptors with Distinct Roles for Ca2+ Signaling and Endolysosomal Trafficking. *Curr Biol* 20(8):703–709.

42. Schieder M, Rotzer K, Bruggemann A, Biel M, Wahl-Schott CA (2010) Characterization of Two-pore Channel 2 (TPCN2)-mediated Ca2+ Currents in Isolated Lysosomes. *J Biol Chem* 285(28):21219–21222.

43. Jha A, Ahuja M, Patel S, Brailoiu E, Muallem S (2014) Convergent regulation of the lysosomal two-pore channel-2 by Mg2+, NAADP, PI(3,5)P2 and multiple protein kinases. *EMBO J* 33(5):501–511.

44. Ruas M, Davis LC, Chen CC, Morgan AJ, Chuang KT, Walseth TF, Grimm C, Garnham C, Powell T, Platt N, Platt FM, Biel M, Wahl-Schott C, Parrington J, Galione A (2015) Expression of Ca2+-permeable two-pore channels rescues NAADP signalling in TPC-deficient cells. *EMBO J* 34(13):1743–1758.

45. Wang X, Zhang X, Dong X-p, Samie M, Li X, Cheng X, Goschka A, Shen D, Zhou Y, Harlow J, Zhu Michael X, Clapham David E, Ren D, Xu H (2012) TPC Proteins Are Phosphoinositide- Activated Sodium-Selective Ion Channels in Endosomes and Lysosomes. *Cell* 151(2):372–383.

46. Lu Y, Hao BX, Graeff R, Wong CWM, Wu WT, Yue J (2013) Two Pore Channel 2 (TPC2) Inhibits Autophagosomal-Lysosomal Fusion by Alkalinizing Lysosomal pH. *J Biol Chem* 288(33):24247–24263.

47. Grimm C, Holdt LM, Chen C-C, Hassan S, Müller C, Jörs S, Cuny H, Kissing S, Schröder B, Butz E, Northoff B, Castonguay J, Luber CA, Moser M, Spahn S, Lüllmann-Rauch R, Fendel C, Klugbauer N, Griesbeck O, Haas A, Mann M, Bracher F, Teupser D, Saftig P, Biel M, Wahl-Schott C (2014) High susceptibility to fatty liver disease in two-pore channel 2-deficient mice. *Nat Commun* 5:4699.

48. Ruas M, Chuang KT, Davis LC, Al-Douri A, Tynan PW, Tunn R, Teboul L, Galione A, Parrington J (2014) TPC1 Has Two Variant Isoforms, and Their Removal Has Different Effects on Endo-Lysosomal Functions Compared to Loss of TPC2. *Mol Cell Biol* 34(21):3981–3992.

49. Sakurai Y, Kolokoltsov AA, Chen CC, Tidwell MW, Bauta WE, Klugbauer N, Grimm C, Wahl-Schott C, Biel M, Davey RA (2015) Two-pore channels control Ebola virus host cell entry and are drug targets for disease treatment. *Science* 347(6225):995–998.

50. Cang C, Zhou Y, Navarro B, Seo Y-j, Aranda K, Shi L, Battaglia-Hsu S, Nissim I, Clapham David E, Ren D (2013) mTOR Regulates Lysosomal ATP-Sensitive Two-Pore Na+ Channels to Adapt to Metabolic State. *Cell* 152(4):778–790.

51. Zoncu R, Bar-Peled L, Efeyan A, Wang S, Sancak Y, Sabatini DM (2011) mTORC1 Senses Lysosomal Amino Acids Through an Inside-Out Mechanism That Requires the Vacuolar H+-ATPase. *Science* 334(6056):678–683.

52. Favia A, Desideri M, Gambara G, D'Alessio A, Ruas M, Esposito B, Del Bufalo D, Parrington J, Ziparo E, Palombi F, Galione A, Filippini A (2014) VEGF-induced neoangiogenesis is mediated by NAADP and two-pore channel-2-dependent Ca2+ signaling. *Proc Natl Acad Sci U S A* 111(44):E4706–E4715.

53. Naylor E, Arredouani A, Vasudevan SR, Lewis AM, Parkesh R, Mizote A, Rosen D, Thomas JM, Izumi M, Ganesan A, Galione A, Churchill GC (2009) Identification of a chemical probe for NAADP by virtual screening. *Nat Chem Biol* 5(4):220–226.

54. Wang G, Lemos JR, Iadecola C (2004) Herbal alkaloid tetrandrine: from an ion channel blocker to inhibitor of tumor proliferation. *Trends Pharmacol Sci* 25(3):120–123.

55. Inubushi Y, Masaki Y, Matsumoto S, Takami F (1968) Total syntheses of optically active natural isotetrandrine, phaeanthine and tetrandrine. *Tetrahedron Lett* 9(30):3399–3402.

56. Hanahan D, Weinberg RA (2000) The Hallmarks of Cancer. *Cell* 100(1):57–70.

57. Elmore S (2007) Apoptosis: A Review of Programmed Cell Death. *Toxicol Pathol* 35(4):495–516.

58. de Bruin EC, Medema JP (2008) Apoptosis and non-apoptotic deaths in cancer development and treatment response. *Cancer Treat Rev* 34(8):737–749.

59. Chaffer CL, Weinberg RA (2011) A Perspective on Cancer Cell Metastasis. *Science* 331(6024):1559–1564.

60. Mosesson Y, Mills GB, Yarden Y (2008) Derailed endocytosis: an emerging feature of cancer. *Nat Rev Cancer* 8(11):835-850.

61. Plathow C, Weber WA (2008) Tumor Cell Metabolism Imaging. *J Nucl Med* 49(Suppl_2):43S-63S.

9 Publications

9.1 Original articles

Lina S. Schneider*, Christian Grimm*, Yu-Kai Chao, Anna Watermann, Melanie Ulrich, Doris Mayr, Christian Wahl-Schott, Martin Biel* and Angelika M. Vollmar*; *Two-pore channel function is crucial for migration of invasive cancer cells;* *These authors contributed equally to this work; Submitted

Lina S. Schneider, Melanie Ulrich, Thorsten Lehr, Dirk Menche, Rolf Müller, Angelika M. Vollmar and Karin von Schwarzenberg; *MDM2 antagonist nutlin-3a sensitizes tumors to V-ATPase inhibition;* Submitted

Siwei Zhang, **Lina S. Schneider**, Binje Vick, Michaela Grunert, Irmela Jeremias, Dirk Menche, Rolf Müller, Angelika M. Vollmar and Johanna Liebl; *Anti-leukemic effects of the V-ATPase inhibitor Archazolid A;* 2015, **Oncotarget**

Anne K. Zaiss, Erin M. Foley, Roger Lawrence, **Lina S. Schneider**, Hamidreza Hoveida, Patrick Secrest, Arthur B. Catapang, Yu Yamaguchi, Ramon Alemany, Dmitry M. Shayakhmetov, Jeffrey D. Esko and Harvey R. Herschman; *Hepatocyte Heparan Sulfate is Required for Adeno-Associated Virus 2 but Dispensable for Adenovirus 5 Liver Transduction In Vivo*; 2015, **Journal of Virology**, JVI.01939-01915

Lina S. Schneider, Karin von Schwarzenberg, Thorsten Lehr, Melanie Ulrich, Rebekka Kubisch-Dohmen, Johanna Liebl, Dirk Menche and Angelika M. Vollmar; *Vacuolar-ATPase inhibition blocks iron metabolism to mediate therapeutic effects in breast cancer;* 2015, **Cancer Research**, 75(14):2863–2874

9.2 Oral presentations

Lina S. Schneider, Karin von Schwarzenberg, Thorsten Lehr, Melanie Ulrich, Rebekka Kubisch-Dohmen, Johanna Liebl, Dirk Menche, and Angelika M. Vollmar; *Interfering with the iron metabolism by V-ATPase inhibition in breast cancer cells*; 6th FOR1406 Meeting, June 30-July 1, 2015, Saarbrücken, Germany

Lina S. Schneider, Karin von Schwarzenberg, Rolf Müller and Angelika M. Vollmar; *Effects of the V-ATPase inhibitor archazolid B on iron metabolism in breast cancer cells*; 4th FOR1406 Meeting, July 16-18, 2013, Saarbrücken, Germany

9.3 Poster presentations

Lina S. Schneider, Karin von Schwarzenberg, Thorsten Lehr, Melanie Ulrich, Rebekka Kubisch-Dohmen, Johanna Liebl, Dirk Trauner, Dirk Menche and Angelika M. Vollmar*; V-ATPase inhibition affects iron metabolism: a novel therapeutic option for breast cancer;* 5th International HIPS-Symposium, July 2, 2015, Saarbrücken, Germany

Lina S. Schneider, Karin von Schwarzenberg, Thorsten Lehr, Melanie Ulrich, Rebekka Kubisch-Dohmen, Johanna Liebl, Dirk Trauner, Dirk Menche and Angelika M. Vollmar*; V-ATPase inhibition affects iron metabolism: a novel therapeutic option for breast cancer;* V-ATPase Symposium, May 13-15, 2015, Milano, Italy

Lina S. Schneider, Karin von Schwarzenberg, Thorsten Lehr, Rebekka Kubisch-Dohmen, Dirk Trauner, Dirk Menche and Angelika M. Vollmar; *V-ATPase inhibition affects iron metabolism: a novel therapeutic option for breast cancer*; Deutsche Pharmazeutische Gesellschaft (DPhG) Jahrestagung 2014, September 24-26, 2014, Frankfurt, Germany

Lina S. Schneider, D. Trauner, R. Müller, A. M. Vollmar and K. von Schwarzenberg; *HIF1α induced by V-ATPase inhibition leads to apoptosis in p53 wild type tumor cells*; 1st European Conference on Natural Products: Research and Applications, September 22-25, 2013, Frankfurt, Germany

Lina S. Schneider, Karin von Schwarzenberg and Angelika M. Vollmar; *HIF1α induced by V-ATPase inhibition leads to apoptosis in p53 wild type tumor cells*; 1st Symposium Tumor Metabolism meets Immunology, April 25-27, 2013, Regensburg, Germany

10 Acknowledgements

Mein allergrößter Dank geht an Frau Prof. Dr. Vollmar. Ich danke Ihnen ganz herzlich, dass Sie mir die Möglichkeit gegeben haben meine Doktorarbeit an Ihrem Lehrstuhl anzufertigen. Sie waren mir mit Ihrem Engagement und Ihrer Freude an der Wissenschaft immer ein Vorbild. Dass Ihre Türe für jegliche Fragen immer offen stand, habe ich sehr wertgeschätzt. Ich möchte mich vor allem auch für das von Ihnen mir entgegengebrachte Vertrauen bedanken, was mir ein sehr eigenständiges Arbeiten ermöglichte und damit zu einer spannenden Zeit in Ihrem Arbeitskreis beitrug. Auch die Teilnahme an verschiedenen Konferenzen, unter anderem im Rahmen der FOR1406, war eine bereichernde Erfahrung für deren Ermöglichung ich mich bei Ihnen herzlich bedanken möchte.

Auch möchte ich mich ganz herzlich bei Herrn Prof. Dr. Zahler bedanken. Vielen Dank für die von Ihnen aufgebrachte Zeit und Mühe mich in die unterschiedlichsten analytischen Methoden einzuweisen. Vor allem einen großen Dank für Ihre kritischen aber konstruktiven Anmerkungen und Fragen nach diversen Vorträgen, die stets zum Überdenken geführt und zur Qualität der Arbeit beigetragen haben.

Ein großer Dank an meinen Zweitprüfer Herrn Prof. Dr. Wahl-Schott dafür, dass Sie meine Arbeit bewertet haben, aber auch für die konstruktiven Diskussionen bezüglich des TPC Projektes.

Herrn Prof. Dr. Zahler und Herrn Prof. Dr. Wagner danke ich ganz herzlich für Ihr Interesse an meiner Arbeit als Dritt- und Viertprüfer, so wie Herrn PD Dr. Michalakis und Herrn Prof. Dr. Bracher als Fünft- und Sechstprüfer.

Hanna und Siwei, euch danke ich für die erfolgreiche Zusammenarbeit im Leukämie Projekt sowie Herrn PD Dr. Dr. Grimm und Herrn Prof. Dr. Biel im TPC Projekt. Rebekka und Melanie, auch euch danke ich für die gute Zusammenarbeit in Bezug auf die Durchführung der Tierversuche.

Liebe Karin, dir möchte ich dafür danken, dass deine Türe für alle Fragen immer offen stand, du mir mit konstruktiven Vorschlägen in den verschiedenen Projekten weiter geholfen hast, mich aber auch meine Ideen verfolgen hast lassen. Auch danke ich dir dafür, dass du mit deiner ruhigen und ausgeglichenen Art immer eine sehr angenehme Arbeitsatmosphäre geschaffen hast.

Es hat mir in den letzten 3 Jahren immer Spaß gemacht in die Arbeit zu gehen und das lag vor allem auch am Team des AK Vollmar. Ich möchte mich hiermit bei allen für die angenehme Zeit bedanken.

Vor allem aber möchte ich mich bei Henri für die wunderbare Freundschaft bedanken. Wir haben schon viel zusammen erlebt, es war immer ein großer Spaß und schön dich dabei gehabt zu haben. Die Doktorarbeit wird nicht das letzte gemeinsame Abenteuer gewesen sein. Genauso möchte ich Katja danken - für all die schönen Momente, die lustigen wie auch „zähen“ Zeiten zu zweit in unserer Box sowie und für die daraus entstandene Freundschaft. Danke euch beiden für die unvergesslichen Jahre der Doktorarbeit mit euch.

Max, Flo und Simon, euch danke ich dafür, dass ihr den Mittagstisch und Kaffeetisch mit euren Männergesprächen bereichert und von Kaloriengesprächen abgelenkt habt. Karin, Christina, Fabi, Meli, Meli und Kerstin, vielen Dank für die schöne Zeit mich euch, ich hab es sehr genossen.

Liebe Tini auch dir möchte ich danken, dass du mich als „Altdoktorandin“ so toll ins Schwarzenberg Team aufgenommen hast und immer eine gute Ansprechpartnerin warst bzw. bist. Sandra und Julia, vielen Dank für die unvergessliche Zeit die wir nicht nur im Labor zusammen erlebt haben.

11 Appendix

In the following, manuscripts I to IV are reprinted.

I. **Lina S. Schneider**, Karin von Schwarzenberg, Thorsten Lehr, Melanie Ulrich, Rebekka Kubisch-Dohmen, Johanna Liebl, Dirk Menche and Angelika M. Vollmar
Vacuolar-ATPase inhibition blocks iron metabolism to mediate therapeutic effects in breast cancer
2015, **Cancer Research**, 75(14):2863–2874

II. Siwei Zhang, **Lina S. Schneider**, Binje Vick, Michaela Grunert, Irmela Jeremias, Dirk Menche, Rolf Müller, Angelika M. Vollmar and Johanna Liebl
Anti-leukemic effects of the V-ATPase inhibitor Archazolid A
2015, accepted for publication in **Oncotarget**

III. **Lina S. Schneider**, Melanie Ulrich, Thorsten Lehr, Dirk Menche, Rolf Müller, Angelika M. Vollmar and Karin von Schwarzenberg
MDM2 antagonist nutlin-3a sensitizes tumors to V-ATPase inhibition
Submitted

IV. **Lina S. Schneider***, Christian Grimm*, Yu-Kai Chao, Anna Watermann, Melanie Ulrich, Doris Mayr, Christian Wahl-Schott, Martin Biel* and Angelika M. Vollmar*
Two-pore channel function is crucial for migration of invasive cancer cells
*These authors contributed equally to this work
Submitted

Therapeutics, Targets, and Chemical Biology

Cancer Research

Vacuolar-ATPase Inhibition Blocks Iron Metabolism to Mediate Therapeutic Effects in Breast Cancer

Lina S. Schneider[1], Karin von Schwarzenberg[1], Thorsten Lehr[2], Melanie Ulrich[1], Rebekka Kubisch-Dohmen[1], Johanna Liebl[1], Dirk Trauner[3], Dirk Menche[4], and Angelika M. Vollmar[1]

Abstract

Generalized strategies to improve breast cancer treatment remain of interest to develop. In this study, we offer preclinical evidence of an important metabolic mechanism underlying the antitumor activity of inhibitors of the vacuolar-type ATPase (V-ATPase), a heteromultimeric proton pump. Specifically, our investigations in the 4T1 model of metastatic breast cancer of the V-ATPase inhibitor archazolid suggested that its ability to trigger metabolic stress and apoptosis associated with tumor growth inhibition related to an interference with hypoxia-inducible factor-1α signaling pathways and iron metabolism. As a consequence of disturbed iron metabolism, archazolid caused S-phase arrest, double-stranded DNA breaks, and p53 stabilization, leading to apoptosis. Our findings link V-ATPase to cell-cycle progression and DNA synthesis in cancer cells, and highlight the basis for the clinical exploration of V-ATPase as a potentially generalizable therapy for breast cancer. *Cancer Res; 75(14); 2863–74. ©2015 AACR.*

Introduction

Breast cancer is a major health issue, which worldwide causes almost 500,000 female fatalities each year, being the most lethal cancer for women (1). Therefore. it is of utmost importance to find new therapeutics to combat this disease. Nature is still one of the most essential sources for new chemotherapeutics, as approximately 60% of the new agents discovered in the last decades were classified as naturally derived or inspired (2). The myxobacterial macrolide archazolid, which was first isolated from *Archangium gephyra* (3), is a highly potent vacuolar-type-ATPase (V-ATPase) inhibitor (4). It showed first promising cytotoxic effects on diverse cancer cells lines (5, 6) proposing pharmacologic V-ATPase inhibition as a new strategy to abrogate solid tumor growth. However, the precise mode of action is not defined yet.

V-ATPases are proton pumps located in the endomembrane system of eukaryotic cells as well as in the plasma membrane. They are heteromultimeric enzymes consisting of two functional domains: the cytosolic hydrolytic active V_1 domain and the membrane integral V_0 complex, which is responsible for proton translocation. V-ATPases actively transport protons from the cytoplasm into intracellular compartments or across the outer membrane. As a consequence of the acidification of endosomes and lysosomes, V-ATPases play a crucial role in the receptor-mediated endocytosis and the endosomal trafficking (7). Besides a variety of transporter and channel proteins, plasma membrane localized V-ATPase is reported to modulate the tumor microenvironment (7, 8). V-ATPase function can be inhibited by the myxobacterial compound archazolid, which binds to subunit c of the membrane integral V_0 domain (4).

Our earlier studies revealed a strong cytostatic effect of archazolid on diverse cancer cell lines *in vitro* and showed an induction of cellular stress response involving the stabilization of the hypoxia-inducible factor 1 α (HIF1α) protein (6). Yet, it stayed unclear how inhibition of V-ATPase generates HIF1α stabilization. The aim of this study was now to illuminate this matter and to extend the *in vitro* data for *in vivo* efficacy. Thereby, we uncover that V-ATPase inhibition impedes the iron metabolism of cancer cells, which opens up new therapeutic options for V-ATPase inhibitors.

This work unveils that the natural derived V-ATPase inhibitor archazolid disrupts endocytotic transferrin receptor (TfR) recycling, leading to iron depletion in the cytosol followed by stabilization of the HIF1α protein and reduction of ribonucleotide reductase (RNR) activity. Finally, this leads to induction of apoptosis *in vitro* and reduction of tumor growth *in vivo*. These results suggest V-ATPase as a highly promising target for breast cancer treatment at the interplay of iron metabolism and apoptotic processes.

Materials and Methods

Cell lines and reagents

The mammary cancer cell lines MDA-MB-231 cells were recently purchased from Cell Line Service Eppelheim, MCF7 from DSMZ, and 4T1-Luc (4T1) from PerkinElmer. MCF7 cells were grown in RPMI-1640 supplemented with 10% FCS, 1% pyruvate,

[1]Department of Pharmacy, Pharmaceutical Biology, Ludwig-Maximilians-University of Munich, Munich, Germany. [2]Clinical Pharmacy, Saarland University, Saarbrücken, Germany. [3]Department of Chemistry, Ludwig-Maximilians-University of Munich, Munich, Germany. [4]Kekulé Institute of Organic Chemistry and Biochemistry, University of Bonn, Bonn, Germany.

Note: Supplementary data for this article are available at Cancer Research Online (http://cancerres.aacrjournals.org/).

Corresponding Author: Angelika M. Vollmar, Department of Pharmacy, Ludwig-Maximilians-University of Munich, Butenandtstraße 5-13, 81377 Munich, Germany. Phone: 49-89-2180-77172; Fax: 49-89-2180-77170; E-mail: angelika.vollmar@cup.uni-muenchen.de

doi: 10.1158/0008-5472.CAN-14-2097

1% nonessential amino acids, and 125 μg/L insulin. MDA-MB-231 cells were cultured in DMEM High Glucose containing 10% FCS and 4T1 cells in RPMI-1640 with 10% FCS. Archazolid was synthesized by Prof. Dirk Trauner (Department of Chemistry, Ludwig-Maximilians-University of Munich, Munich, Germany) and isolated from Prof. Dirk Menche (Institute of Organic Chemistry, University of Bonn, Bonn, Germany), QVD was purchased from R&D Systems, ferric citrate, deferoxamine, 3-aminopyridine-2-carboxaldehyde thiosemicarbazone (3-AP), doxorubicin, pifithrin-α from Sigma Aldrich, and KU55933 from Santa Cruz Biotechnology.

In vivo mouse model

Sixteen female BALB/cByJRj mice (Janvier) were locally shaved and 2×10^6 4T1 cells were injected subcutaneously into the flank of each mouse. Mice were divided into two groups and treated intravenously with 0.3 mg/kg archazolid in 5% DMSO/10% solutol/PBS or equal amounts of 5% DMSO/10% solutol/PBS. Mice were treated three times a week. Measurement of tumors was done every 2 to 3 days with a caliper, using the formula $a \times b^2/2$. The average tumor volumes of the two groups were compared over time. Tumor volume was modeled using a sequential exponential-linear growth model. IHC analysis of tumor tissue sections was performed as described previously (9) using anti-active-caspase-3-antibody and Hoechst from Sigma. Modeling was performed using the non-linear mixed effects modeling technique with the software NONMEM 7.3 (10). Animal experiments were approved by the District Government of Upper Bavaria in accordance with the German animal welfare and institutional guidelines.

Western blot analysis

Protein lysis was performed as described before (6). Antibodies given below were used: HIF1α (Becton Dickinson), Hexokinase II, PARP-1, γH2AX, p53, CREB (Cell Signaling Technology), ATP6V0C (Novus), β-actin (Millipore), HRP-goat-antirabbit (Bio-Rad), HRP-goat-antimouse (Santa Cruz Biotechnology), and AlexaFluor 680-goat-antirabbit (Invitrogen).

Cell transfection

For silencing experiments, 2×10^6 cells were transfected using the Amaxa Nucleofector kit V (Lonza) program A-23. HIF1α and ATP6V0C were silenced using ON-TARGETPlus SMARTpool siRNA (2 μg) from Dharmacon and nontargeting siRNA as a control.

Oxygen consumption assay

Oxygen consumption was analyzed with the MitoXpress-Xtra-HS Kit (Luxcel Biosciences). A total of 8×10^6 MCF7 cells were used. Phosphorescence signal was measured according to the manufacturer's instructions with SpectraFluor Plus reader (Tecan).

Measurement of metabolic activity

CellTiter-Blue Assay (Promega) was used according to the manufacturer's instructions to measure metabolic activity.

Measurement of intracellular iron levels

For analysis of intracellular iron levels, cells were stained with 10 nmol/L calcein-AM (Santa Cruz Biotechnology) for 15 minutes. Fluorescence intensity was determined with FACSCalibur (Becton). In addition, treated cells seeded on μ-slides 8-well ibidiTreat (IBIDI) were stained with 10 nmol/L calcein-AM for 15 minutes and analyzed by confocal microscopy.

TfR internalization assay

Cells seeded on μ-slides 8-well ibidiTreat were starved for 2 hours. Subsequently, cells were incubated with transferrin (Tf) -rhodamine conjugate (Invitrogen) for 15 minutes at 37°C and fixed with 4% paraformaldehyde for 20 minutes. Cells were mounted with PermaFluor mounting medium (Beckman Coulter) and analyzed with a Zeiss LSM 510 Meta confocal microscope (Jena).

Mammospheres

MCF7 spheroids were grown using the hanging drop protocol as described before (11).

Measurement of cell death and cell cycle

Cells were considered as dead when cell membrane was permeable for propidium iodide (PI; Sigma Aldrich). Trypsinized and washed cells were resuspended in PBS containing 5 μg/mL PI and analyzed by flow cytometry. Cells with higher fluorescence intensities compared with control were examined as dead. To quantify percentage of cells with sub-G_1 DNA content, cell pellet was resuspended in hypotonic-fluorochrome solution containing 0.1%Triton X-100 and 50 μg/mL PI. Cells appearing left of G_1 -peak were considered as apoptotic. In some experiments, cell cycle was analyzed with FlowJo 7.6.

Clonogenic assay

Clonogenic assay was performed as described previously (6).

Measurement of dCTP levels

dCTP levels were measured as described previously (12). Therefore, 3×10^6 cells were seeded on 10-cm culture dishes, allowed to grow over night and treated for 24 hours.

qRT-PCR analysis

Total RNA was extracted using the RNeasy mini Kit (Qiagen GmbH) according to the manufacturer's instructions. For cDNA synthesis, the High Capacity cDNA Rerverse Transcription Kit (Applied Biosystems) was used. qRT-PCR was performed with the AB 7300 RealTime PCR system, the TaqMan Gene Expression Master Mix (Applied Biosystems) and the SYBR Green PCR Master Mix (Applied Biosystems) according to the manufacturer's instructions. All designed primers were purchased from Metabion. ATP6V0C primers were purchased from Applied Biosystems.

Nuclei extraction

Stimulated MCF7 cells were trypsinized. Cell pellet was resuspended in nuclear extraction buffer A (10 mmol/L HEPES, pH 7.9, 10 mmol/L KCl, 0.1 mmol/L EDTA, 0.1 mmol/L EGTA, 1 mmol/L DTT, 0.5 mmol/L PMSF, 1 mmol/L Complete EDTAfree; Roche) and incubated on ice for 15 minutes. Nonidet P-40 (0.625%) was added, probes were vortex and centrifuged. Pellet was resuspended in nuclear extraction buffer B (20 mmol/L HEPES, pH 7.9, 0.4 mmol/L NaCl, 0.1 mmol/L EDTA, 0.1 mmol/L EGTA, 1 mmol/L DTT, 0.5 mmol/L PMSF, 25% glycerol, 1 mmol/L Complete EDTAfree). After 15-minute incubation on ice and centrifugation, supernatants were used for Western blot analysis.

Statistical analysis

GraphPad Prism Software was used for all statistical analysis. Error bars indicate SEM. Synergism was calculated with the Bliss formula: $\nu = x_{\text{combination}}/((x_A - x_B) - (x_A \times x_B))$, with $\nu > 1$ indicating synergism (13).

Results

Archazolid abrogates tumor growth *in vivo* and induces HIF1α stabilization *in vitro*

To start with, archazolid was confirmed to induce cell death in breast cancer cell lines MDA-MB-231 and MCF-7 as well as in mouse 4T1 cells (Supplementary Fig. S1). These results were extended by an *in vivo* model based on the 4T1 mouse mammary tumor cell line to assess therapeutic relevance of V-ATPase inhibition. In fact, archazolid reduced the tumor growth rate significantly with an average reduction of 24.4%, while the mean mouse weight did not differ (Fig. 1A). Tumor tissues of archazolid-treated mice showed induced caspase-3 activity (Fig. 1B).

To explore the molecular mechanism of archazolid-induced cell death, the HIF1α protein came into focus. We confirmed a strong HIF1α expression after 24 hours of archazolid treatment in MCF7 and MDA-MB-231 breast cancer cell lines (Fig. 1C). Importantly, silencing of ATP6V0C, the subunit c of V-ATPase, by siRNA resulted in stabilization of HIF1α in both cell lines after 72 hours (Fig. 1C), suggesting a V-ATPase–dependent effect. Silencing efficiency is shown in Supplementary Fig. S2 both on the mRNA and protein level. In addition to the expression status of the HIF1α protein, we analyzed the mRNA levels via qPCR analysis in MDA-MB-231 cells after 24 hours of treatment, which showed no significant changes (Supplementary Fig. S3), indicating an effect on stabilization of HIF1α by archazolid.

As HIF1α has many target genes involved in glycolysis, we investigated the impact of archazolid on glycolysis and oxidative phosphorylation. Western blot analysis after 24 hours of archazolid treatment showed induced hexokinase II protein levels in breast cancer cell lines (Fig. 1D) as well as other glycolytic gene products [6-phosphofructo-2-kinase/fructose-2, 6-bisphosphatase-3 (6PF2K3), aldolase C, Supplementary Fig. S4]. Moreover, measurement of oxygen consumption demonstrated a reduction in MCF7 cells after 4 hours of archazolid treatment compared with control cells (Fig. 1E). Oligomycin served as a positive control. Interestingly, the ratio of metabolic activity of MCF7 cells grown in medium with glucose to cells cultivated with galactose increases after 48 hours of archazolid treatment further implicating a shift to glycolysis (Fig. 1F). Galactose forces the cells to derive their energy by oxidative phosphorylation. Hence, an increased ratio of metabolic activity in glucose to galactose medium implicates a mitochondrial impairment.

Iron depletion leads to HIF1α stabilization

To unveil how V-ATPase is implicated in HIF1α stabilization, it is important to know that the hydroxylation of HIF1α by prolyl hydroxylases (PHD) requires oxygen, 2-oxoglutarate and iron. To examine whether a lack of iron is responsible for the stabilization of HIF1α after V-ATPase inhibition, cell culture medium was supplemented with iron citrate. Indeed, Western blot analysis of breast cancer cells after 24 hours of treatment showed a complete abolishment of archazolid-induced HIF1α stabilization in the presence of additional iron (Fig. 2A). Hence, expression of HIF1α is due to iron depletion in the cell.

Disruption of TfR recycling leads to iron depletion

To verify iron deprivation in the cytosol through V-ATPase inhibition, confocal microscopy analysis was performed using the fluorescence dye calcein-AM. Of note, in MDA-MB-231 cells, the fluorescence intensity increased after 24 hours of high-dose archazolid treatment and could be compensated by adding iron citrate to the medium (Fig. 2B). Flow-cytometric analysis in calcein-AM–stained breast cancer cell lines after 24-hour treatment confirmed these findings (Fig. 2C). Interestingly, mRNA level of ferritin, a protein serving as an iron storage in the cell as well as mRNA of transferrin and RRM2 were increased in MCF7 after 24 hours of archazolid treatment and could be abolished by iron (Supplementary Fig. S5). To further investigate the underlying mechanisms that lead to a lack of cellular iron by V-ATPase inhibition, internalization of TfR was analyzed. TfR binds Tf-bound iron and is taken up by endocytosis. Tf-rhodamine conjugate was added and cells were analyzed by confocal microscopy. Noteworthy, after 24 hours of archazolid treatment recycling of Tf/TfR was disrupted in breast cancer cells (Fig. 2D).

Iron depletion is responsible for archazolid-induced cell death

Next, we investigated whether iron depletion is responsible for archazolid-induced cell death. Interestingly, flow-cytometric analysis of MCF7 and MDA-MB-231 cells after 48 hours of archazolid treatment showed a reduction of PI-positive cells when iron citrate was added (Fig. 3A). In addition, 4T1 cells showed rescue of metabolic activity in medium with iron excess (Supplementary Fig. S6). PARP-1 cleavage was abolished in human breast cancer cell lines after 48 hours by adding iron (Fig. 3B). Along this line, we could see a synergistic cell death induction in MCF7 cells after 48 hours by combining archazolid with the iron chelators deferoxamine and 3-AP (Fig. 3C). In MDA-MB-231 cells, combination of archazolid and 3-AP led to reduced formation of colonies after 24 hours of treatment (Fig. 3D). We could verify these findings in three-dimensional growing MCF7 mammospheres after 48 hours of treatment by PI staining (Fig. 4A and B) and CTB assay (Fig. 4C).

Iron depletion leads to dysfunction of RNR

To more deeply analyze the consequences of archazolid-induced iron depletion, we took a closer look at the iron-dependent target RNR. The formation of deoxyribonucleotides (dNTP) in a cell is iron dependent and catalyzed by RNR (14). For analyzing RNR activity, dCTP levels were measured as described previously (12). Interestingly, treatment of MCF7 and MDA-MB-231 cells with archazolid for 24 hours resulted in reduced dCTP levels in both cells lines (Fig. 5A). As dNTPs are needed for DNA synthesis, cell-cycle analysis was examined in MDA-MB-231 cells 48 hours after archazolid treatment, showing S-phase block, which could be rescued by adding iron (Fig. 5B). Phosphorylation of the H2AX histone (γH2AX), indicating double-strand breaks (DSB), was seen after 48 hours of archazolid treatment in all three cell lines, further suggesting a reduced RNR activity after archazolid treatment. Again, these effects were abolished by additional iron (Fig. 5C and Supplementary Fig. S7). Combination of the DNA intercalating drug doxorubicin with archazolid showed reduced formation of colonies in MDA-MB-231 cells (Fig. 5D). These findings connect V-ATPase inhibition to fundamental cellular processes such as DNA synthesis and DNA repair.

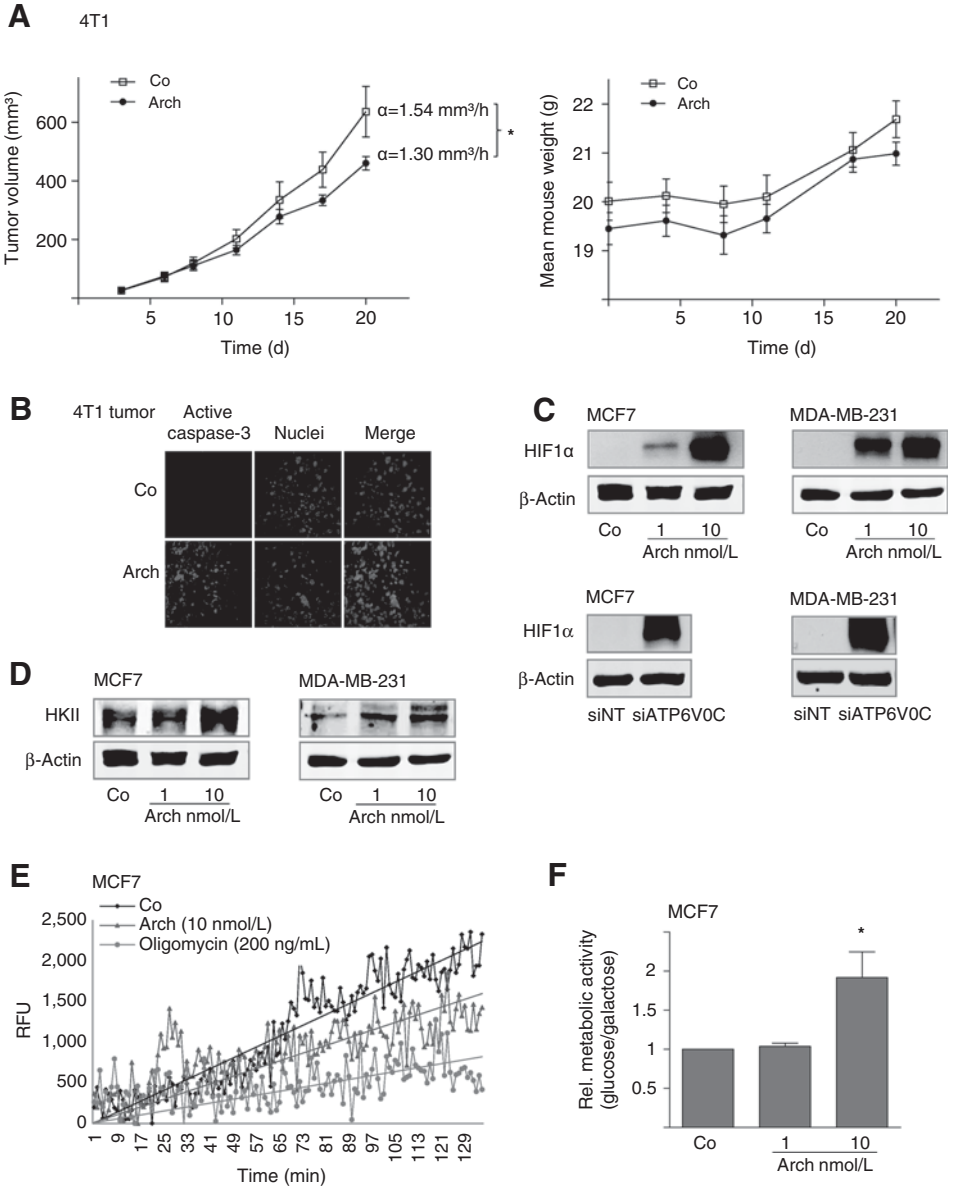

Figure 1.
Archazolid inhibits tumor growth *in vivo* and stabilizes HIF1α *in vitro*. A, 4T1 tumor cells were subcutaneously injected into the flanks of 16 Balb/cByJRj mice. Mice were divided in two groups and treated three times a week intravenously with archazolid or equal amounts of solvent. Growth rate α of tumors is indicated (Co, $\alpha = 1.54$ mm^3/hour vs. archazolid, $\alpha = 1.30$ mm^3/hour), *, $P = 0.0165$. B, paraffin sections of tumors were stained for active caspase-3 and nuclei. Representative images of control and archazolid-treated mice are shown. C, HIF1α expression was detected by Western blot analysis upon archazolid treatment (24 hours) and downregulation of ATP6V0C (72 hours) in MCF7 cells and MDA-MB-231 cells. D, expression of hexokinase II was analyzed by Western blot analysis in MCF7 cells and MDA-MB-231 cells after 24 hours of archazolid treatment. E, oxygen consumption was measured with the MitoXpress probe kit in MCF7 cells after 24 hours of archazolid treatment. C–E, representative experiments out of three independent experiments are shown. F, metabolic activity of MCF7 cells treated with archazolid (24 hours) was assessed with CTB assay. Ratio of metabolic activity of cells grown in normal medium and cells seeded in galactose medium was calculated. Bars are the SEM of three independent experiments performed in triplicates; *, $P < 0.05$ (one-way ANOVA, Newman–Keuls multiple comparison test).

p53 is implicated in archazolid-induced cell death in p53 wild-type MCF7 cells

As the HIF1α protein and the occurrence of DSB are known inducers of the p53 protein, we analyzed its implication in archazolid-induced cell death in p53 wild-type MCF7 cells. Figure 6A shows elevated p53 mRNA levels after 24 hours of V-ATPase inhibition, which was compensated by additional iron. Along this line, archazolid-treated MCF7 cells indicate higher p53 protein levels after 48 hours within the nucleus (Fig. 6B). Silencing HIF1α in MCF7 cells reduced the induction of p53 protein levels (Fig. 6C) revealing an impact of HIF1α on p53 expression in this context. The ataxia telangiectasia mutated (ATM) kinase mediates the induction of p53 upon DSB. To unveil whether in addition the presence of DSB elevates p53 protein levels, we used the ATM inhibitor KU55933. Western blot analysis after 48 hours of archazolid treatment in MCF7 cells indicates that this is the case (Fig. 6D). Finally, to prove that p53 plays a role in archazolid induced cell death, we used the p53 inhibitor pifithrin-α. Flow-cytometric analysis of MCF7 cells after 48 hours shows a significant reduction of cell death in the presence of pifithrin-α (Fig. 6E) providing evidence that p53 is involved in V-ATPase–dependent cell death.

To sum up in a cartoon, Fig. 7 illustrates that V-ATPase inhibition by archazolid leads to cell death induction, which is mediated by iron depletion, resulting in the stabilization of the HIF1α protein and the inhibition of RNR together leading to p53 induction.

Discussion

Our data suggest V-ATPase as a highly interesting and druggable target to abrogate solid breast tumors by interfering with the iron homeostasis of cancer cells.

Since the first advent of V-ATPase inhibitors, evidence is increasing that V-ATPases are implicated in cancer. Reports show that

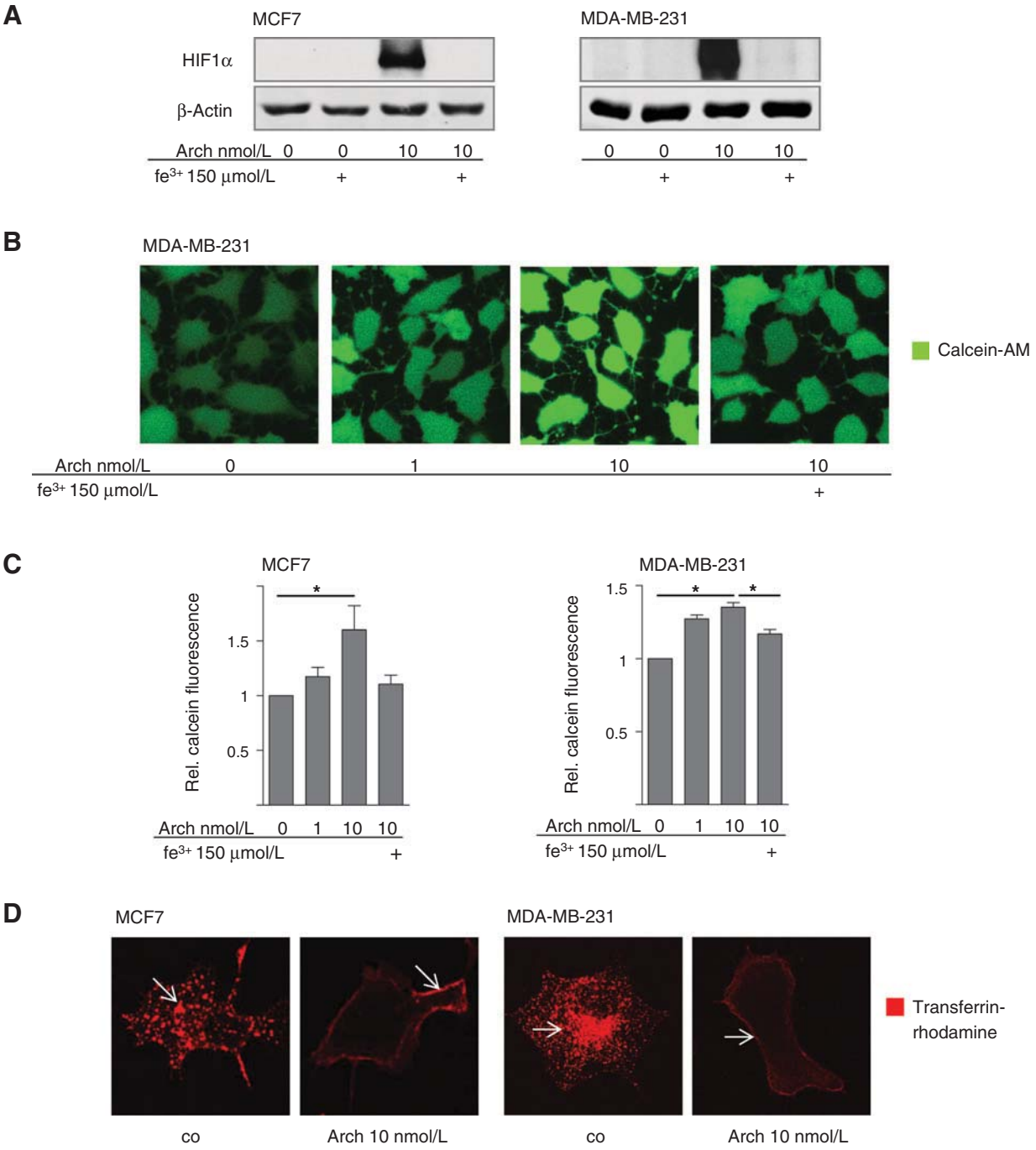

Figure 2.
Archazolid affects Tf/TfR internalization and induces iron depletion. A, HIF1α expression was detected by Western blot analysis upon archazolid and iron citrate treatment (24 hours). B, archazolid-treated MDA-MB-231 cells (24 h) were incubated with calcein-AM for 30 minutes and analyzed by confocal microscopy. C, calcein-AM–stained MCF7 and MDA-MB-231 cells were analyzed by flow cytometry after 24 hours of archazolid and iron citrate treatment. Bars are the SEM of three independent experiments performed in triplicates; *, $P < 0.05$ (one-way ANOVA, Newman–Keuls multiple comparison test). D, MCF7 and MDA-MB-231 cells were incubated with Tf-rhodamine conjugate after 24 hours of archazolid treatment. Cells were analyzed by confocal microscopy. A, B, and D, representative experiments out of three independent experiments are shown.

V-ATPase is overexpressed in invasive pancreatic tumors (15) and that the mass of V-ATPases located at the plasma membrane of breast cancer cells correlates with their invasiveness (16). Among various other transporter proteins such as monocarboxylate transporter (MTC), Na^+/H^+ exchanger (NHE1), carbonic anhydrase IX (CAIX) plasma membrane located V-ATPase contribute to dysregulated pH in the tumor microenvironment favoring tumor progression and metastasis (8, 17). Moreover, overexpression of

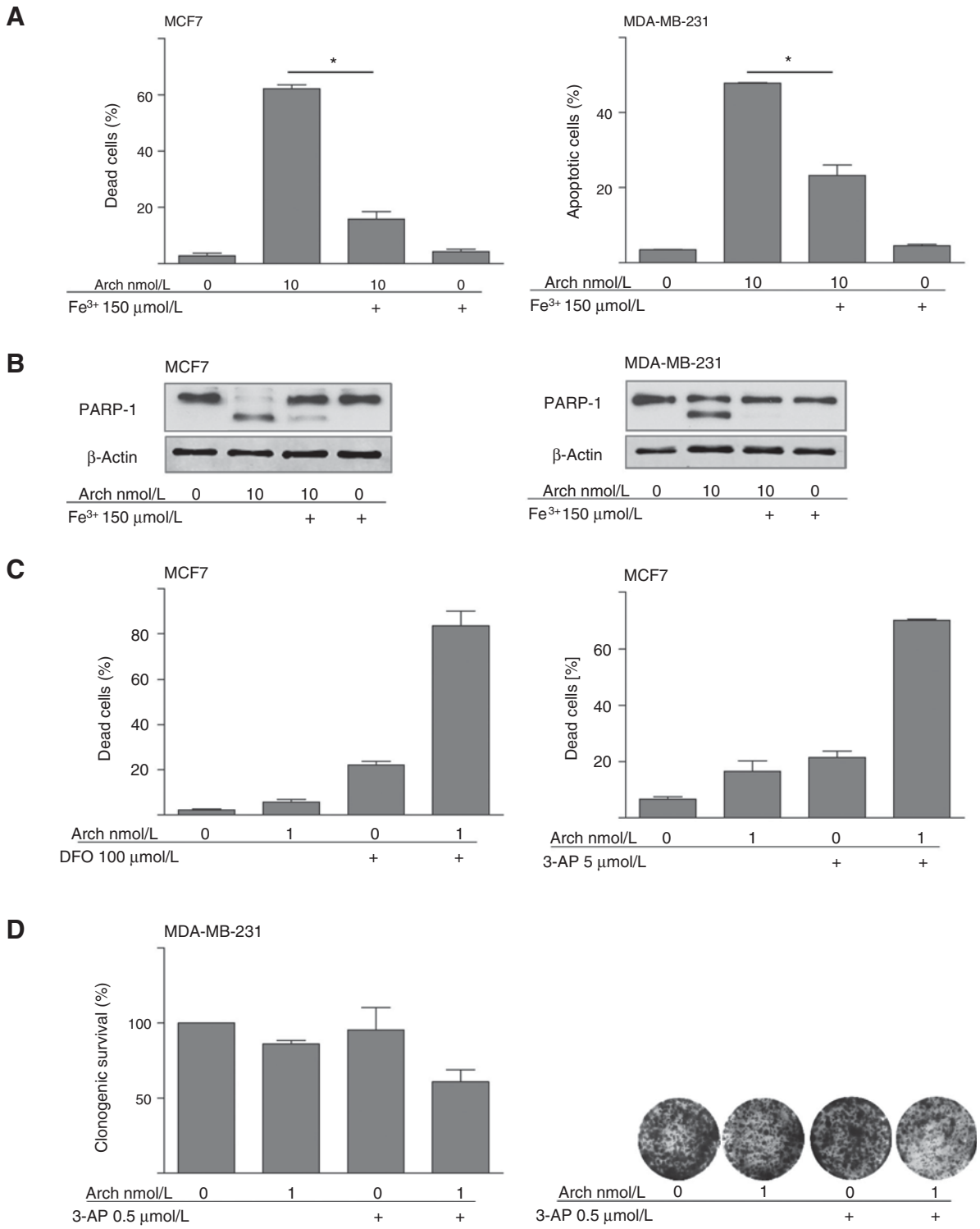

Figure 3.
Induced iron deprivation leads to archazolid-induced cell death. A and C, cell death induction after archazolid, iron citrate, deferoxamine (DFO), and 3-AP treatment (48 hours in MCF7 cells and 72 hours in MDA-MB-231 cells) was assessed by flow cytometry. Bars are the SEM of three independent experiments performed in triplicates, *, $P < 0.05$ (one-way ANOVA, Newman–Keuls multiple comparison test). C, synergism was calculated with the Bliss formula (value for deferoxamine, 3; value for 3-AP, 1,93). B, PARP-1 cleavage was detected by Western blot analysis upon archazolid and iron citrate treatment (MCF7 cells, 48 hours; MDA-MB-231, 72 hours). One representative blot out of three independent experiments is shown. D, clonogenic survival after 20 hours of archazolid and 3-AP treatment (4 hours archazolid pretreatment) was analyzed by crystal violet staining. Absorption of resolved crystal violet was measured with SpectraFluor Plus reader. Bars are the SEM of three independent experiments performed in triplicates. Synergism was calculated with the Bliss formula (value: 2,05)

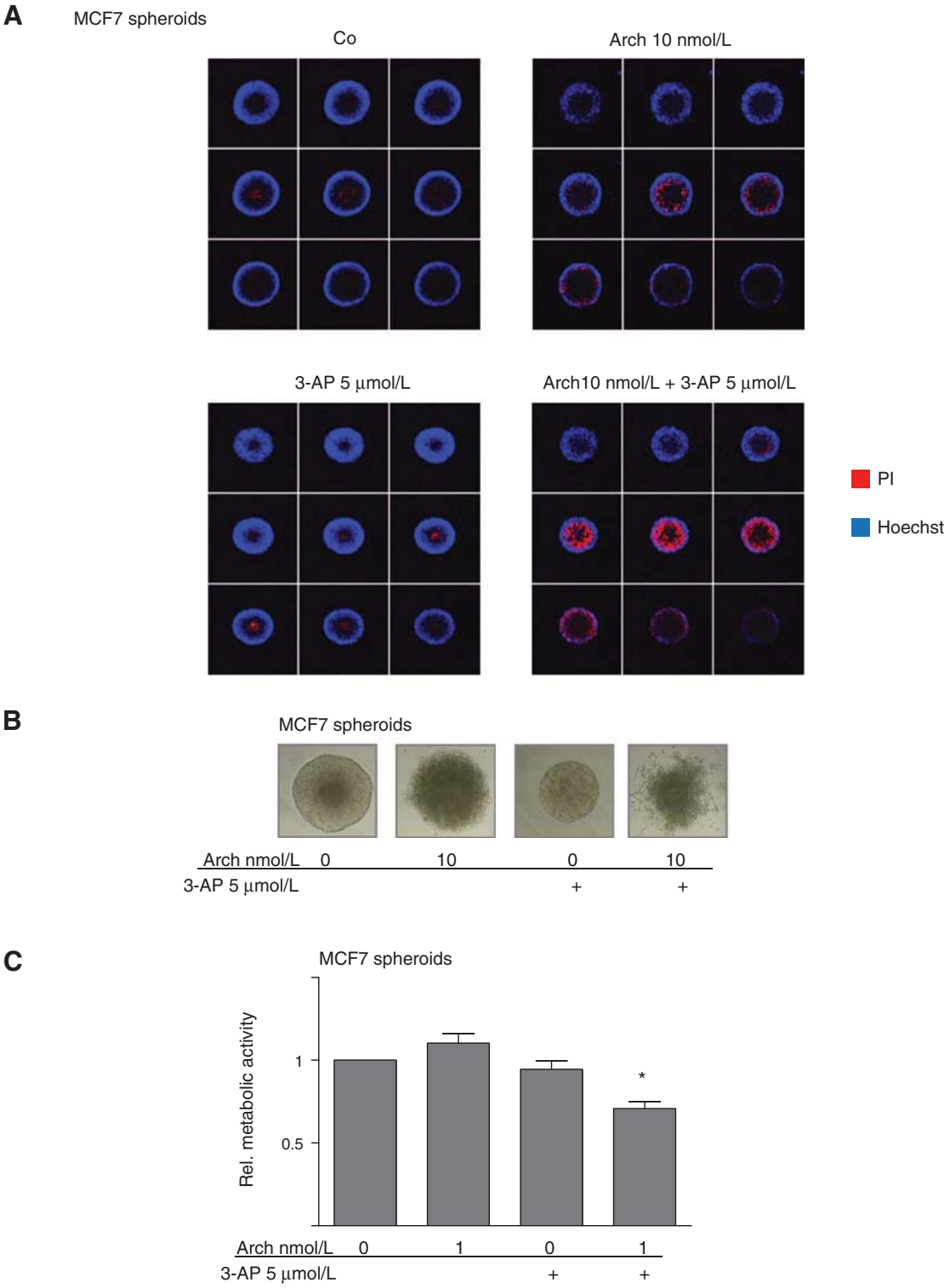

Figure 4.
Combination of archazolid and 3-AP induces synergistic cell death in mammospheres. A, MCF7 mammospheres were treated with archazolid for 48 hours, stained with PI and Hoechst, and analyzed by confocal microscopy. B, MCF7 mammospheres seeded in Poly-HEMA plates were incubated with archazolid and 3-AP for 48 hours. A and B, representative experiments out of three independent experiments are shown. C, metabolic activity of MCF7 mammospheres after archazolid and 3-AP treatment was assessed by CTB assay. Bars are the SEM of three independent experiments performed in triplicates. *, $P < 0.05$ (one-way ANOVA, Newman–Keuls multiple comparison test).

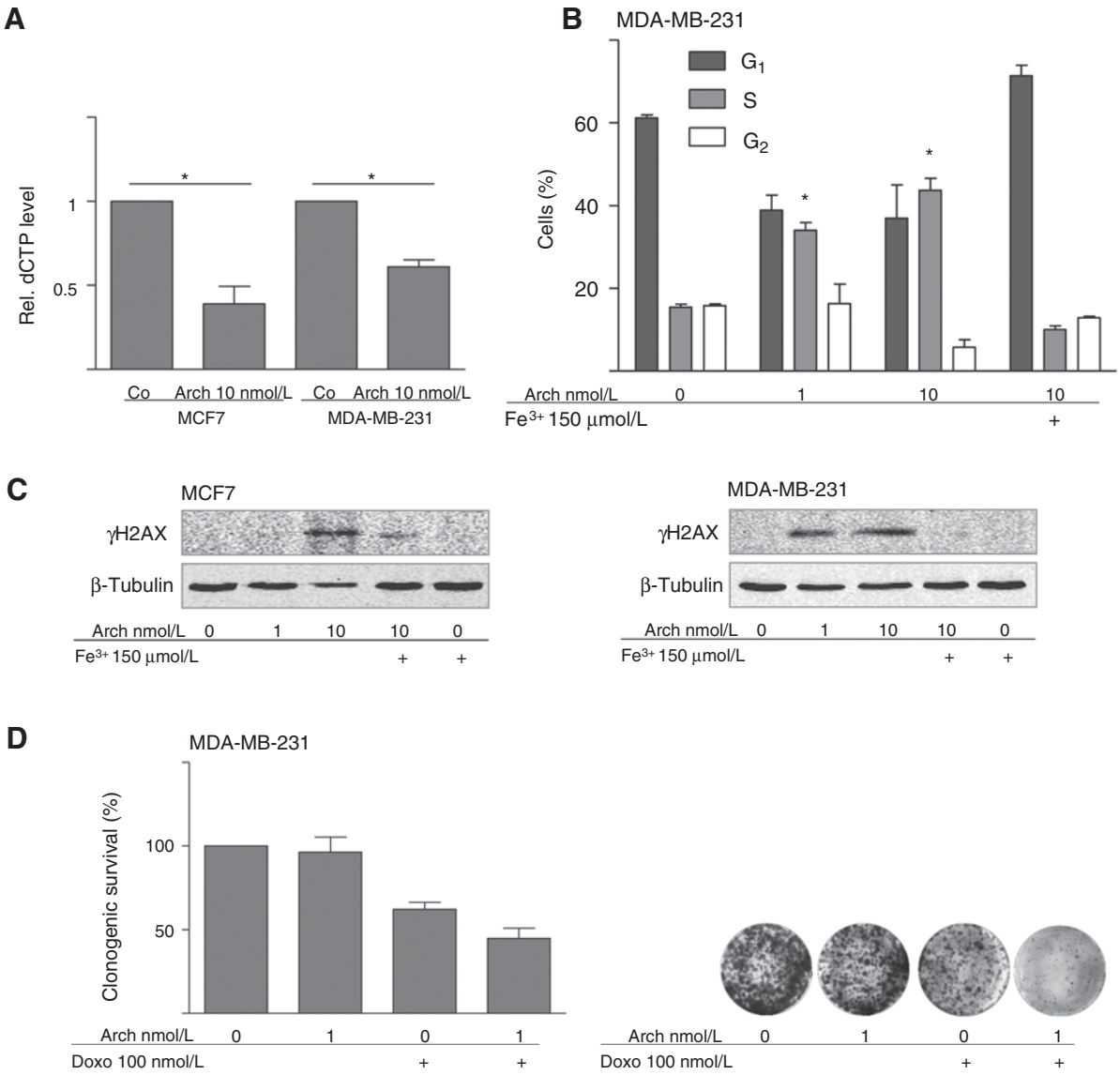

Figure 5.
Archazolid reduces RNR activity. A, relative dCTP amounts after archazolid treatment (24 hours) were detected with the AB 7300 RealTime PCR system in MCF7 and MDA-MB-231 cells. B, cell-cycle was analyzed by flow cytometry in MDA-MB-231 cells after 48 hours of archazolid and iron citrate stimulation. A and B, bars are the SEM of A two B three independent experiments performed in triplicates; *, $P < 0.05$ (one-way ANOVA, Newman–Keuls multiple comparison test). C, expression of phosphorylated H2AX was detected by Western blot in MCF7 and MDA-MB-231 cells after 48 hours of archazolid and iron citrate treatment. One representative blot out of three independent experiments is shown. D, clonogenic survival after 20 hours of archazolid and doxorubicin treatment (4 hours archazolid pretreatment) was analyzed by crystal violet staining. Absorption of resolved crystal violet was measured with SpectraFluor Plus reader. Bars are the SEM of three independent experiments performed in triplicates. Synergism was calculated with the Bliss formula (value: 1,38)

subunit c of V-ATPase in *Drosophila* induces a tumor-like tissue transformation (18). Nontumor cells showed less cytotoxic sensitivity toward V-ATPase inhibition compared with breast carcinoma cells and hepatoblastoma cells (6, 19). It has been shown that V-ATPase inhibition abrogates tumor cell migration and dissemination through disturbed endocytotic activation of Rac1 (20). Furthermore, cell death induction was observed in various cancer cell lines by bafilomycin, a V-ATPase inhibitor from the first family (21–23). Consistently, we did find induced apoptosis in breast cancer cells through archazolid treatment. Here, we could show for the first time that V-ATPase inhibition by archazolid reduced the growth rate of 4T1 mammary tumors significantly *in vivo*, indicating therapeutic relevance of V-ATPase inhibition.

Although cell death induction through V-ATPase inhibition was extensively studied, the precise causal mechanisms are still not well understood. Wu and coworkers attributed the induction of apoptosis in colon cancer by bafilomycin to the inhibition of macroautophagy (21). Others suggested a mechanism in which proteases are released after lysosomal dysfunction, leading to caspase-3 activation (22). Our group postulated a mechanism that involves the induction of a cellular stress response, including

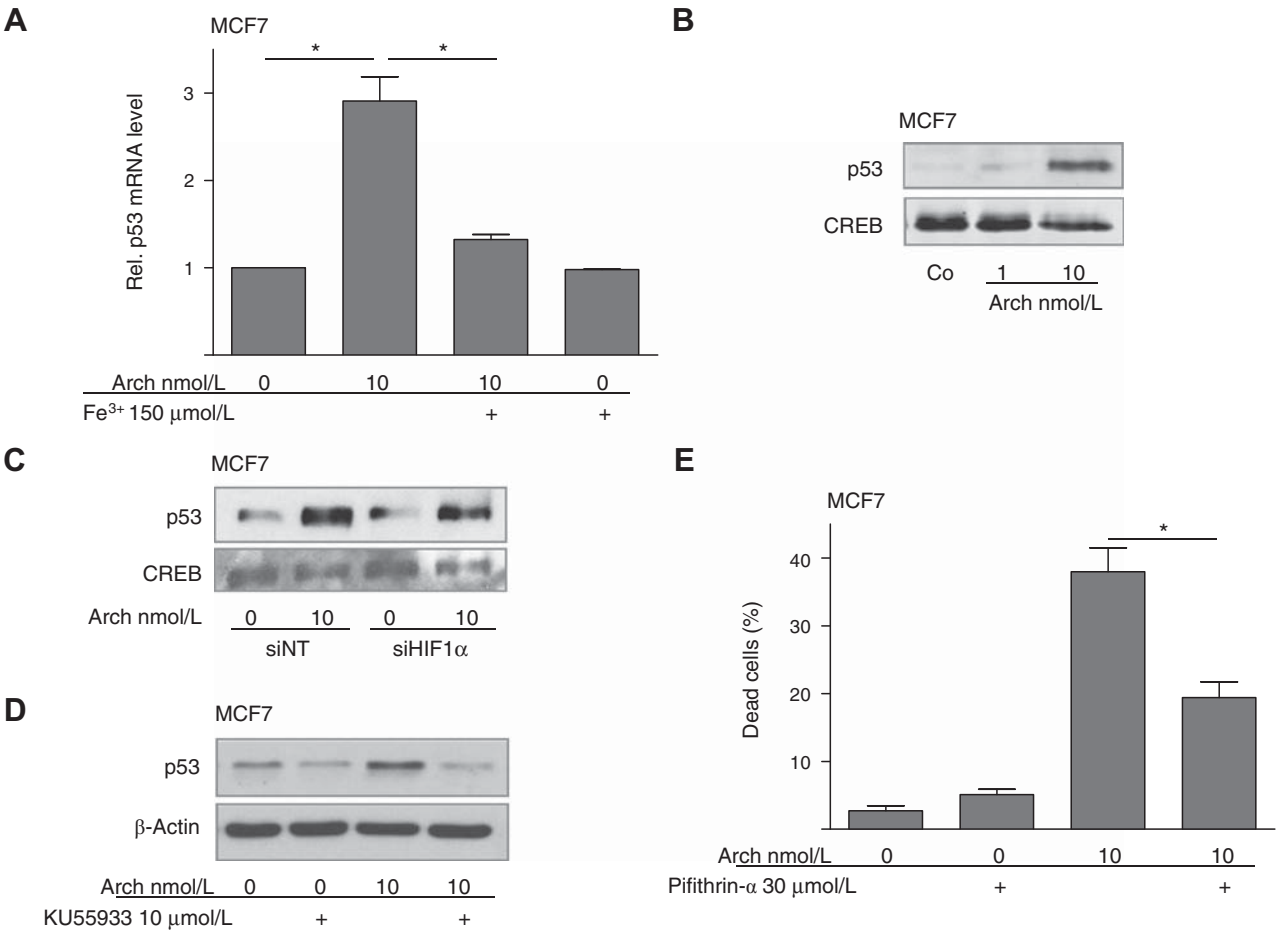

Figure 6.
Implication of p53 in archazolid induced cell death. A, SYBR Green qRT-PCR analysis was performed to assess p53 mRNA levels in archazolid-treated (24 hours) MCF7 cells. B and C, expression of p53 in nuclei was analyzed by Western blot analysis in MCF7 cells after 48 hours of archazolid treatment C upon HIF1α silencing. CREB served as a loading control. D, expression of p53 was analyzed by Western blot analysis in MCF7 cells after 48 hours of archazolid and KU55933 treatment. E, cell death was assessed by flow cytometry analysis in archazolid and pifithrin-α–treated MCF7 cells after 48 hours. A and E, bars are the SEM of three independent experiments performed in triplicates; *, $P < 0.05$ (one-way ANOVA, Newman–Keuls multiple comparison test). B–D, one representative blot out of three independent experiments is shown.

autophagy and the stabilization of HIF1α (6). This study here ties in with our earlier work and reveals a role for V-ATPase at the interplay of iron metabolism and apoptotic processes. Our findings illuminate that the cytotoxicity of V-ATPase inhibitors is mainly due to disturbed TfR recycling, which impairs the iron supply of cancer cells. As a consequence, the activity of iron-dependent enzymes is reduced, leading to DSB, S-phase arrest, and induction of p53.

In the last decades, it became more and more evident that iron is implicated in cancer development. Induction of malignant tumors by injecting iron dextran into rat was first reported in 1959 (24). This was confirmed later by the observation that patients injected with iron preparations developed sarcomas (25). Consistently, epidemiologic reports from the 1980s associated high body iron with the risk of cancer (26). The iron supply of cancer cells is mainly mediated by the TfR. The clearly defined function of the TfR is the interaction with the iron loaded plasma glycoprotein Tf initiating its endocytotic up take (27). Since it has been reported that TfR is overexpressed in cancer cells (28, 29), targeted therapy became an attractive strategy for cancer treatment. In different studies, antibodies against TfR have successfully been used to abrogate tumor progression (30, 31). Others used toxic moieties conjugated to Tf to selectively target cancer cells (32). After internalization of Tf/TfR, iron dissociates from the receptor-ligand complex and enters the cytosol forming the labile iron pool whereas the complex gets recycled to the cell surface. Essential for the dissociation is the acid pH in the endosomes (33), which is maintained by V-ATPases. It is known that an inadequate acidification of endosomes inhibits trafficking out of them although precise mechanisms are not defined yet (34). Consistently, a role for V-ATPase in the internalization or processing of receptors has been shown such as for Notch (35, 36). Our present study in breast cancer cells shows impaired TfR internalization after archazolid treatment and connects this with disturbed iron metabolic pathways. The generated iron deprivation eventually induces apoptotic processes, leading to cell death. Therefore, we suggest inhibition of V-ATPase as a

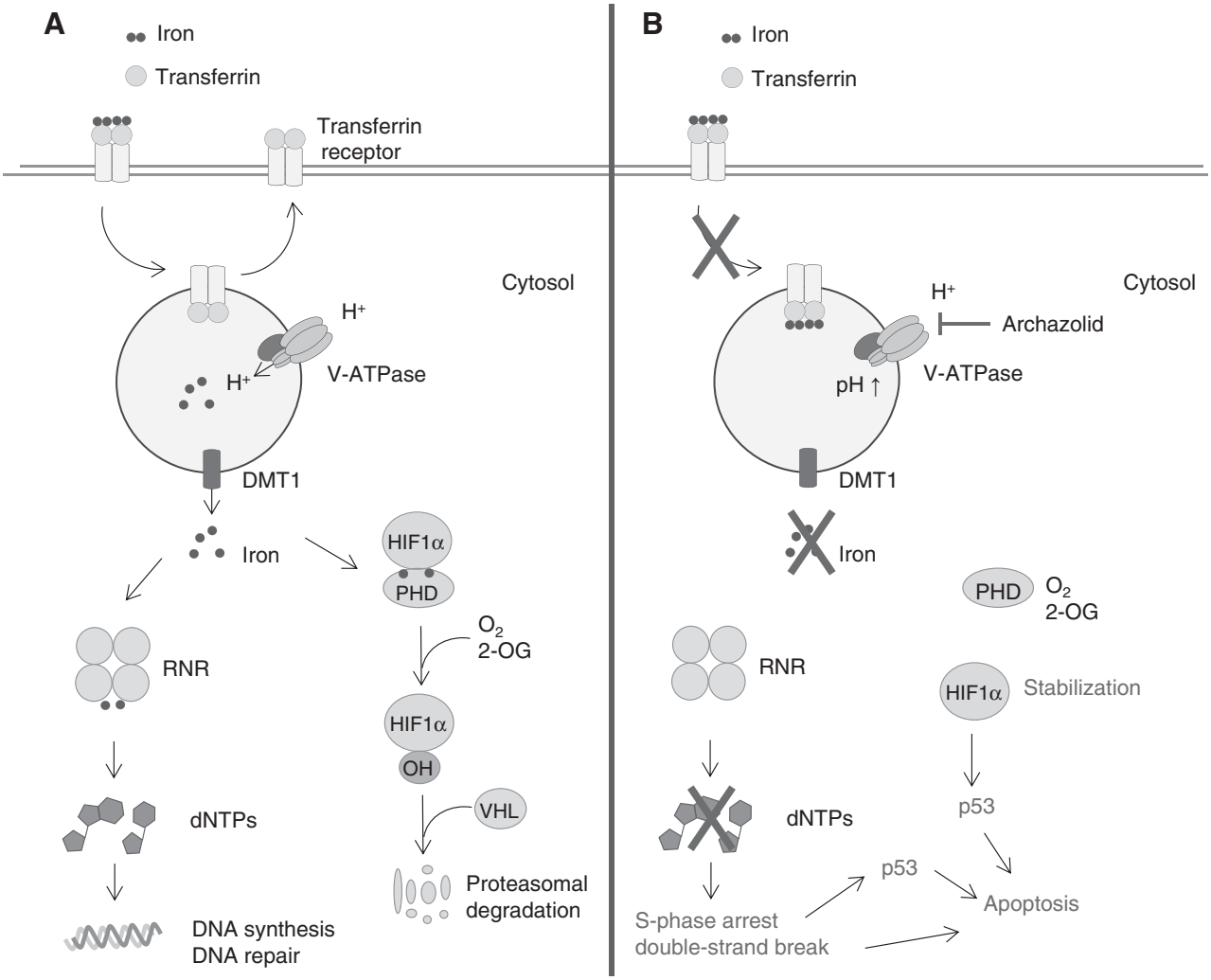

Figure 7.
Proposed mode of action for archazolid induced apoptosis. A, Tf-bound iron is taken up by endocytosis. The low pH of the lysosomes releases the iron from Tf, reaching the cytosol through divalent metal transporters 1 (DMT1) where it forms the labile iron pool. Iron is an essential cofactor for the hydroxylation of HIF1α via PHDs, initiating its degradation. Furthermore, catalytic formation of dNTPs by RNR is iron dependent. 2-OG, 2-oxoglutatrate. B, archazolid inhibits acidification of endosomes, resulting in disrupted TfR internalization. Induced iron deprivation stabilizes HIF1α and reduces RNR activity. In consequence, dNTP levels are decreased in the cytosol, generating S-phase block and DSB, finally leading to p53-dependent and p53-independent apoptosis.

new and effective way to target and interfere with the iron metabolism in cancer cells.

Interestingly, there are other approaches to abrogate tumor growth by targeting iron homeostasis. Iron chelators such as deferoxamine and 3-AP showed antitumor effects in different reports (37). Combination of these iron chelators with archazolid showed synergistic cytotoxicity in breast cancer cells, which allowed for the reduction of both chelator and inhibitor concentrations. Up to now there are further chelators under evaluation as anticancer agents such as ciclopirox, tachpyridine, and deferasirox (38).

Sufficient amount of labile iron is essential for fundamental cellular processes such as DNA synthesis and repair (39). The enzyme that connects these processes to iron homeostasis is the RNR. It catalyzes the formation of dNTPs by reducing the corresponding ribonucleotides (14). In mammalians, class I enzymes of RNR are present using an iron center for the catalytic reaction (40). Not surprisingly, depleted labile iron in the cytosol of cells affects the activity of RNR (41), thereby reducing the dNTP pool. Consistently, our observations show decreased dCTP levels after V-ATPase inhibition. As a consequence of reduced dNTP levels, RNR inhibitors show an interruption of DNA synthesis and DNA damage as reported for hydroxyurea (42, 43) and seen by archazolid treatment. Various clinical cytostatics interfere with DNA synthesis of cancer cells such as the DNA intercalating agent doxorubicin (44). Along this line, the combination of doxorubicin and archazolid was successful in reducing breast cancer colonies synergistically, indicating a potential therapeutic relevance of V-ATPase inhibition.

Besides the regulation of DNA metabolism, iron affects the signaling through HIF1α. HIF1α is a crucial transcription factor activated by hypoxia, upon which it influences the survival of

tumor cells and shifts the cellular metabolism toward glycolysis (45). For the proteasomal degradation of HIF1α via the von Hippel–Lindau tumor suppressor, HIF1α has to be hydroxylated by PHDs (46). This catalytic reaction is dependent on the presence of oxygen, 2-oxogutarat, and iron (47). Consistently, archazolid-induced iron depletion stabilizes HIF1α modifying the cellular glucose metabolism.

DNA damage as well as HIF1α can evoke the stabilization of the tumor suppressor p53 (48, 49). After activation of p53, it is able to induce either cell-cycle arrest or apoptosis, thereby reducing tumor progression. Cell-type origin, strength of p53-activating stimulus, and others can influence the outcome of p53 activation (50). p53 is widely mutated in tumors but at least 50% of all cancers are p53 wild-type tumors. Therefore, a lot of effort was put into the development of p53 activators. Up to now, the most advanced p53 activators are RG7112, MI-773, and DS-3032b being in phase I clinical trials (51). Nevertheless, it has been reported that DNA damage can trigger apoptosis independent of p53 in p53-deficient cells (52). Our work in p53 wild-type tumor cells (MCF7 cells) showed a clear involvement of p53 in V-ATPase–dependent cell death. Furthermore, archazolid successfully induced cell death in p53-mutated breast cancer cells (MDA-MB-231) and p53-null breast cancer cells (4T1). Hence this indicates that targeting the iron metabolism of cancer cells by V-ATPase inhibition can hit p53 wild-type tumors as well as mutated. Nonetheless one might speculate that a xenograft mouse model using a cell line expressing wild-type p53 should be more sensitive to tumor mass reduction than our p53-null 4T1 model.

Our observations that V-ATPase inhibition generates iron deprivation in the cell, thereby influencing activity of the iron-dependent enzymes PHDs and RNR evokes new options for interfering with the iron metabolism in cancer therapy. The depicted mechanism of action connects V-ATPase inhibition to fundamental cellular processes such as DNA synthase and repair. We like to point to the fact that the growth-inhibiting effects of archazolid seen *in vitro* are recapitulated in a solid tumor growth model *in vivo*, suggesting inhibition of V-ATPase as highly promising and viable strategy for breast cancer treatment.

Disclosure of Potential Conflicts of Interest

No potential conflicts of interest were disclosed.

Authors' Contributions

Conception and design: L.S. Schneider, K. von Schwarzenberg, A.M. Vollmar
Development of methodology: L.S. Schneider, D. Trauner, A.M. Vollmar
Acquisition of data (provided animals, acquired and managed patients, provided facilities, etc.): R. Kubisch-Dohmen
Analysis and interpretation of data (e.g., statistical analysis, biostatistics, computational analysis): L.S. Schneider, K. von Schwarzenberg, T. Lehr, M. Ulrich, J. Liebl
Writing, review, and/or revision of the manuscript: L.S. Schneider, T. Lehr, D. Menche, A.M. Vollmar
Administrative, technical, or material support (i.e., reporting or organizing data, constructing databases): K. von Schwarzenberg, D. Menche, A.M. Vollmar
Study supervision: A.M. Vollmar

Grant Support

This work was financially supported by the German Research foundation (DFG, FOR 1406, Vo 376-14/15; A.M. Vollmar).

The costs of publication of this article were defrayed in part by the payment of page charges. This article must therefore be hereby marked *advertisement* in accordance with 18 U.S.C. Section 1734 solely to indicate this fact.

Received July 16, 2014; revised February 24, 2015; accepted April 28, 2015; published OnlineFirst May 27, 2015.

References

1. Jemal A, Bray F, Center MM, Ferlay J, Ward E, Forman D. Global cancer statistics. CA Cancer J Clin 2011;61:69–90.
2. Newman DJ, Cragg GM. Natural products as sources of new drugs over the 30 years from 1981 to 2010. J Nat Prod 2012;75:311–35.
3. Sasse F, Steinmetz H, Höfle G, Reichenbach H. Archazolids, new cytotoxic macrolactones from archangium gephyra (Myxobacteria) production, isolation, physico-chemical and biological properties. J Antibiot 2003;56:520–5.
4. Bockelmann S, Menche D, Rudolph S, Bender T, Grond S, von Zezschwitz P, et al. Archazolid A binds to the equatorial region of the c-ring of the vacuolar H+-ATPase. J Biol Chem 2010;285:38304–14.
5. Huss M, Sasse F, Kunze B, Jansen R, Steinmetz H, Ingenhorst G, et al. Archazolid and apicularen: novel specific V-ATPase inhibitors. BMC Biochem 2005;6:13.
6. von Schwarzenberg K, Wiedmann RM, Oak P, Schulz S, Zischka H, Wanner G, et al. Mode of cell death induction by pharmacological vacuolar H+-ATPase (V-ATPase) inhibition. J Biol Chem 2012;288:1385–96.
7. Forgac M. Vacuolar ATPases: rotary proton pumps in physiology and pathophysiology. Nat Rev Mol Cell Biol 2007;8:917–29.
8. Barar J, Omidi Y. Dysregulated pH in tumor microenvironment checkmates cancer therapy. Bioimpacts 2013;3:149–62.
9. Foerster F, Braig S, Moser C, Kubisch R, Busse J, Wagner E, et al. Targeting the actin cytoskeleton: selective antitumor action via trapping PKCε. Cell Death Dis 2014;5:e1398.
10. Simeoni M, Magni P, Cammia C, De Nicolao G, Croci V, Pesenti E, et al. Predictive pharmacokinetic-pharmacodynamic modeling of tumor growth kinetics in xenograft models after administration of anticancer agents. Cancer Res 2004;64:1094–101.
11. Braig S, Kressirer CA, Liebl J, Bischoff F, Zahler S, Meijer L, et al. Indirubin derivative 6BIO suppresses metastasis. Cancer Res 2013;73:6004–12.
12. Wilson PM, LaBonte MJ, Russell J, Louie S, Ghobrial AA, Ladner RD. A novel fluorescence-based assay for the rapid detection and quantification of cellular deoxyribonucleoside triphosphates. Nucleic Acids Res 2011;39:e112.
13. Bliss CI. The calculation of microbial assays. Bacteriol Rev 1956;20:243–58.
14. Elledge SJ, Zhou Z, Allen JB. Ribonucleotide reductase: regulation, regulation, regulation. Trends Biochem Sci 1992;17:119–23.
15. Ohta T, Numata M, Yagishita H, Futagami F, Tsukioka Y, Kitagawa H, et al. Expression of 16 kDa proteolipid of vacuolar-type H(+)-ATPase in human pancreatic cancer. Br J Cancer 1996;73:1511–7.
16. Hinton A, Sennoune SR, Bond S, Fang M, Reuveni M, Sahagian GG, et al. Function of a subunit isoforms of the V-ATPase in pH homeostasis and *in vitro* invasion of MDA-MB231 human breast cancer cells. J Biol Chem 2009;284:16400–8.
17. Pinheiro C, Longatto-Filho A, Azevedo-Silva J, Casal M, Schmitt FC, Baltazar F. Role of monocarboxylate transporters in human cancers: state of the art. J Bioenerg Biomembr 2012;44:127–39.
18. Petzoldt AG, Gleixner EM, Fumagalli A, Vaccari T, Simons M. Elevated expression of the V-ATPase C subunit triggers JNK-dependent cell invasion and overgrowth in a Drosophila epithelium. Dis Model Mech 2013;6:689–700.
19. Morimura T, Fujita K, Akita M, Nagashima M, Satomi A. The proton pump inhibitor inhibits cell growth and induces apoptosis in human hepatoblastoma. Pediatr Surg Int 2008;24:1087–94.
20. Wiedmann RM, von Schwarzenberg K, Palamidessi A, Schreiner L, Kubisch R, Liebl J, et al. The V-ATPase-inhibitor archazolid abrogates tumor metastasis via inhibition of endocytic activation of the Rho-GTPase Rac1. Cancer Res 2012;72:5976–87.
21. Wu YC, Wu WKK, Li Y, Yu L, Li ZJ, Wong CCM, et al. Inhibition of macroautophagy by bafilomycin A1 lowers proliferation and induces

apoptosis in colon cancer cells. Biochem Biophys Res Commun 2009; 382:451–6.
22. Nakashima S. Vacuolar H+-ATPase inhibitor induces apoptosis via lysosomal dysfunction in the human gastric cancer cell line MKN-1. J Biochem 2003;134:359–64.
23. Ohta T, Arakawa H, Futagami F, Fushida S, Kitagawa H, Kayahara M, et al. Bafilomycin A1 induces apoptosis in the human pancreatic cancer cell line Capan-1. J Pathol 1998;185:324–30.
24. Richmond HG. Induction of sarcoma in the rat by iron-dextran complex. Br Med J 1959;1:947–9.
25. Greenberg G. Sarcoma after intramuscular iron injection. Br Med J 1976; 1:1508–9.
26. Stevens RG, Jones DY, Micozzi MS, Taylor PR. Body iron stores and the risk of cancer. New Engl J Med 1988;319:1047–52.
27. Ponka P, Lok CN. The transferrin receptor: role in health and disease. Int J Biochem Cell Biol 1999;31:1111–37.
28. Ryschich E, Huszty G, Knaebel HP, Hartel M, Büchler MW, Schmidt J. Transferrin receptor is a marker of malignant phenotype in human pancreatic cancer and in neuroendocrine carcinoma of the pancreas. Eur J Cancer 2004;40:1418–22.
29. Law S. Overexpression of transferrin receptor CD71 and its tumorigenic properties in esophageal squamous cell carcinoma. Oncol Rep 2014; 31:1296–304.
30. Brooks D, Taylor C, Dos Santos B, Linden H, Houghton A, Hecht TT, et al. Phase Ia trial of murine immunoglobulin A antitransferrin receptor antibody 42/6. Clin Cancer Res 1995;1:1259–65.
31. Taetle R, Castagnola J, Mendelsohn J. Mechanisms of growth inhibition by anti-transferrin receptor monoclonal antibodies. Cancer Res 1986;46: 1759–63.
32. Daniels TR, Bernabeu E, Rodríguez JA, Patel S, Kozman M, Chiappetta DA, et al. The transferrin receptor and the targeted delivery of therapeutic agents against cancer. Biochim Biophys Acta 2012;1820:291–317.
33. Dautry-Varsat A, Ciechanover A, Lodish HF. pH and the recycling of transferrin during receptor-mediated endocytosis. Proc Natl Acad Sci U S A 1983;80:2258–62.
34. Mellman I, Fuchs R, Helenius A. Acidification of the endocytic and exocytic pathways. Annu Rev Biochem 1986;55:663–700.
35. Kozik P, Hodson NA, Sahlender DA, Simecek N, Soromani C, Wu J, et al. A human genome-wide screen for regulators of clathrin-coated vesicle formation reveals an unexpected role for the V-ATPase. Nat Cell Biol 2012; 15:50–60.
36. Kobia F, Duchi S, Deflorian G, Vaccari T. Pharmacologic inhibition of vacuolar H+ ATPase reduces physiologic and oncogenic Notch signaling. Mol Oncol 2014;8:207–20.
37. Yu Y, Wong J, Lovejoy DB, Kalinowski DS, Richardson DR. Chelators at the cancer coalface: desferrioxamine to Triapine and beyond. Clin Cancer Res 2006;12:6876–83.
38. Torti SV, Torti FM. Iron and cancer: more ore to be mined. Nat Rev Cancer 2013;13:342–55.
39. Robbins E, Pederson T. Iron: its intracellular localization and possible role in cell division. Proc Natl Acad Sci U S A 1970;66:1244–51.
40. Reichard P. From RNA to DNA, why so many ribonucleotide reductases? Science 1993;260:1773–7.
41. Furukawa T, Naitoh Y, Kohno H, Tokunaga R, Taketani S. Iron deprivation decreases ribonucleotide reductase activity and DNA synthesis. Life Sci 1992;50:2059–65.
42. Koc A, Wheeler LJ, Mathews CK, Merrill GF. Hydroxyurea arrests DNA replication by a mechanism that preserves basal dNTP pools. J Biol Chem 2003;279:223–30.
43. Osterman Golkar S, Czene S, Gokarakonda A, Haghdoost S. Intracellular deoxyribonucleotide pool imbalance and DNA damage in cells treated with hydroxyurea, an inhibitor of ribonucleotide reductase. Mutagenesis 2013;28:653–60.
44. Box VGS. The intercalation of DNA double helices with doxorubicin and nagalomycin. J Mol Graphics Model 2007;26:14–9.
45. Piret J-P, Mottet D, Raes M, Michiels C. Is HIF-1α a pro- or an anti-apoptotic protein? Biochem Pharmacol 2002;64:889–92.
46. Denko NC. Hypoxia, HIF1 and glucose metabolism in the solid tumour. Nat Rev Cancer 2008;8:705–13.
47. Tuderman L, Myllyla R, Kivirikko KI. Mechanism of the prolyl hydroxylase reaction. 1. Role of co-substrates. Eur J Biochem 1977;80:341–8.
48. Sermeus A, Michiels C. Reciprocal influence of the p53 and the hypoxic pathways. Cell Death Dis 2011;2:e164.
49. Lee JH, Paull TT. Activation and regulation of ATM kinase activity in response to DNA double-strand breaks. Oncogene 2007;26:7741–8.
50. Fridman JS, Lowe SW. Control of apoptosis by p53. Oncogene 2003;22: 9030–40.
51. Hoe KK, Verma CS, Lane DP. Drugging the p53 pathway: understanding the route to clinical efficacy. Nat Rev Drug Discov 2014; 13:217–36.
52. Lips J, Kaina B. DNA double-strand breaks trigger apoptosis in p53-deficient fibroblasts. Carcinogenesis 2001;22:579–85.

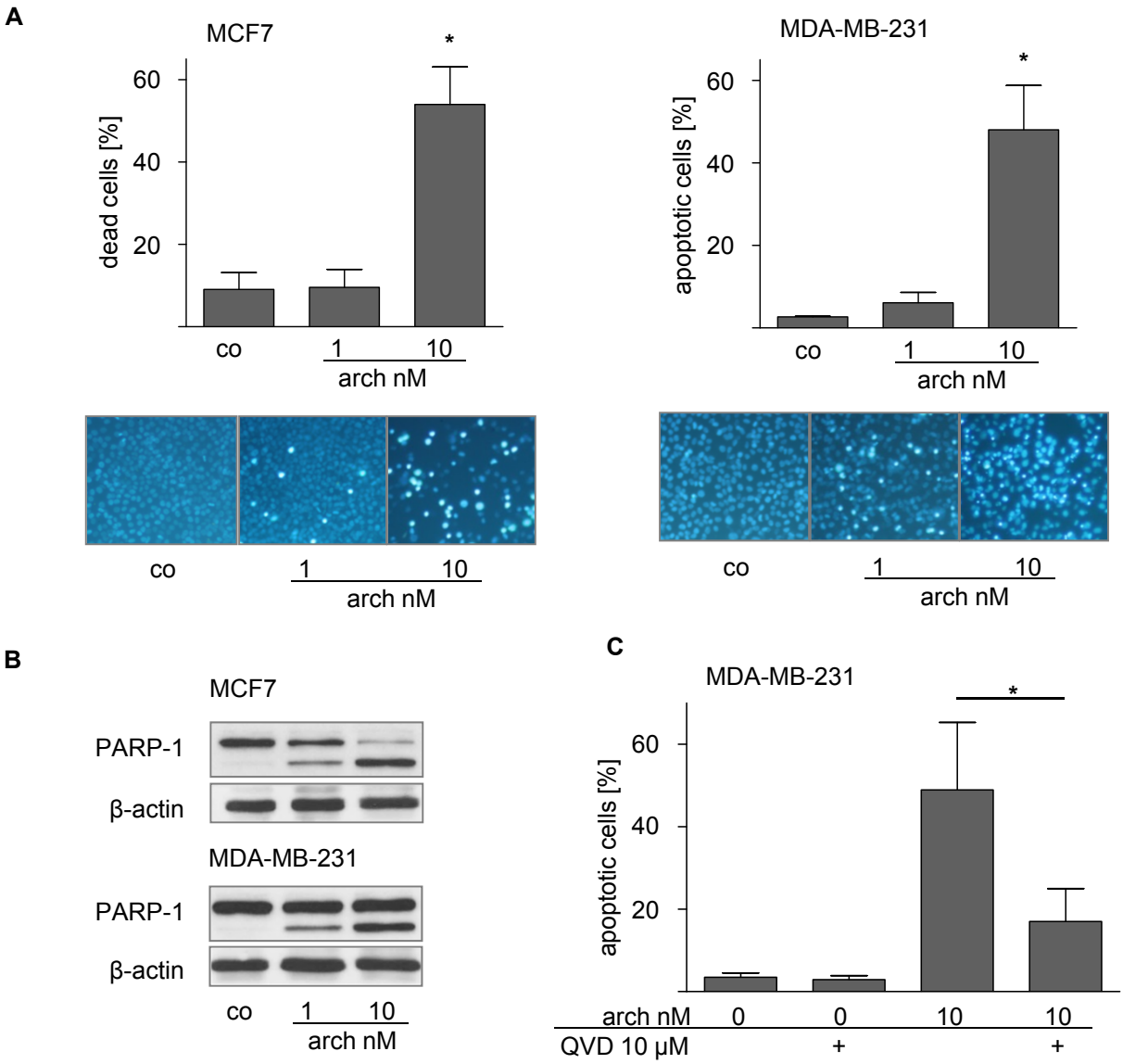

Supplementary Figure S1

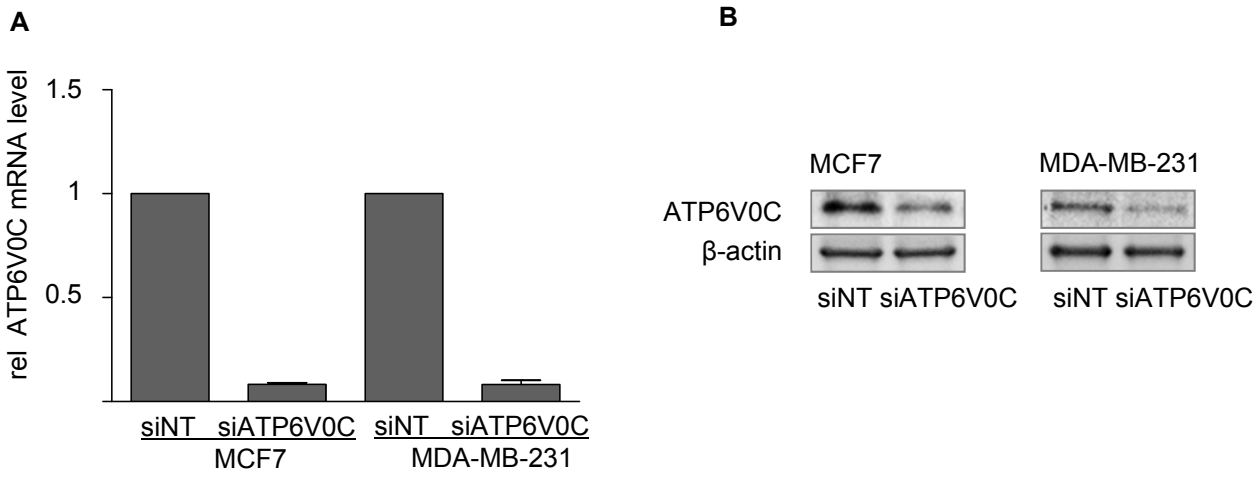

Supplementary Figure S2

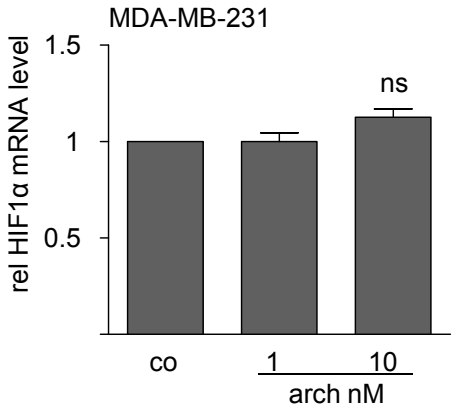

Supplementary Figure S3

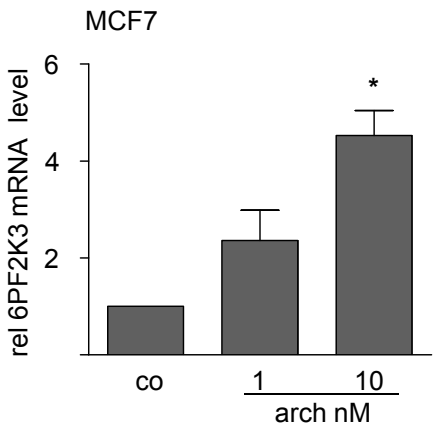

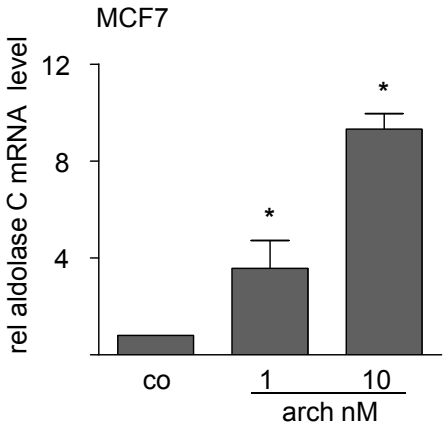

Supplementary Figure S4

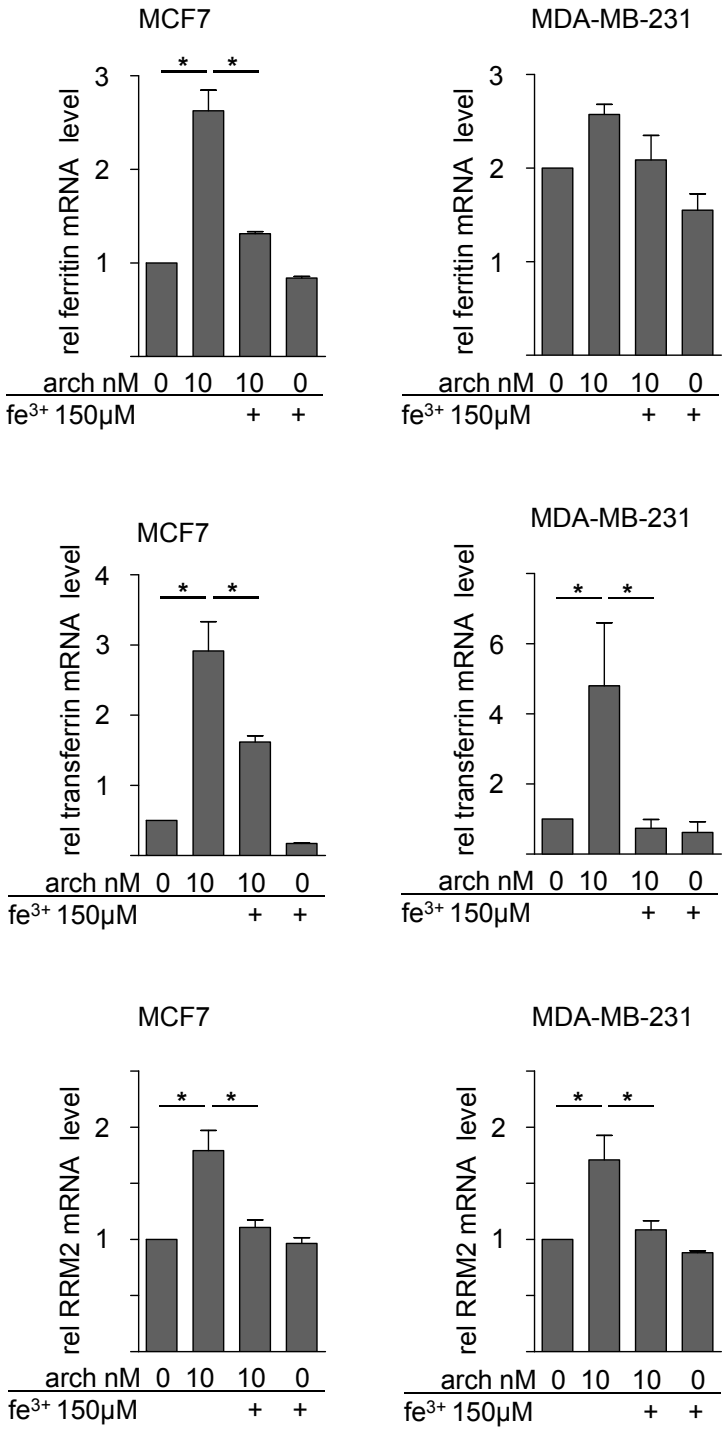

Supplementary Figure S5

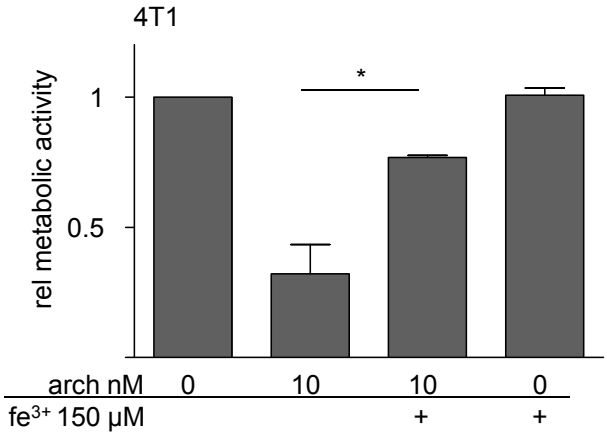

Supplementary Figure S6

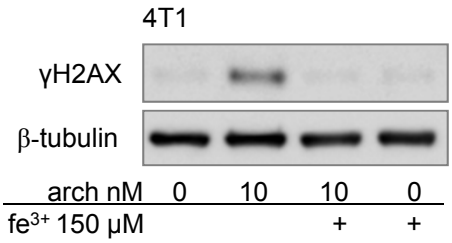

Supplementary Figure S7

SUPPLEMENTARY FIGURE LEGENDS

Supplementary Figure S1 Archazolid induces apoptosis in breast cancer cells in vitro. (A, C, D) Cell death was assessed by flow cytometry analysis in archazolid (**C** and QVD) treated MCF7 cells after 48 h, MDA-MB-231 cells after 72 h and 4T1 cells after 24 h. Bars are the SEM of three independent experiments performed in triplicates, *p<0.05 (One-way ANOVA, Newman-Keuls multiple comparison test). Condensed chromatin was visualized by Hoechst staining after 48 h of archazolid treatment in MCF7 cells and 72 h in MDA-MB-231 cells. One representative experiment out of three independent experiments is shown. **(B)** PARP-1 cleavage was detected by western blot upon 48 h and respectively 72 h of archazolid treatment in MCF7 and MDA-MB-231 cells. One representative blot out of three experiments is shown.

Supplementary Figure S2: mRNA levels of ATP6V0C after knockdown. MCF7 and MDA-MB-231 cells were transfected with siRNA-ATP6V0C and **(A)** mRNA was extracted after 72 h. qPCR analysis was assessed with the TaqMan Gene Expression Master Mix. Bars are the SEM of three independent experiments performed in triplicates. **(B)** ATP6V0C protein levels were detected by western blot after 72 h of transfection. One representative blot is shown.

Supplementary Figure S3: Archazolid has no influence on HIF1α mRNA levels in MDA-MB-231 cells. MDA-MB-231 cells were stimulated with archazolid for 24 h and mRNA levels were assessed by SYBR® Green qPCR analysis. Bars are the SEM of three independent experiments performed in triplicates, p*<0.05, ns=not significant (One-way ANOVA, Newman-Keuls multiple comparison test).

Supplementary Figure S4: Archazolid induces 6PF2K3 and aldolase C mRNA levels. MCF7 cells were treated with archazolid for 24 h. SYBR® Green qPCR was performed to analyze 6PF2K3 and aldolase C mRNA levels. Bars are the SEM of three independent experiments performed in triplicates, p*<0.05 (One-way ANOVA, Newman-Keuls multiple comparison test).

Supplementary Figure S5: Archazolid induces ferritin, transferrin and RRM2 mRNA levels. MCF7 cells and MDA-MB-231 cells were treated with archazolid for 24 h. SYBR® Green qPCR was performed to analyze ferritin, transferrin and RRM2 mRNA levels. Bars are the SEM of three independent experiments performed in triplicates, p*<0.05 (One-way ANOVA, Newman-Keuls multiple comparison test).

Supplementary Figure S6: Iron rescues archazolid induced reduction of metabolic activity in 4T1 cells. Metabolic activity of 4T1 cells after archazolid and iron citrate treatment was assessed by CTB assay. Bars are the SEM of three independent experiments performed in triplicates, p*<0.05 (One-way ANOVA, Newman-Keuls multiple comparison test).

Supplementary Figure S7: Archazolid induces DSB in 4T1 cells, which is compensated by iron. Expression of phosphorylated H2AX was detected by western blot in 4T1 cells after 48 h of archazolid and iron citrate treatment. One representative blot out of three independent experiments is shown.

SUPPLEMENTARY MATERIALS AND METHODS

Analysis of chromatin condensation

After treatment nuclei were stained with 0.5 µg/mL Hoechst33258® (Sigma Aldrich) for 10 min to visualize condensed chromatin by fluorescence microscopy using a Zeiss Axiovert 25 (Jena, Germany).

Anti-leukemic effects of the V-ATPase inhibitor Archazolid A

Siwei Zhang[1], Lina S. Schneider[1], Binje Vick[2,4], Michaela Grunert[2], Irmela Jeremias[2,3,4], Dirk Menche[5], Rolf Müller[6], Angelika M. Vollmar[1] and Johanna Liebl[1]

[1] Department of Pharmacy, Pharmaceutical Biology, Ludwig-Maximilians-University, Munich, Germany

[2] Department of Gene Vectors, Helmholtz Zentrum München, German Research Center for Environmental Health, Munich, Germany

[3] Department of Oncology/Hematology, Dr. von Haunersches Kinderspital, Munich, Germany

[4] German Cancer Consortium (DKTK), German Cancer Research Center (DKFZ), Heidelberg, Germany

[5] Kekulé-Institut für Organische Chemie und Biochemie der Universität Bonn, Bonn, Germany

[6] Helmholtz Institute for Pharmaceutical Research Saarland, Helmholtz Centre for Infection Research and Department of Pharmaceutical Biotechnology, Saarland University, Saarbrücken, Germany

***Correspondence to**: Johanna Liebl, **email**: johanna.liebl@cup.uni-muenchen.de*

Keywords: Archazolid, leukemia, natural compounds

***Received**: May 20, 2015* ***Accepted**: October 07, 2015* ***Published**: October 19, 2015*

ABSTRACT

Prognosis for patients suffering from T-ALL is still very poor and new strategies for T-ALL treatment are urgently needed. Our study shows potent anti-leukemic effects of the myxobacterial V-ATPase inhibitor Archazolid A. Archazolid A reduced growth and potently induced death of leukemic cell lines and human leukemic samples. By inhibiting lysosomal acidification, Archazolid A blocked activation of the Notch pathway, however, this was not the mechanism of V-ATPase inhibition relevant for cell death induction. In fact, V-ATPase inhibition by Archazolid A decreased the anti-apoptotic protein survivin. As underlying mode of action, this work is in line with recent studies from our group demonstrating that Archazolid A induced S-phase cell cycle arrest by interfering with the iron metabolism in leukemic cells. Our study provides evidence for V-ATPase inhibition as a potential new therapeutic option for T-ALL.

INTRODUCTION

T-cell acute lymphoblastic leukemia (T-ALL) is an aggressive hematopoietic malignancy. Despite advances in understanding of the molecular basis of T-ALL and intensified treatment regimens that have improved outcome of therapy, some patients fail conventional chemotherapy and T-ALL remains fatal in 20% of children and more than 50% of adults [1]. Along this line, new therapeutic approaches are urgently needed to improve patient prognosis.

Activating mutations in Notch1 occur in more than 50% of T-ALLs, highlighting Notch1 as key player in T-ALL [2, 3]. In fact, constitutive activation of Notch1 signaling represents the most prominent oncogenic pathway in T-cell transformation [1]. Therefore, targeted therapies to inhibit the Notch1 pathway have been developed. γ-secretase inhibitors (GSIs) that prevent Notch1 activating cleavage have been widely tested in preclinical models and clinical trials. However, the role of Notch in leukemia is still not entirely clear: on the one hand, it was shown that Notch signaling promotes cell survival and apoptosis resistance in leukemia [4, 5] and that Notch blockade by γ-secretase inhibition exerts pro-apoptotic effects in leukemia [6]. On the other hand, activation of Notch or of the Notch downstream target Hes1 inhibits leukemia development, growth and survival [7-9]. Furthermore, GSIs have shown only modest and temporary responses in leukemia therapy. These controversial results about Notch in leukemia demand for better understanding of the mechanisms that contribute to Notch signaling in leukemia in order to develop novel strategies to inhibit Notch1 signaling with alternative mechanism different from GSIs as potential promising approaches for T-ALL therapy.

Besides Notch activation at the plasma membrane

where ligand binding initiates y-secretase dependent cleavage of the Notch receptor, and subsequently NICD generation and translocation to the nucleus, Notch signaling in part depends on endocytosis. Recent reports showed that Notch can be activated in endosomes: in *drosophila*, Notch signaling is abolished when endosomal entry is blocked but is enhanced when endosomal retention is increased [10]. Moreover, in *drosophila*, acidification of endosomes by the V-ATPase is required for Notch activation [11].

Along this line, we hypothesized that inhibition of V-ATPase might be a promising strategy for T-ALL treatment. V-ATPase is an ATP-dependent proton pump that regulates pH homeostasis by translocating protons across membranes. The main function of V-ATPase is to regulate the acidification of intracellular compartments like lysosomes [12, 13]. V-ATPases are multisubunit heteromeric protein complexes with two functional domains: the V1 domain that is composed of eight subunits (A-H) mediates ATP hydrolysis and the V0 domain that is composed of five subunits (a, c, c'', d, e) regulates proton translocation [14]. The V-ATPase is localized at endosomes and lysosomes and is essential for endocytotic processes, receptor internalization and recycling, and finally lysosomal degradation [13]. Therefore, V-ATPase is implicated in fundamental physiological processes, like neurotransmitter uptake, renal acidification, bone resorption or sperm maturation and is associated with pathologic conditions including osteopetrosis, renal tubular acidosis and disease-related processes such as entry of toxins and viruses [13].

Recent reports indicate important functions of V-ATPase in tumors. Augmented expression of V-ATPase in cancer cells was demonstrated to contribute to metastasis, survival and growth of cancer cells [15-18]. Localization of V-ATPase at the plasma membrane was associated with invasiveness of various types of cancer including breast, pancreatic, prostate, and melanoma cancer cells [14, 19-21]. V-ATPase was shown to localize to the plasma membrane in sarcoma cells as well and was elucidated as a promising target for Ewing sarcoma, osteosarcoma, chondrosarcoma or rhabdomyosarcoma [22, 23] as well as glioblastoma [24, 25]. Along this line, V-ATPase inhibition could represent a promising approach for tumor therapy. Although only few V-ATPase inhibitors have been described so far, their V-ATPase binding properties and mode of action are well-investigated. Amongst others, a class of natural compounds - the Archazolids - inhibits V-ATPase activity by binding to the V-ATPase V0 subunit [26-28] that is responsible for proton transport across the membrane [29]. Archazolids are macrolides that have originally been isolated from the myxobacterium *Archangium gephyra* [30], and are available also by chemical synthesis [31, 32]. Archazolids have attracted attention as highly potent V-ATPase inhibitors that exert promising anti-tumor effects [15-18, 33-36].

Because Notch signaling activation in part depends on endocytosis [10, 11, 37] and V-ATPase has therefore been linked with the Notch pathway [35, 38], we hypothesized that V-ATPase inhibition might represent an alternative option to target leukemic cells. Therefore, we had a closer look on the functional effects and the mechanism of action, including the Notch pathway and cellular stress response, of the V-ATPase inhibitor Archazolid A in leukemic cells.

RESULTS

V-ATPase in leukemic cells

First, we analyzed the expression of the V-ATPase subunits in different leukemic cell lines including the T-ALL cell lines Jurkat and CEM, the AML cell line HL60, and the CML cell line K562 in comparison to non-tumor primary human PBMCs. Most of the V-ATPase subunits were comparably expressed in non-tumor PBMCs, Jurkat, CEM, and HL60 cells and some subunits were increased in K562 cells (Table 1). Immunostainings show that subunit c ATP6V0C which is targeted by Archazolid A, is localized to the lysosomal system and to the plasma membrane of leukemic cells (Figure 1A). As V-ATPase is essential for endo-lysosomal function, we analyzed the size of the endo-lysosomal compartment. In fact, the size of the endosomal compartment was increased in leukemic cell lines compared to non-tumor primary human peripheral blood mononuclear cells (PBMCs) (Figure 1B). This set of data suggests a potential function of V-ATPase in leukemia.

V-ATPase inhibition by Archazolid A impairs growth and induces death of leukemic cell lines

Archazolid A inhibited V-ATPase activity in leukemic cells as shown by staining of lysosomes with a pH-sensitive fluorescence dye (LysoTracker) (Figure 2A). Archazolid A impaired proliferation of leukemic cell lines Jurkat (EC50 0.56 nM) and CEM (EC50 0.51 nM) (Figure 2B, 2C). In line, clonogenic growth of Jurkat and CEM cells was reduced by V-ATPase inhibition (Figure 2D, 2E).

Moreover, as shown by Nicoletti assay (Figure 3A, 3B) and Annexin V staining (Figure 3C), Archazolid A potently induced death of leukemic cell lines. In line with a previous report from our group [15], Archazolid A induced cleavage of procaspase-3, procaspase-9, and PARP, increased the pro-apoptotic protein BNIP3, and decreased the anti-apoptotic protein Bcl-XL in leukemic cells (Figure 3D). Moreover, the pan-caspase inhibitor QVC-OPh

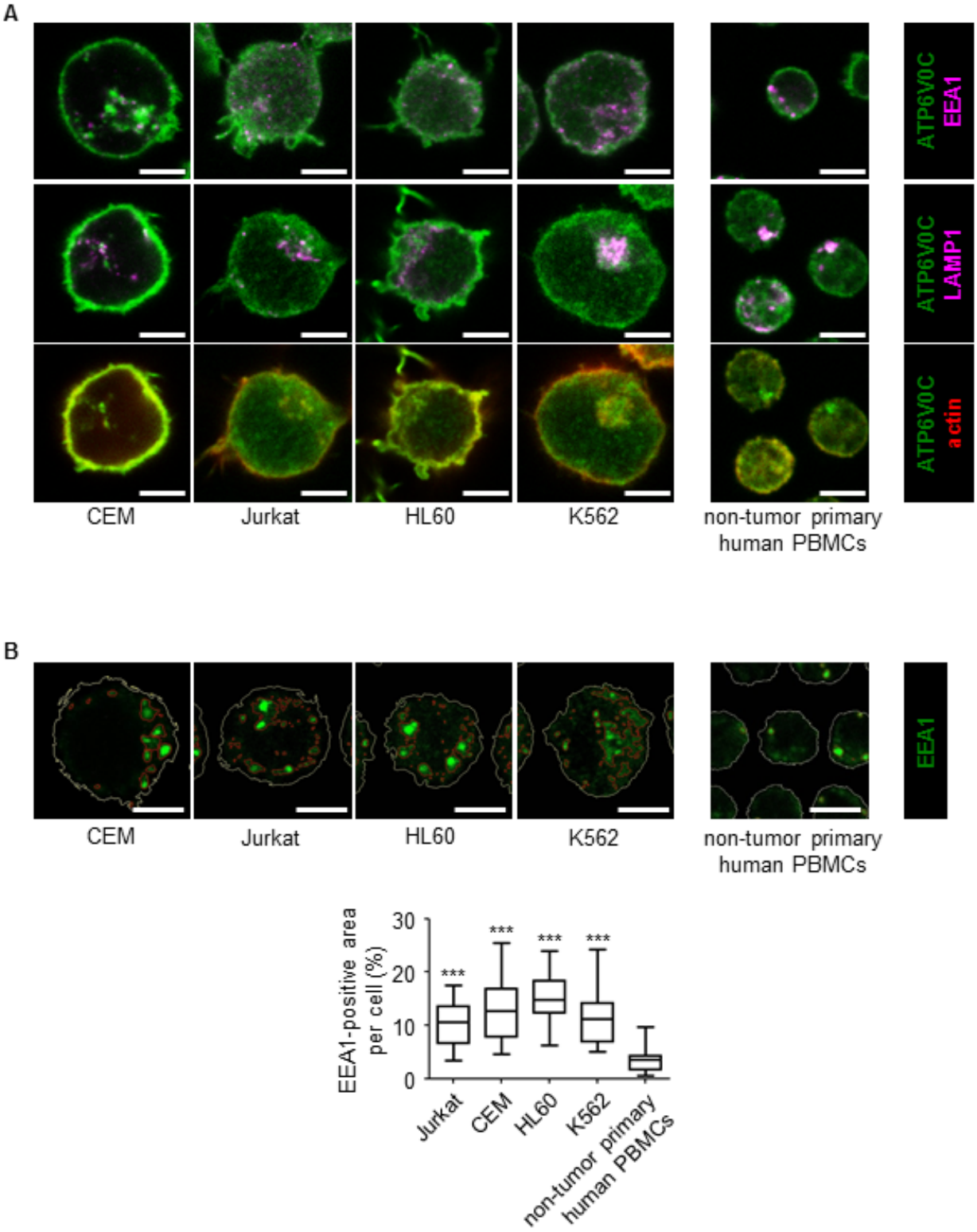

Figure 1: V-ATPase in leukemic cell lines. A. V-ATPase localization in leukemic cell lines is shown. Immunostaining of non-tumor primary human peripheral blood mononuclear cells (PBMCs) and leukemic cell lines (Jurkat, CEM, HL60, K562) for V-ATPase c-subunit (ATP6V0C, green) together with EEA1 (magenta), LAMP1 (magenta) and actin (red) is shown. Scale bar 5 µm. **B.** The size of the endo-lysosomal compartment in leukemic cell lines is shown. Staining of non-tumor primary human PBMCs and leukemic cell lines (Jurkat, CEM, HL60, K562) for EEA1 (green) is shown. Scale bar 5 µm. The white line labels the cell border. The red lines label the endosome area (EEA1-positive area). Endosome area per cell was calculated and is shown in the graph. One-Way ANOVA, Tukey's post test, ***$p \leq$ 0.001 (compared to non-tumor primary PBMCs).

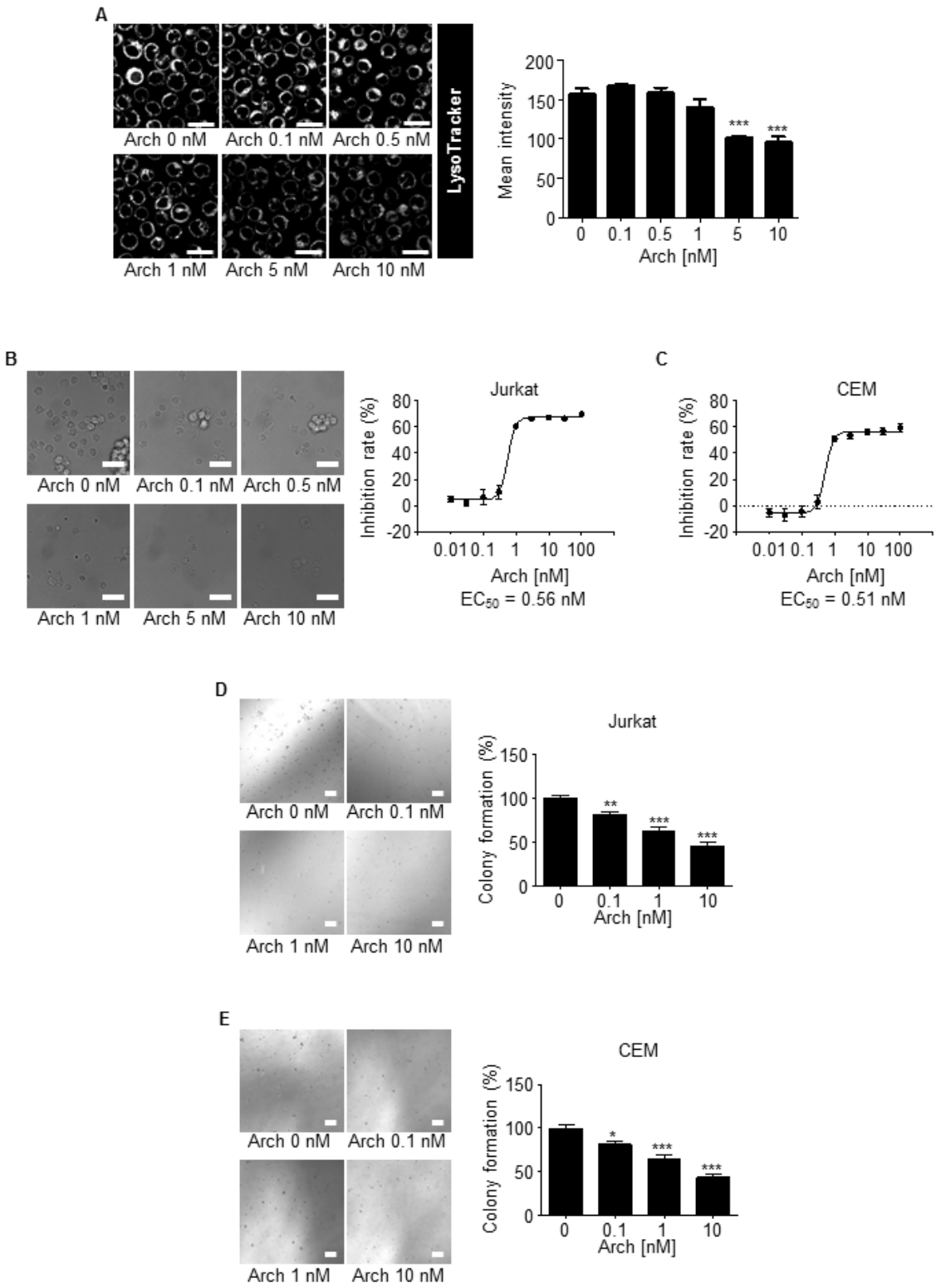

Figure 2: Archazolid A inhibits growth of leukemic cell lines. A. Archazolid A inhibits lysosome acidification. Stainings of Jurkat cells treated with Archazolid A (Arch, 0, 0.1, 0.5, 1, 5, 10 nM, 24h) with the pH-sensitive LysoTracker are shown. $n = 3$. Scale bar 20 µm. Quantification of LysoTracker staining is displayed (***$p \leq 0.001$, One-Way ANOVA, Tukey, $n = 3$). **B.**, **C.** Archazolid A inhibits the proliferation of leukemic cells. Inhibition rates of proliferation of Jurkat **B.** and CEM cells **C.** after treatments with Archazolid A (Arch) at indicated concentrations for 72h are shown. EC50 is indicated. $n = 3$. Scale bar 50 µm. **D.**, **E.** Archazolid A inhibits clonogenic growth. Colony formation of Jurkat **D.** and CEM cells **E.** after treatments with Archazolid A (Arch) at indicated concentrations is shown. Scale bar 100 µm. One-Way ANOVA, Tukey's post test, *$p \leq 0.05$, **$p \leq 0.01$, ***$p \leq 0.001$, $n = 3$.

Table 1: mRNA expression of V-ATPase subunits of the V1 domain (A-H) and the V0 domain (a, c, c", d, e) is shown in human leukemic cell lines related to non-tumor primary human PBMCs

V-ATPase subunit	S-Jurkat	CEM	K562	HL60
ATP6V1A	0.70±0.07	1.41±0.11	2.83±0.47	0.70±0.05
ATP6V1B1	0.43±0.16	1.16±0.60	1.24±1.13	0.36±0.19
ATP6V1B2	0.52±0.07	0.63±0.10	0.88±0.10	0.68±0.12
ATP6V1C1	0.90±0.06	0.93±0.09	2.59±0.22	0.83±0.09
ATP6V1C2	0.79±0.21	0.48±0.11	0.75±0.15	34.28±15.71
ATP6V1D	0.96±0.01	1.19±0.14	1.87±0.05	0.24±0.01
ATP6V1E1	1.00±0.05	0.97±0.01	3.43±0.44	0.89±0.06
ATP6V1E2	0.51±0.05	0.37±0.03	0.65±0.06	0.17±0.01
ATP6V1F	1.12±0.27	1.64±0.34	5.27±0.39	1.00±0.06
ATP6V1G1	1.00±0.17	1.06±0.06	1.61±0.13	0.60±0.04
ATP6V1G2	0.12±0.03	1.00±0.14	0.11±0.03	0.06±0.01
ATP6V1G3	0.18±0.07	0.69±0.25	0.10±0.00	0.11±0.04
ATP6V1H	0.85±0.04	1.16±0.06	2.32±0.08	0.66±0.04
ATP6V0A1	0.48±0.01	1.07±0.06	10.67±0.87	0.60±0.05
ATP6V0A2	0.78±0.03	0.66±0.21	1.55±0.10	0.30±0.04
ATP6V0A3	0.01±0.00	0.11±0.01	0.37±0.24	0.68±0.07
ATP6V0A4	0.82±0.31	1.46±0.23	1.26±0.71	0.83±0.28
ATP6V0B	1.53±0.12	1.47±0.14	4.78±0.53	1.46±0.49
ATP6V0C	0.67±0.06	0.81±0.07	2.39±0.36	0.90±0.10
ATP6V0D1	0.38±0.03	0.44±0.04	1.26±0.12	0.86±0.09
ATP6V0D2	0.10±0.04	0.19±0.17	9.09±4.84	18.38±5.61
ATP6V0E1	0.34±0.08	0.72±0.16	0.84±0.03	0.62±0.04
ATP6V0E2	1.97±0.08	2.62±0.15	0.54±0.05	0.07±0.01

Table 2: Clinical characteristics of patients from which the PDX cells have been generated are shown.

number	Type of Leukemia	Disease stage	sex	age	cytogenetics
ALL-169	cALL	diagnosis	m	pediatric	unknown
ALL-233	pre B ALL	diagnosis	m	pediatric	t(2;15)(p13;q15)
ALL-256	cALL	unknown		pediatric	+8, t(9;22)(q34;q11)
ALL-363	pre B ALL	diagnosis	m	adult	BCR/ABL translocation
AML-372	AML	relapse	m	adult	Complex, including -17
AML-412	AML	diagnosis	f	adult	CN, FLT3-ITD, NPM1+
ALL-435	pre B ALL	unknown		pediatric	t(11;19)

partially rescued Archazolid A induced apoptosis (Figure 3E). This suggests that apoptosis by Archazolid A is at least partially mediated via the mitochondrial pathway.

V-ATPase inhibitor Archazolid A induces death of primary human leukemic cells

To analyze the potential therapeutic relevance of V-ATPase inhibition by Archazolid A, patient derived xenograft (PDX) leukemic cells were studied. Clinical characteristics are listed in Table 2. PDX cells enable repetitive *in vitro* testing on viable patient-derived cells, by passaging primary tumor cells in severely immuno-compromised mice. These cells resemble the primary patient cells to a very high extent [39, 40]. In accordance with cell culture experiments, Archazolid A reduced viability (Figure 4A) and induced death of PDX human leukemic cell samples from different patients which was again shown by PI exclusion assays (Figure 4B) and Annexin V staining (Figure 4C). Moreover, Archazolid A induced cleavage of procaspase-3 in PDX samples (Figure 4D). This set of data demonstrates that V-ATPase inhibition by Archazolid A exerts anti-leukemic properties.

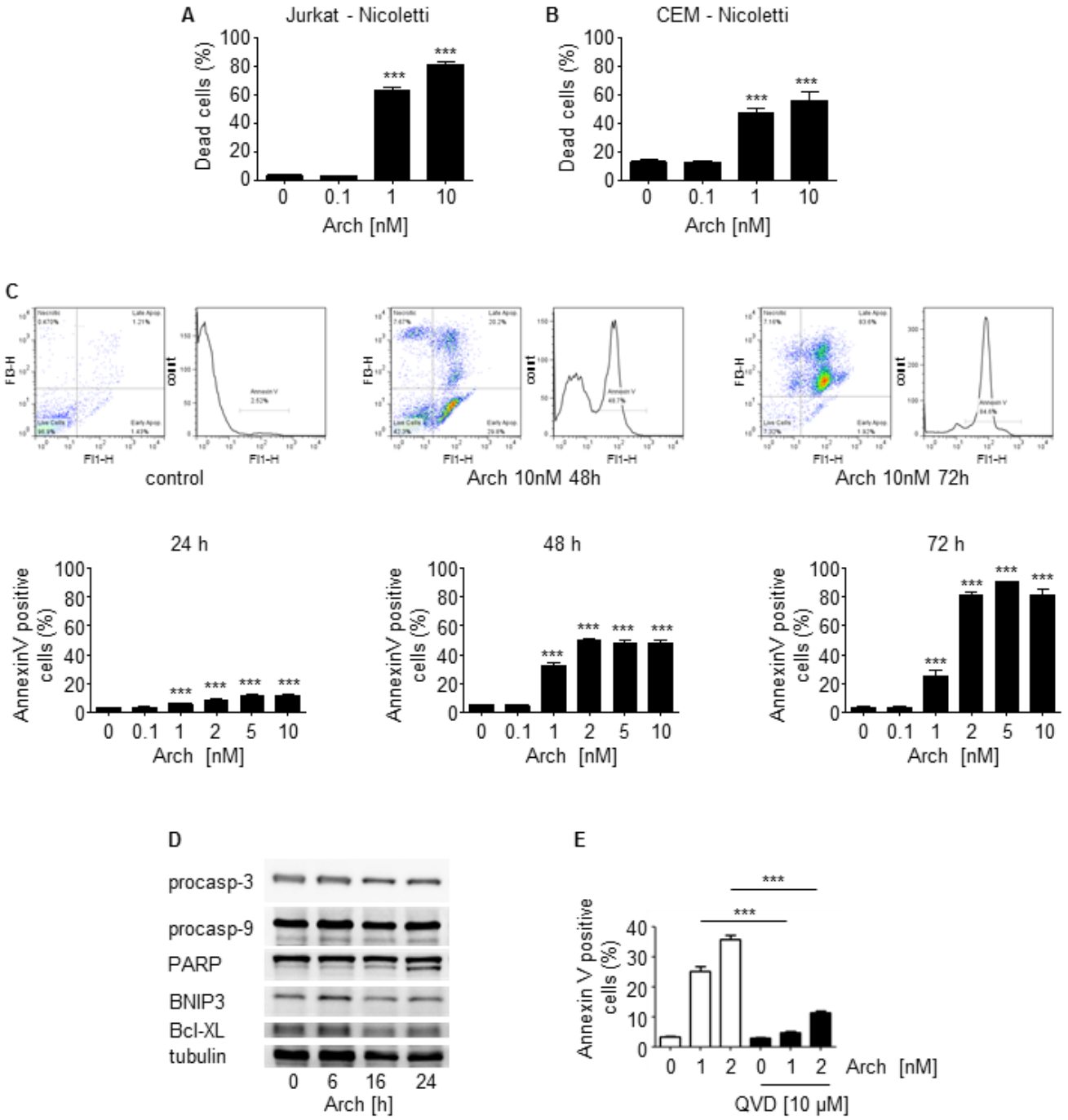

Figure 3: Archazolid A induces death of leukemic cell lines. A., **B.** Apoptosis rate determined by Nicoletti assay of Jurkat **A.** and CEM cells **B.** after treatments with Archazolid A (Arch) at indicated concentrations for 72h is shown. One-Way ANOVA, Tukey's post test, ***$p \leq 0.001$, $n = 3$. **C.** Pictures display Annexin V staining of Jurkat cells after treatments with Archazolid A (Arch). Bar graphs show the apoptosis rate determined by Annexin V staining of Jurkat cells after treatments with Archazolid A (Arch) at indicated concentrations for 24h, 48h, and 72h. One-Way ANOVA, Tukey's post test, ***$p \leq 0.001$, $n = 3$. **D.** Immunoblots of Jurkat cells treated with Archazolid A (10 nM) for the indicated times for procaspase-3 (procasp-3), procaspase-9 (procasp-9), PARP, BNIP3, and Bcl-XL are shown. The immunoblot for tubulin indicates equal loading. $n = 3$. **E.** Annexin V/PI staining of cells treated with Archazolid A at indicated concentrations for 48h and with/without the pan-caspase inhibitor QVD-OPh (QVD) at 10 µM for 48h is shown. One-Way ANOVA, Tukey's post test, ***$p \leq 0.001$, $n = 3$.

Because Archazolid A did not induce cell death of non-tumor primary human PBMCs (Figure 4E) it might represent an option for anti-leukemic treatment.

V-ATPase inhibition by Archazolid A addresses Notch1 signaling in leukemic cells, but the Notch pathway is not responsible for Archazolid A induced cell death

In order to evaluate the mechanism of Archazolid A to induce leukemic cell death, the Notch pathway gained our attention. Expression of the Notch1 downstream target Hes1 was reduced by Archazolid A as well as by the y-secretase inhibitor (GSI) Dibenzazepine (DBZ) that served as positive control for Notch signaling inhibition (Figure 5A). Archazolid A reduced levels of Notch1 intracellular domain (NICD) and the Notch1 downstream target c-myc (Figure 5B). As expected, DBZ treatment decreased NICD and c-myc as well. NICD expression revealed that the Notch1 pathway was active in PDX samples (Figure 5C). Archazolid A-mediated decrease of NICD (Figure 5C) proved that Archazolid A addressed the Notch1 pathway in PDX cells. Archazolid A induced cell death in these PDX samples as well (Figure 4C and 10A), suggesting sensitivity of leukemic cells with Notch1 pathway activation towards Archazolid A. Moreover, Archazolid A increased levels of the Notch1 whole receptor (Figure 5B). This was further analyzed by immunostainings which demonstrate again that Archazolid A abrogated NICD levels whereas the Notch1 whole receptor was increased (Figure 5D). Stainings for the lysosomal marker LAMP1 revealed large lysosomes that contained increased amounts of Notch1 in Archazolid A treated cells (Figure 5E). This suggested that Archazolid A inhibits Notch1 signaling in a way different from GSI: by capturing the Notch1 whole receptor in lysosomes and therefore inhibiting Notch1 cleavage and NICD generation at endolysosomal membranes.

However, NICD overexpression could not rescue from Archazolid A-mediated cell death (Figure 6A), suggesting no causal relationship between the Notch1 pathway and Archazolid A-induced leukemic cell death. Nevertheless, NICD overexpression induced Notch1 downstream target gene expression (Figure 6B) and rescued DBZ-induced inhibition of proliferation (Figure 6C), proving that NICD overexpression was functional. In order to better understand the inter-connection between V-ATPase and Notch1, we analyzed whether Notch inhibition affects levels of V-ATPase c-subunit. V-ATPase c-subunit expression was not affected by DBZ treatment (Figure 6D). This set of data indicated that Notch1 signaling inhibition is not the major relevant downstream signaling of Archazolid A in leukemic cell death induction.

Inhibition of y-secretase impairs growth but does not induce death of leukemic cell lines

DBZ-mediated γ-secretase inhibition reduced proliferation of leukemic cell lines Jurkat (EC50 15.5 μM) and CEM (EC50 12.7 μM) (Figure 7A, 7B) as well as clonogenic growth (Figure 7C, 7D). However, DBZ neither induced death of leukemic cell lines (Figure 7E-7G), nor of human leukemic PDX samples (Figure 7H). This set of data suggests that the Notch1 pathway is not essential for the effects of Archazolid A on leukemic cell death.

Archazolid A decreases survivin by inducing cell cycle arrest and interfering with the iron metabolism in leukemic cells

In search for other pathways of Archazolid A responsible for cell death, we analyzed the anti-apoptotic protein survivin, a crucial regulator of cell death in leukemic cells [41-43]. In fact, Archazolid A decreased survivin protein levels (Figure 8A, 8B and Supplementary Figure 1) which was not due to changed survivin mRNA (Figure 8C). In contrast, DBZ showed no significant effect on survivin (Figure 8A-8C), again providing evidence that Archazolid A-mediated anti-leukemic effects are not based on Notch1 inhibition. Because survivin expression strongly depends on the cell cycle [41-43], subsequently, cell cycle analysis was performed. In fact, cells without Archazolid A treatment pass S-phase (8h) to reach (16h) and accumulate (20h, 24h) in G2-phase. In contrast, Archazolid A treated cells accumulate in S-phase (8h, 16h, 20h) but do not traverse to G2-phase. This suggests that Archazolid A treated cells die during S-phase which is confirmed by cell death analysis showing that Archazolid A-induced S-phase arrest is in parallel with apoptosis induction (Figure 8D).

In line with recent studies from our group [15, 44] that elucidated that interference of Archazolid with the iron metabolism leads to S-phase cell cycle arrest in breast cancer, Archazolid A stabilized Hif1α in leukemic cells (Figure 9A-9C) which was abrogated by simultaneous treatment with iron citrate (Figure 9C). In contrast, Notch inhibition by DBZ did not affect Hif1α (Figure 9D). As shown previously [44], Archazolid A-mediated cell death was partially rescued by iron citrate (Figure 9E). Because Hif1α stabilization is generally pro-proliferative, but also anti-proliferative and cell death inducing properties have been described [45-48], we analyzed the effects of Hif1α induction on cell death and survivin expression in leukemic cells. Induction of Hif1α by deferoxamine (DFO) induced leukemic cell death and decreased survivin, which was even enhanced by concomitant Archazolid A treatment (Figure 9F, 9G). This set of data suggests that interference of Archazolid A with the iron metabolism

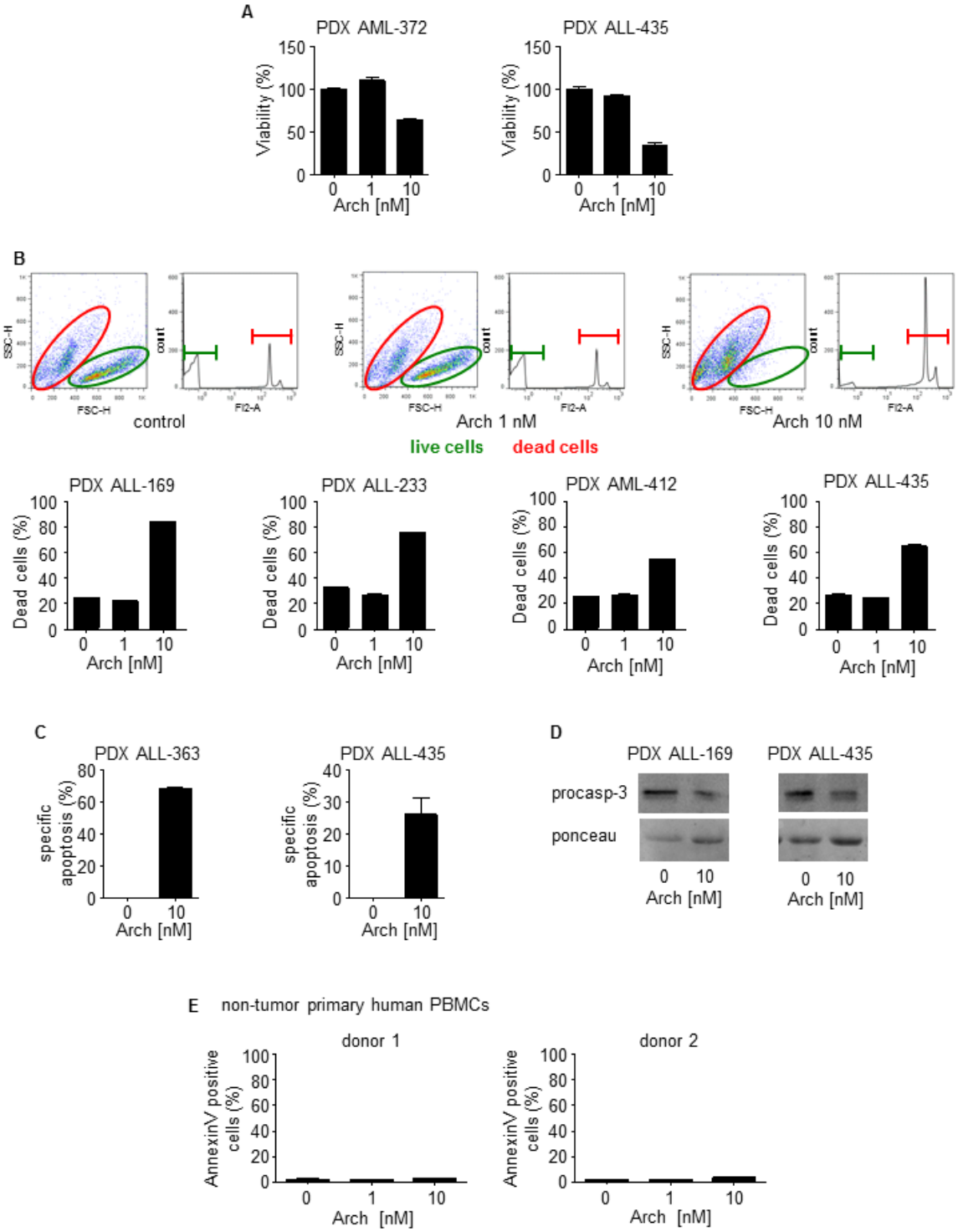

Figure 4: Archazolid A induces cell death in human patient derived xenograft (PDX) samples. A. Viability of leukemic PDX samples with/without treatment with Archazolid A (Arch) for 72h at indicated concentrations is shown. **B.** PI exclusion staining of leukemic PDX samples with/without treatment with Archazolid A (Arch) for 48h at indicated concentrations is shown. Upper panels display dot plots and histograms of PDX leukemic cells from one respective patient (PDX ALL-169). Dead cells are stained by PI and are marked in red. Live cells without PI staining are displayed in green. Lower panels show apoptosis rate of PDX leukemic cells treated with Archazolid A (Arch) at indicated concentrations. **C.** The specific apoptosis rate determined by Annexin V/PI staining of PDX cells after treatments with Archazolid A (Arch) at indicated concentrations for 48h is shown. **D.** Immunoblots of PDX samples treated with Archazolid A (10 nM, 48h) for procaspase-3 (procasp-3) are shown. Ponceau staining indicates equal loading. **E.** Archazolid A does not induce cell death in non-tumor primary human PBMCs. Apoptosis rate determined by Annexin V/PI staining and of non-tumor primary human PBMCs (FACS analysis with gating for lymphocytes) of two different donors treated with Archazolid A (Arch) at indicated concentrations for 48h is shown.

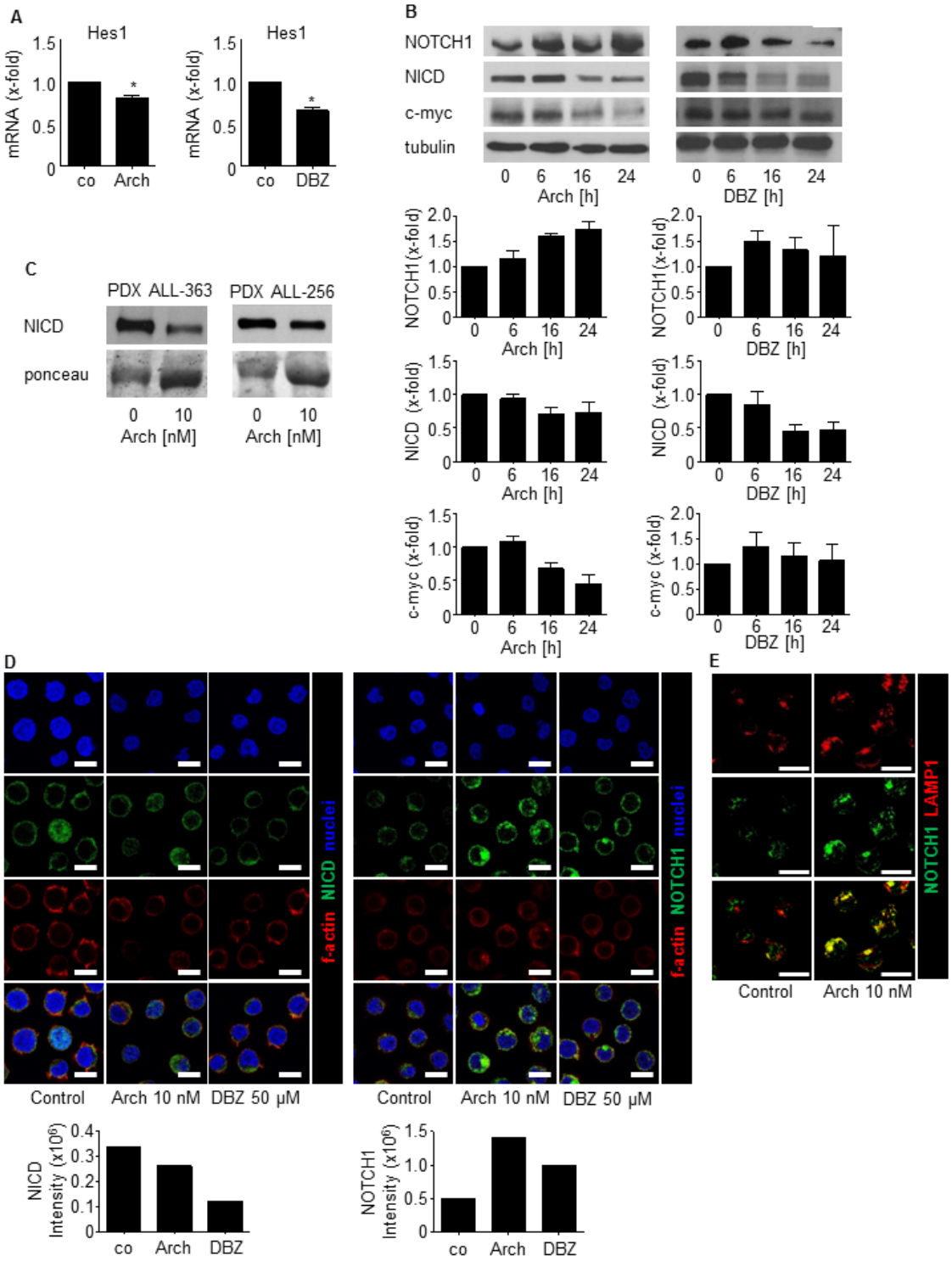

Figure 5: Archazolid A inhibits Notch1 signaling. A. Hes1 mRNA expression of Jurkat cells treated with Archazolid A (Arch, 10 nM, 24h) or DBZ (50 µM, 24h) is shown. Archazolid A: paired *t*-test, **p* = 0.0341, *n* = 3. DBZ: paired *t*-test, **p* = 0.0090, *n* = 3. **B.** Immunoblots from Jurkat cells treated with Archazolid A (Arch, 10 nM, left panel) or DBZ (10 µM, right panel) for the indicated times and probed with antibodies for Notch, NICD, and c-myc are shown. Immunoblots for β-tubulin indicate equal loading. Bar graphs display quantitative evaluations of immunoblots for Notch1, NICD, and c-myc. *n* = 3. **C.** Immunoblots from PDX cells treated with Archazolid A (10 nM, 24h) and probed with antibodies for NICD are shown. Ponceau staining is used as loading control. **D.** Immunostainings from Jurkat cells treated with Archazolid A (Arch, 10 nM, 24h) or DBZ (50 µM, 24h) for NICD (green, left panels) and Notch1 (green, right panels) are shown. *n* = 3. Scale bar 10 µm. Bar graphs display quantitative evaluations of NICD and Notch1 intensities. **E.** Immunostainings from Jurkat cells treated with Archazolid A (Arch, 10 nM, 24h) for LAMP1 (red) and Notch1 (green) are shown. Merged pictures indicate colocalization of LAMP1 and Notch1 (yellow). *n* = 3. Scale bar 10 µm.

contributes to cell death in leukemic cells.

Finally, coincident with apoptosis induction, survivin levels were decreased by Archazolid A treatment of PDX human patient samples as shown for the PDX samples PDX ALL-363 and PDX ALL-256 (Figure 10A, Figure 4C). Moreover, survivin overexpression partially rescued Archazolid A induced cell death in leukemic cells (Figure 10B). This set of data suggests decreased survivin as relevant mechanism of Archazolid A to induce leukemic cell death.

DISCUSSION

Our study demonstrates that V-ATPase inhibition by Archazolid A exerts anti-leukemic effects, suggesting V-ATPase inhibition as potential option for T-ALL treatment.

During recent years, V-ATPase has emerged as interesting target for cancer therapy. Amongst others, including various studies of our group, it has been shown that V-ATPase is implicated in cancer cell metastasis [16, 49], invasion [50, 51], tumor cell death [15, 52], anoikis resistance [17], cellular stress response [15], breast cancer trastuzumab resistance [34], and regulation of the secretion profile of cancer and cancer-associated cells [18, 53]. Only few reports point to a function of V-ATPase in leukemia or hematopoietic cells in general. In detail, it was shown that proton pump inhibitors induce apoptosis of human B-cells [54] and lysosome disruption has been associated with anti-leukemic effects in acute myeloid leukemia (AML) [55]. Moreover, V-ATPase was suggested to regulate

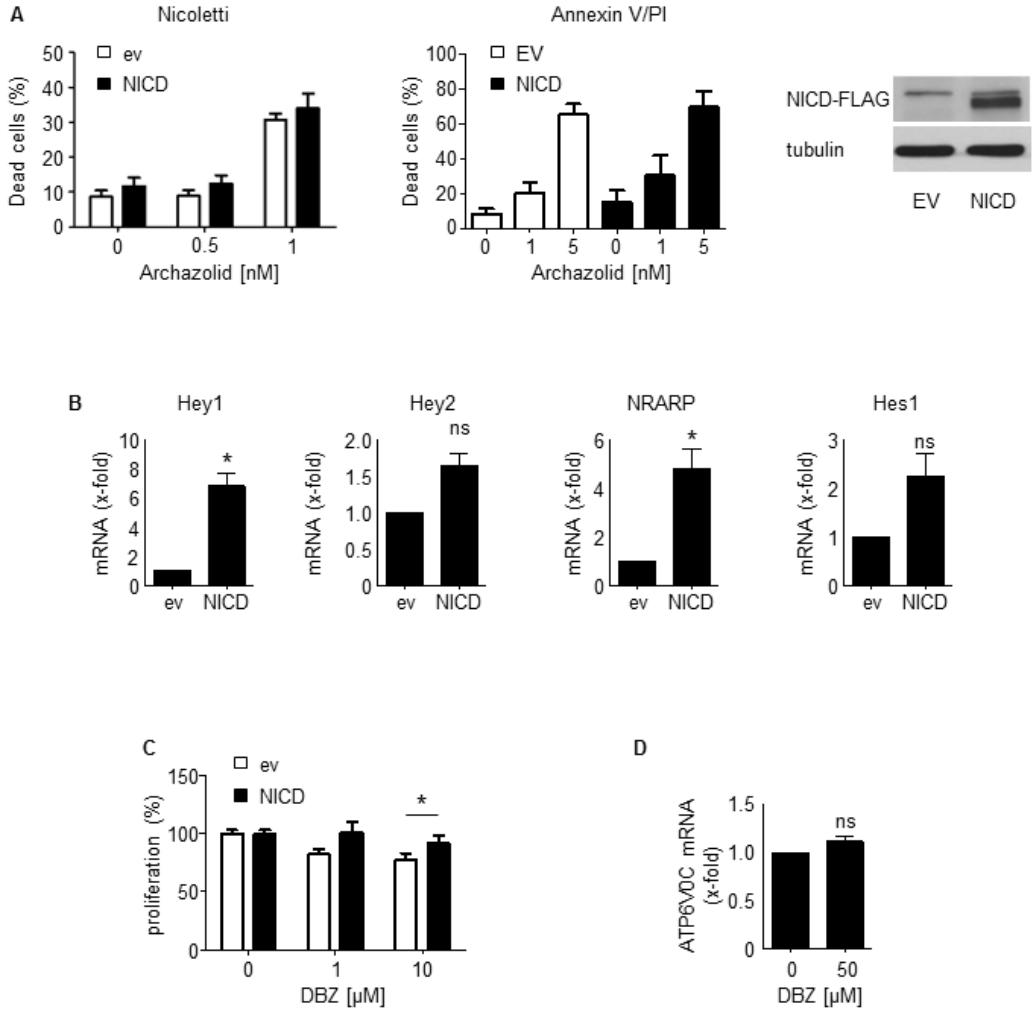

Figure 6: NICD cannot rescue Archazolid A mediated induction of apoptosis. A. Apoptosis rate determined by Nicoletti assay (left bar graph) and by Annexin V/PI staining (right bar graph) of Jurkat cells overexpressing either empty vector or NICD after treatment with Archazolid A (48h) is shown. Immunoblots show NICD overexpression. $n = 3$. **B.** Increased expression of Notch downstream targets Hey1 (paired t-test, $^*p = 0.0197$), Hey2 (paired t-test, $p = 0.0576$), NRARP (paired t-test, $^*p = 0.0407$), Hes1 (paired t-test, $p = 0.1117$) after NICD overexpression (24h) is shown. $n = 3$. **C.** Proliferation of Jurkat cells overexpressing either empty vector or NICD after treatment with DBZ at indicated concentrations for 72h is shown. t-test, $^*p = 0.0209$, $n = 3$. **D.** Expression of V-ATPase subunit c (ATP6V0C) of Jurkat cells treated with DBZ (50 µM, 24h) is shown. Non-significant (ns), paired t-test, $p = 0.1886$.

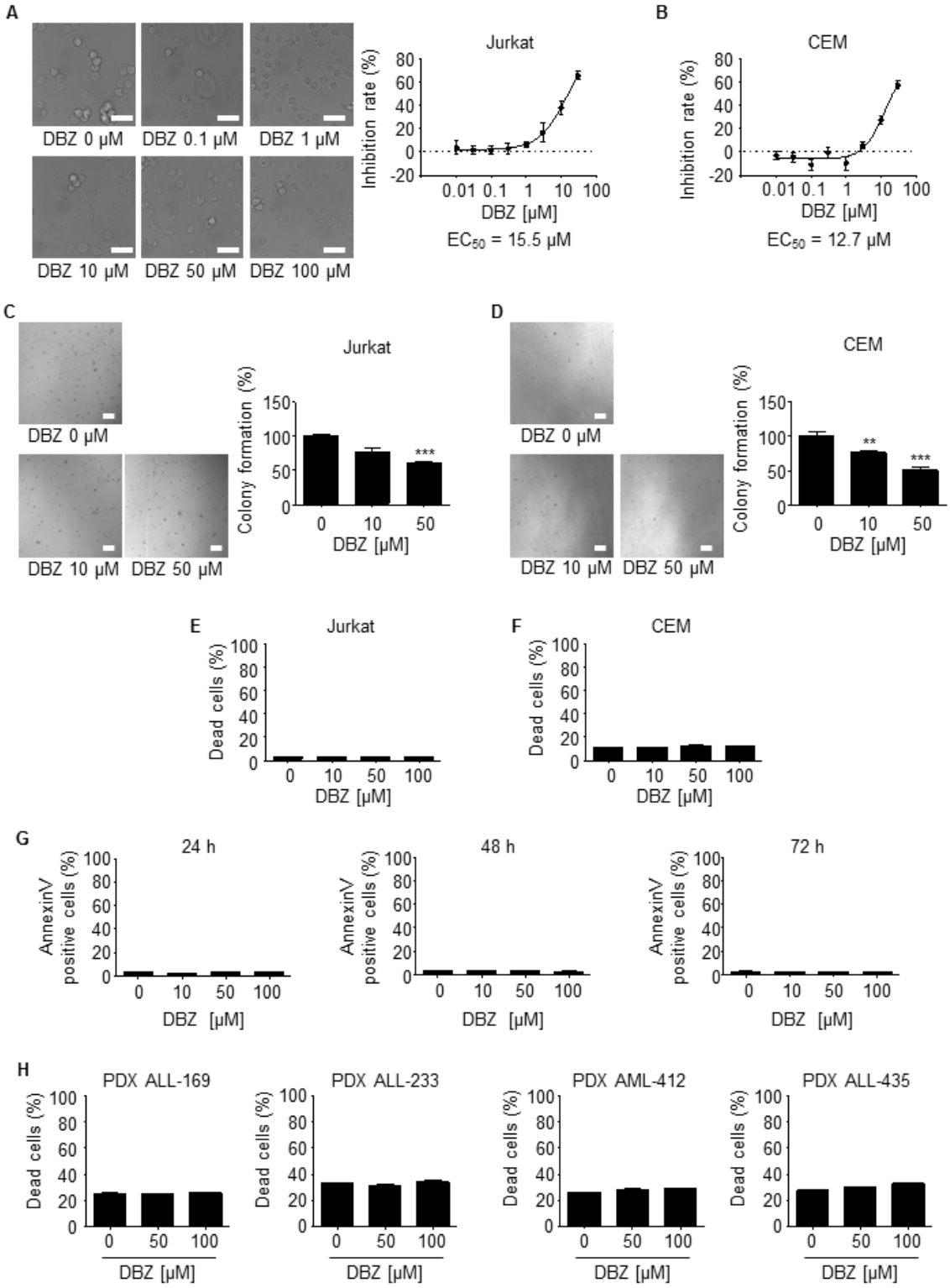

Figure 7: y-secretase inhibition by DBZ inhibits growth but does not induce leukemic cell death. A., **B.** DBZ inhibits proliferation of leukemic cells. Inhibition rates of proliferation of Jurkat **A.** and CEM cells **B.** after treatment with DBZ for 72h at indicated concentrations are shown. EC50 is indicated. $n = 3$. Scale bar 50 µm. **C.**, **D.** Colony formation of Jurkat **C.** and CEM cells **D.** after treatments with DBZ at indicated concentrations is shown. Scale bar 100 µm. One-Way ANOVA, Tukey, $^{**}p \leq 0.01$, $^{***}p \leq 0.001$, $n = 3$. **E.**, **F.** Apoptosis rate determined by Nicoletti assay of Jurkat **E.** and CEM cells **F.** after treatments with DBZ at indicated concentrations for 72h is shown. $n = 3$. **G.** Apoptosis rate determined by Annexin V/PI staining of Jurkat cells after treatments with DBZ at indicated concentrations for 24h, 48h, and 72h is shown. 24h and 48h: $n = 2$. 72h: $n = 3$. **H.** Apoptosis rate determined by PI exclusion of PDX leukemic cells with/without treatments with DBZ (48h) at indicated concentrations is shown.

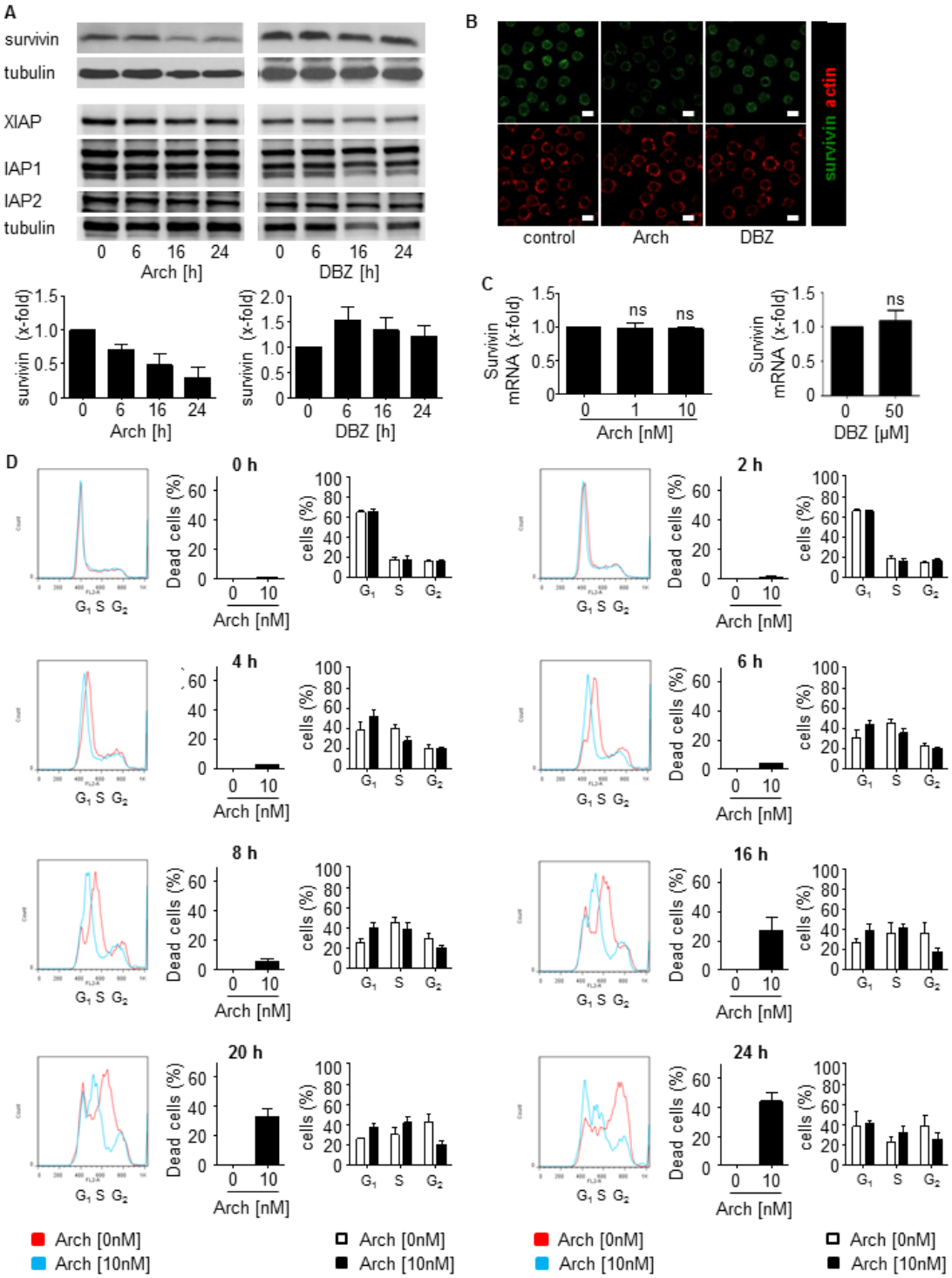

Figure 8: Archazolid A decreases the anti-apoptotic protein survivin and interferes with the cell cycle in leukemic cells. A. Archazolid A decreases the anti-apoptotic protein survivin. Immunoblots from Jurkat cells treated with Archazolid A (Arch, 10 nM, left panel) or DBZ (50 µM, right panel) for the indicated times and probed with antibodies for survivin, XIAP, IAP1, and IAP2 are shown. Immunoblots for tubulin indicate equal loading. $n = 3$. Bar graphs display the quantitative evaluation of survivin expression. **B.** Immunostainings for survivin (green) and actin (red) after treatment with/without Archazolid A (Arch, 10 nM, 24h) and DBZ (50 µM, 24h) is shown. Scale bar 10 µm. **C.** Archazolid A (Arch) and DBZ do not interfere with survivin mRNA expression. Survivin mRNA levels from Jurkat cells treated with Archazolid A (1 and 10 nM) and DBZ (50 µM) for 24h are shown. Not significant (ns), Archazolid A: One-Way ANOVA, DBZ: paired *t*-test, $n = 3$. **D.** Archazolid A (Arch) induces S-phase cell cycle arrest of Jurkat cells. Cell cyle analysis and apoptosis measurement after aphidicolin synchronization (24h) and subsequent treatment with Archazolid A for indicated times is shown. Control cells (untreated, Archazolid A 0 nM) are indicated in red, Archazolid A (Arch, 10 nM) treated cells are indicated in blue. One representative out of three independent experiments is shown.

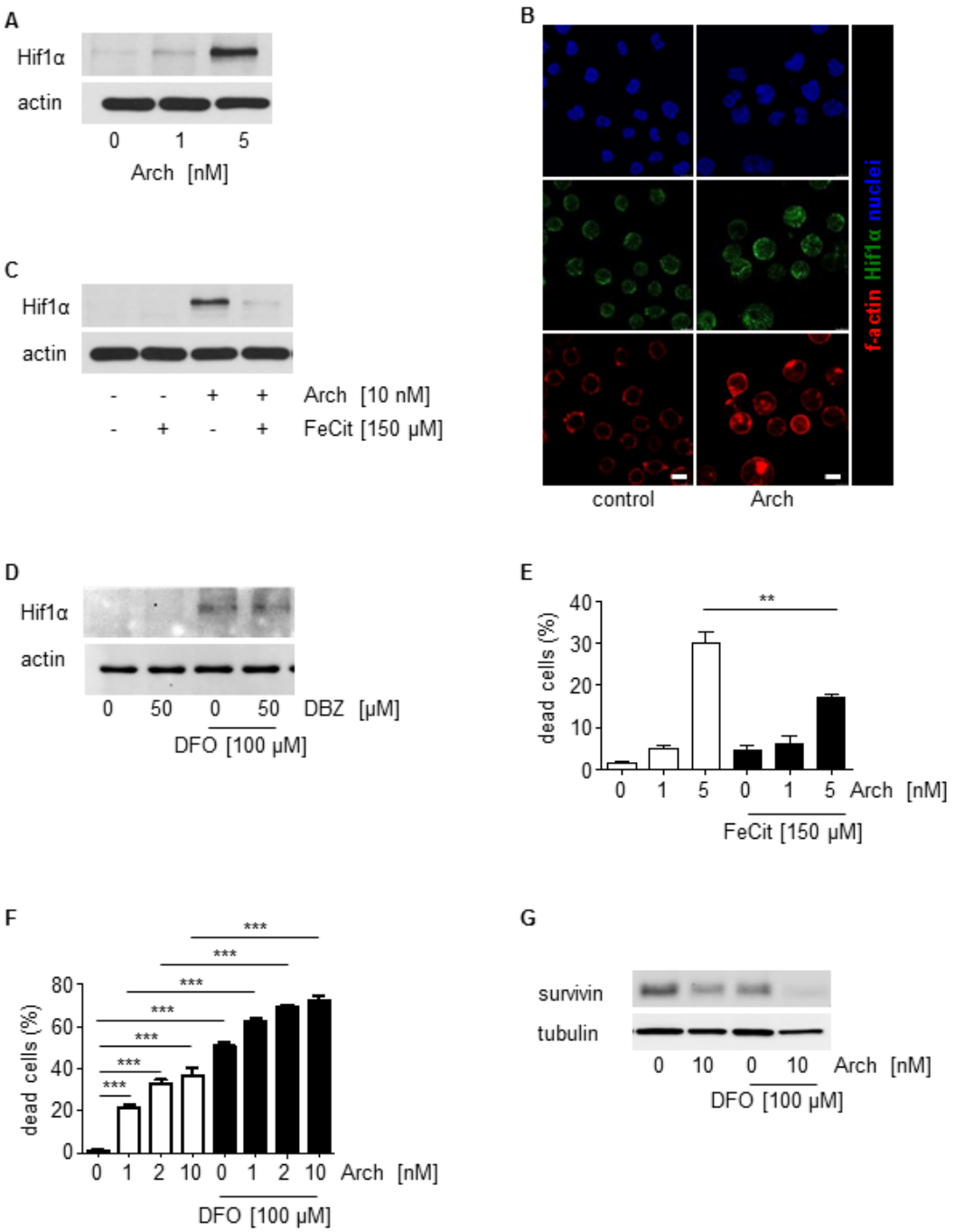

Figure 9: Archazolid A interferes with the iron metabolism in leukemic cells. A. Archazolid A increases Hif1α. Immunoblots show Hif1α levels of Jurkat cells with/without Archazolid A (Arch) treatment at indicated concentrations for 24h. Actin indicates equal loading. **B.** Immunostainings for Hif1α (green) and f-actin (red) after treatment with/without Archazolid A (Arch, 10 nM, 24h) is shown. Nuclei are labeled with Hoechst33342 (blue). Scale bar 7.5 μm. **C.** Archazolid A mediated Hif1α increase is abrogated by iron citrate. Immunoblots show Hif1α levels of Jurkat cells with/without Archazolid A (Arch) and iron citrate (FeCit) treatment at indicated concentrations for 24h. Actin indicates equal loading. $n = 3$. **D.** Inhibition of Notch by DBZ does not influence Hif1α. Immunoblots of Jurkat cells treated with DBZ and deferoxamine (DFO) at indicated concentrations for 24h for Hif1α and actin (loading control) are shown. **E.** Archazolid A mediated cell death is partially rescued by iron citrate. The graph shows cell death of Jurkat cells treated with/without Archazolid A (Arch) and iron citrate (FeCit) at indicated concentrations for 48 h. Mann Whitney test, $^{**}p = 0.0022$, $n = 3$. **F.** DFO induces cell death in Jurkat cells and is enhanced by Archazolid A. Nicoletti assay of cells treated with/without Archazolid A (Arch) and DFO at indicated concentrations for 48 h is shown. One-Way ANOVA, Tukey's post test, $^{***}p \leq 0.001$, $n = 3$. **G.** Survivin is decreased by DFO which is enhanced by Archazolid A. Immunoblots for survivin and tubulin (loading control) from cells treated with/without DFO (100 μM) and Archazolid A (Arch, 10 nM) for 48h are shown; $n = 3$.

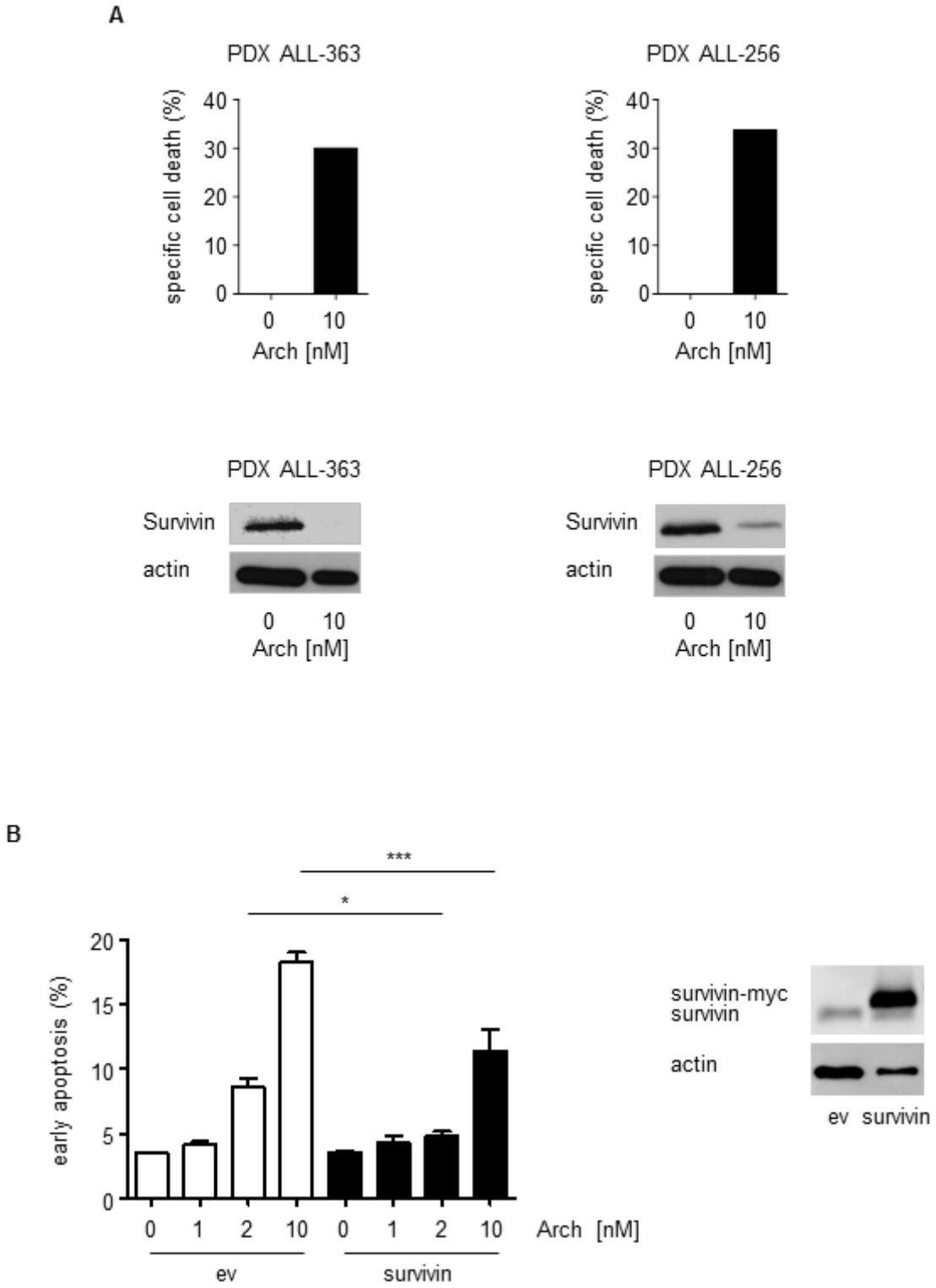

Figure 10: Archazolid A-induced apoptosis in PDX is in line with decreased levels of the anti-apoptotic protein survivin. A. Upper panels show apoptosis rates (specific cell death) determined by PI exclusion staining of PDX leukemia samples treated with Archazolid A (Arch, 10 nM, 48 h). Lower panels display immunoblots from PDX cells from the same patients treated with Archazolid A (Arch, 10 nM, 24 h) and probed with antibodies for survivin. Immunoblots for actin indicate equal loading. **B.** Archazolid A mediated cell death is partially rescued by survivin overexpression. The graph shows early apoptosis (AnnexinV-positive and PI-negative cells) determined by AnnexinV/PI staining of Jurkat cells overexpressing either empty vector (ev) or survivin and treated with/without Archazolid A (Arch) at indicated concentrations for 48 h. One-Way ANOVA, Tukey, $*p \leq 0.05$, $***p \leq 0.001$, $n = 3$. Immunoblots show overexpression of empty vector (ev) and survivin 24h after transfection; actin indicates equal loading.

leukemic cell adhesion [56] and V-ATPase inhibition by Bafilomycin A reduced leukemic cell growth [35].

In search for the signaling pathway responsible for the anti-leukemic effects of Archazolid A-mediated V-ATPase inhibition, first the Notch pathway was analyzed as it is one of the most prominent oncogenic pathways in T-ALL [57]. Targeted therapies addressing the Notch pathway have been proposed as auspicious options for T-ALL treatment. Despite promising *in vitro* results and initial clinical effectiveness of GSIs that block Notch activatory cleavage, this benefit only in some studies translates into improved overall survival [58-60]. In fact, most human T-ALL cell lines are resistant to GSIs that fail to induce leukemic cell death [57]. Therefore, to inhibit Notch signaling with a mechanism different from GSIs might be a promising approach. Our study shows that V-ATPase reduces Notch1 signaling by capturing the Notch whole receptor in the endolysosomal compartment and inhibiting its activatory cleavage. This is in line with reports demonstrating that impaired endolysosomal function by V-ATPase inhibition blocks γ-secretase mediated Notch activatory cleavage at the endolysosomal membrane [11, 35, 37, 38]. However, our rescue experiments revealed that leukemic cell death by Archazolid A was not caused by inhibition of Notch signaling. Moreover, although our results revealed that GSI treatment reduced leukemic cell growth, cell death was not induced. Thus, Archazolid A-mediated induction of leukemic cell death was not based on Notch1 pathway inhibition.

Our work suggests the anti-apoptotic protein survivin as target addressed by Archazolid A to induce leukemic cell death. Survivin exerts multiple cellular functions: it participates in the regulation of cell division, apoptosis, stress response, migration, and metastasis. Whereas it is nearly absent in normal tissues, it is overexpressed in most human tumors, including hematopoietic malignancies [42, 43, 61-63]. Survivin expression has been associated with leukemia progression and poor clinical outcome [64-66]. In consequence, survivin is addressed in cancer therapy by molecular antagonists like antisense oligonucleotides, siRNA, or hammerhead ribozymes, as well as small molecules or cancer immunotherapeutics [67]. Inhibition of survivin has shown clinical benefits and chemosensitizing effects in leukemia [42, 43, 68-70]. By describing potent anti-leukemic effects of Archazolid A, our study probably expands the class of small molecule survivin antagonists.

Survivin expression strongly depends on the cell cycle, i.e. survivin is upregulated and stabilized during G2-phase [41]. Besides regulation at the transcriptional level, changes in protein stability essentially contribute to survivin expression during the cell cycle: proteasome-dependent destruction of survivin has been shown in interphase cells whereas at metaphase, mitotic phosphorylation of survivin by Cdk1 has been associated with increased protein stability [71]. In fact, in line with recent studies from our group addressing V-ATPase in cancer [15, 44], our results presented here suggest that Archazolid decreased survivin at the protein level by inducing S-phase cell cycle arrest in leukemic cells which probably was due to its interference with the iron metabolism.

In line with previous studies from our group showing that Archazolid B led to cellular stress response and induction of Hif1α [15, 44], our present study suggests that the induction of Hif1α contributes to Archazolid A induced leukemic cell death. Although the stabilization of Hif1α during hypoxia is generally pro-proliferative as stabilization of Hif1α influences the survival of tumor cells, Hif1α has also tumor-inhibiting properties. In detail, Hif1α overexpression inhibits cell proliferation by expressing cell cycle inhibitors like p53, p21, and p27 and promotes apoptosis by inducing pro-apoptotic molecules such as p53, Nip3, and Noxa [45-48].

A recent study from our group demonstrated that inhibition of V-ATPase by Archazolid B led to iron depletion by disruption of transferrin receptor recycling which subsequently reduced ribonucleotide reductase (RNR) activity, induced S-phase cell cycle arrest and finally caused cell death [44]. Interestingly, iron overload due to inefficient erythropoiesis or blood transfusion represents a major problem in patients suffering from myelodysplastic syndromes (MDS), clonal disorders with ineffective hematopoiesis and an increased risk of transformation into acute myeloid leukemia. Iron overload is associated with osteopenia and osteoporosis in these patients [72, 73]. In consequence, V-ATPase inhibition in hematopoietic diseases might be an interesting object for further studies.

To conclude, our study provides evidence for V-ATPase inhibition as new alternative strategy and Archazolid A as interesting new compound for T-ALL therapy.

MATERIALS AND METHODS

Cells

Cell lines: Human leukemia Jurkat T cells (J16, S-Jurkat) were kindly provided by P.H. Krammer and H. Walczak, Heidelberg, Germany. S-Jurkat cells were cultured in RPMI 1640 (PAN Biotech, Aidenbach, Germany) containing 10% FCS (PAA Laboratories, Cölbe, Germany) and 1% pyruvate (Merck, Darmstadt, Germany). CCRF-CEM cells were kindly provided by Dr. Joachim Arend (Mainz, Germany) and cultured in RPMI 1640 containing 10% FCS.

Reagents

The γ-secretase inhibitor DBZ was purchased from Merck Millipore. The pan-caspase inhibitor QVD-OPh (551476) was purchased from Calbiochem. Deferoxamine (DFO) was purchased from Sigma.

Patient-derived xenograft (PDX) leukemic cells

The xenograft mouse model, the transplantation of patient's primary tumor cells, and the cell amplification have been described previously [39, 40]. In detail, primary leukemic cells were obtained from diagnostic bone marrow aspiration or peripheral blood sampling before onset of treatment. Xenografts were established by injecting 10^7 fresh or frozen/thawed primary leukemic cells into NSG mice (NOD SCID gamma mice, i.e. mice with dysfunctional gamma chain of the IL-2R receptor) by tail vein injection. Development of leukemia was monitored by repetitive blood sampling in mice and by determining human leukemic cells in flow cytometry upon staining of murine CD45 and human CD38. At clear leukemic engraftment or by latest after 25 weeks, mice were sacrificed and human patient-derived xenograft (PDX) leukemic cells were isolated either from bone marrow or from spleens of mice using Ficoll purification. Phenotypic markers and genetic aberrations in PDX cells compared to primary leukemic tumor cells remained mainly stable as shown before [25]. For stimulation and during experiments, cells were maintained in RPMI 1640 medium containing 20% FCS and 1% glutamine. Freshly isolated PDX leukemic cells were stimulated as indicated *in vitro*.

Primary non-tumor human peripheral blood mononuclear cells (PBMCs)

Isolation of primary non-tumor human PBMCs was performed using the "Ficoll-Paque PLUS" kit from GE Healthcare according to the manufacturer's instructions. Briefly, EDTA (1.5mg/ml) blood (2 ml) was mixed with balanced salt solution (2 ml), added on top of Ficoll-Paque PLUS (3ml) in a 15ml centrifuge tube, and centrifuged (400×g, 40min, RT). Afterwards, PBMCs were carefully withdrawn from the interface between the upper plasma layer and the lower Ficoll-Paque PLUS layer, washed twice by 3 volumes of balanced salt solution, centifuged (100×g, 10 min, RT) and resuspended in culture medium (RPMI 1640+20%FCS+1%Glutamine). PBMCs were directly used for the respective assays.

For FACS analysis, gating of lymphocytes was performed and only these cells were included in the evaluation.

Tansfection of cells

Cell transfection was performed by using the Amaxxa system with the cell line nucleofector kit V (Lonza, VCA-1003) according to the manufacturer's instructions. 1×10^6 cells were electroporated (program X-001). NICD plasmid was from addgene (20183). Survivin plasmid was from Sino Biologicals (pCMV3-BIRC5-myc, HG10356-CM G09AU4M62). For respective assays, cells were used 24h (NICD) or 48h (survivin) after transfection.

Proliferation

CellTiter-Blue® assay was performed according manufacturer's instructions. Briefly, cells were seeded (96 well plates, 3×10^3 cells/well) for 24 h, treated with Archazolid A or DBZ at indicated concentrations and incubated for 70 h. CTB solution (20µl) was added and cells were incubated for 2h. Fluorescence was measured with a Tecan reader (Maennedorf, Austria).

PDX viability

PDX leukemic cells were seeded (96 well plates, $1x10^5$ cells/well) and the cells were treated with Archazolid A at indicated concentrations for 72h. Cell Titer Blue assay was performed according manufacturer's instructions as described before at "proliferation". For calculating viability, the value from the time of plating was subtracted.

Apoptosis and cell cycle

Apoptosis and cell cycle analysis were performed according to the Nicoletti method [74]. In brief, cells were seeded (24 well plates, 0.5×10^4 cells/well for 48 h, 2.5×10^4 cells/well for 72 h) and treated with Archazolid A or DBZ at indicated concentrations. For DNA staining, cells were permeabilized and stained by resuspension in hypotonic fluorochrome solution (HFS) containing propidium iodide (PI, 50 µg/ml) and incubated at 4°C overnight. Subsequently, flow cytometry was performed on a FACSCalibur (Becton Dickinson, Heidelberg, Germany). The sub-G1 peak accounts for apoptotic cells and was determined according to Nicoletti [74]. Cell cycle was analyzed by using FlowJo 7.6 (Tree Star Unc., Ashland, USA).

PI exclusion

Cells were seeded (96 well plates, 1×10^5 cells/well and treated with Archazolid A or DBZ at indicated

concentrations. Subsequently, cells were incubated with PI (5 µg/ml, 5 min) that was added to the cell suspension before analysis by flow cytometry. Subsequently, flow cytometry was performed on a FACSCalibur (Becton Dickinson, Heidelberg, Germany) using the Fl-2 laser.

As cells were not permeabilized, PI staining was exclusive for dead cells, whereas viable cells were not stained by PI. For quantification, PI positive dead cells can be seen in dot plots at the left and in histograms at the right and are shown in red; PI negative viable cells can be seen in dot plots at the right and in histograms at the left and are shown in green (Figure 4A).

Annexin V/PI staining

Annexin V/PI staining was performed by using the Annexin V-FITC Apoptosis Detection Kit (eBioscience Dx, BMS500FI/300CE) according to the manufacturer's protocol. Briefly, cells were treated as indicated, collected, centrifuged (600g, 4 °C, 10min), washed with PBS, centrifuged again (600g, 4 °C, 10min) and resuspended in binding buffer. 5µl AnnexinV-FITC were added to 195µl of cell suspension, cells were mixed and incubated at RT for 10 min (cover from light), centrifuged (600g, 4 °C, 10min), washed with 200µl Binding Buffer and resuspended in Binding Buffer. 10µl PI (20µg/ml) was added to 190 µl of cell suspension and FACS analysis was performed using Fl-2 and Fl-3 lasers. AnnexinV positive cells have been considered as apoptotic. AnnexinV positive and PI negative cells have been considered as early apoptotic.

For primary PDX leukemic cells, the specific apoptosis was calculated according to the following formula: % specific apoptosis = 100 × (% total apoptosis of treated cells - % total apoptosis of untreated cells) / (100 - % total apoptosis untreated cells) [75].

For primary non-tumor human PBMCs, gating of lymphocytes was performed and only these cells were included in the evaluation.

Colony formation

Cells were seeded (6 well plates, 5×10^5 cells/well) and treated with Archazolid A or DBZ at indicated concentrations for 24h. Cells were freshly plated (96 well plates, 5×10^3 cells/well) in RPMI 1640 Medium containing 40% FCS, 0.52% Methylcellulose, and 1% Sodium Pyruvate and incubated for 11 d. Images from each well were taken with a Zeiss 510 Meta Confocal Microscope. Colonies were counted by using Image J with the cell counter plugin.

Immunoblotting

Immunoblotting was performed as described [76]. The following primary antibodies were used: actin (MAB1501 Millipore), BCL-XL (2762 Cell Signaling), BNIP3 (ab10433 Abcam), Caspase 3 (sc-7148 Santa Cruz), Caspase 9 (9506 Cell Signaling), Hif1α (610958 BD), IAP-1 (4952 Cell Signaling), IAP-2 (3130 Cell Signaling), NICD (4147 Cell Signaling), Notch1 (4380 Cell Signaling), c-Myc (sc-788 Santa Cruz), survivin (2803 Cell Signaling), β-tubulin (2164 Cell Signaling), XIAP (610717 BD).

RT-PCR

mRNA was isolated using the Qiagen RNeasy Mini Kit. For reverse transcription the High-Capacity cDNA Reverse Transcription Kit (Applied Biosystems) was used. RT-PCR was performed with the 7300 Real Time PCR System.

For RT-PCR of Notch downstream targets, the following Taqman gene expression assays were used: Hes1 Hs00172878, HEY1 Hs00232618, HEY2 Hs00232622, NRARP Hs01104102 (Life Technologies Corporation, Carlsbad, CA, USA). GAPDH was used as housekeeper.

For RT-PCR for V-ATPase subunits, SYBR® Green PCR Master Mix (4309155, Life Technologies) was used. A list with the primer sequences for all V-ATPase subunits is included in Supplementary Table 1.

Confocal microscopy

For Immunostaining with antibodies, cells were treated as indicated, collected, resuspended and seeded on chrome alum-gelatin (0.05% $CrK(SO_4)_2\cdot12H_2O$, 0.4% gelatine in H_2O) coated coverslips (30 min). Cells were fixed (4% PFA, 10mins), permablized (0.2% Triton X 100 in PBS, 5min), blocked (0.2% BSA in PBS, 1 h), incubated with primary antibodies (0.2% BSA in PBS, 1h) and subsequently secondary antibodies (0.2% BSA in PBS, 1h) and mounted. The following primary antibodies were used: EEA1 (sc-6415, Santa Cruz), LAMP1 (H4A3, Developmental Studies Hybridoma Bank), NICD (4147 Cell Signalling), Notch1 (4308, Cell Signaling). Alexa Fluor conjugated secondary antibodies (Molecular Probes) were used.

For LysoTracker experiment, cells were treated as indicated, collected, and stained with LysoTracker (Molecular Probes) for 45min. After Hoechst33342 staining (5 µg/ml, 5min), confocal microscopy was performed with a Zeiss LSM 510 META confocal microscope.

For the evaluation of the size of the endolysosomal compartment, EEA1 staining was performed. The size

of the endolysosomal compartment was analyzed by calculating the EEA1-positive area per cell by using ImageJ. Approximately 20 cells per cell line were randomly selected for the evaluation.

The quantification of the intensities of Notch1 and NICD staining was performed by using Image J. The total intensity of the whole image was divided by the number of cells. Cells on the border of the images were excluded.

Statistic evaluation

All experiments were performed at least 3 times in duplicates/triplicates. Results are expressed as mean value ± SEM. One-way ANOVA/Tukey and individual t-tests were conducted using GraphPad Prism (version 5.04, GraphPad Software, Inc.). P values less than 0.05 were considered as significant.

ACKNOWLEDGMENTS

The authors thank Kerstin Loske and Jana Peliskova for their help with the experiments.

FUNDING

S.Z. was supported by the Chinese Scholarship Council (CSC). A.M.V. received financial support by the German Research Foundation (DFG, FOR 1406, Vo 376-14/15)

CONFLICTS OF INTEREST

The authors declare no conflict of interest.

REFERENCES

1. Van Vlierberghe P and Ferrando A. The molecular basis of T cell acute lymphoblastic leukemia. J Clin Invest. 2012; 122:3398-3406.
2. Koch U and Radtke F. Notch in T-ALL: new players in a complex disease. Trends Immunol. 2011; 32:434-442.
3. Pancewicz J and Nicot C. Current views on the role of Notch signaling and the pathogenesis of human leukemia. BMC Cancer. 2011; 11:502.
4. De Falco F, Sabatini R, Del Papa B, Falzetti F, Di Ianni M, Sportoletti P, Baldoni S, Screpanti I, Marconi P and Rosati E. Notch signaling sustains the expression of Mcl-1 and the activity of eIF4E to promote cell survival in CLL. Oncotarget. 2015; 6:16559-16572.
5. Rosati E, Sabatini R, Rampino G, Tabilio A, Di Ianni M, Fettucciari K, Bartoli A, Coaccioli S, Screpanti I and Marconi P. Constitutively activated Notch signaling is involved in survival and apoptosis resistance of B-CLL cells. Blood. 2009; 113:856-865.
6. Rosati E, Sabatini R, De Falco F, Del Papa B, Falzetti F, Di Ianni M, Cavalli L, Fettucciari K, Bartoli A, Screpanti I and Marconi P. gamma-Secretase inhibitor I induces apoptosis in chronic lymphocytic leukemia cells by proteasome inhibition, endoplasmic reticulum stress increase and notch down-regulation. Int J Cancer. 2013; 132:1940-1953.
7. Tian C, Yu Y, Jia Y, Zhu L and Zhang Y. HES1 activation suppresses proliferation of leukemia cells in acute myeloid leukemia. Annals of hematology. 2015; 94:1477-83.
8. Kannan S, Sutphin RM, Hall MG, Golfman LS, Fang W, Nolo RM, Akers LJ, Hammitt RA, McMurray JS, Kornblau SM, Melnick AM, Figueroa ME and Zweidler-McKay PA. Notch activation inhibits AML growth and survival: a potential therapeutic approach. J Exp Med. 2013; 210:321-337.
9. Kato T, Sakata-Yanagimoto M, Nishikii H, Ueno M, Miyake Y, Yokoyama Y, Asabe Y, Kamada Y, Muto H, Obara N, Suzukawa K, Hasegawa Y, Kitabayashi I, Uchida K, Hirao A, Yagita H, et al. Hes1 suppresses acute myeloid leukemia development through FLT3 repression. Leukemia. 2015; 29:576-585.
10. Vaccari T, Lu H, Kanwar R, Fortini ME and Bilder D. Endosomal entry regulates Notch receptor activation in Drosophila melanogaster. J Cell Biol. 2008; 180:755-762.
11. Vaccari T, Duchi S, Cortese K, Tacchetti C and Bilder D. The vacuolar ATPase is required for physiological as well as pathological activation of the Notch receptor. Development. 2010; 137:1825-1832.
12. Nishi T and Forgac M. The vacuolar (H+)-ATPases—nature's most versatile proton pumps. Nat Rev Mol Cell Biol. 2002; 3:94-103.
13. Forgac M. Vacuolar ATPases: rotary proton pumps in physiology and pathophysiology. Nat Rev Mol Cell Biol. 2007; 8:917-929.
14. Cotter K, Capecci J, Sennoune S, Huss M, Maier M, Martinez-Zaguilan R and Forgac M. Activity of plasma membrane V-ATPases is critical for the invasion of MDA-MB231 breast cancer cells. J Biol Chem. 2015; 290:3680-3692.
15. von Schwarzenberg K, Wiedmann RM, Oak P, Schulz S, Zischka H, Wanner G, Efferth T, Trauner D and Vollmar AM. Mode of cell death induction by pharmacological vacuolar H+-ATPase (V-ATPase) inhibition. J Biol Chem. 2013; 288:1385-1396.
16. Wiedmann RM, von Schwarzenberg K, Palamidessi A, Schreiner L, Kubisch R, Liebl J, Schempp C, Trauner D, Vereb G, Zahler S, Wagner E, Muller R, Scita G and Vollmar AM. The V-ATPase-inhibitor archazolid abrogates tumor metastasis via inhibition of endocytic activation of the Rho-GTPase Rac1. Cancer Res. 2012; 72:5976-5987.
17. Schempp CM, von Schwarzenberg K, Schreiner L, Kubisch R, Muller R, Wagner E and Vollmar AM. V-ATPase inhibition regulates anoikis resistance and metastasis of cancer cells. Mol Cancer Ther. 2014; 13:926-937.

18. Kubisch R, Frohlich T, Arnold GJ, Schreiner L, von Schwarzenberg K, Roidl A, Vollmar AM and Wagner E. V-ATPase inhibition by archazolid leads to lysosomal dysfunction resulting in impaired cathepsin B activation *in vivo*. Int J Cancer. 2014; 134:2478-2488.

19. Chung C, Mader CC, Schmitz JC, Atladottir J, Fitchev P, Cornwell ML, Koleske AJ, Crawford SE and Gorelick F. The vacuolar-ATPase modulates matrix metalloproteinase isoforms in human pancreatic cancer. Laboratory investigation; a journal of technical methods and pathology. 2011; 91:732-743.

20. Nishisho T, Hata K, Nakanishi M, Morita Y, Sun-Wada GH, Wada Y, Yasui N and Yoneda T. The a3 isoform vacuolar type H(+)-ATPase promotes distant metastasis in the mouse B16 melanoma cells. Mol Cancer Res. 2011; 9:845-855.

21. Michel V, Licon-Munoz Y, Trujillo K, Bisoffi M and Parra KJ. Inhibitors of vacuolar ATPase proton pumps inhibit human prostate cancer cell invasion and prostate-specific antigen expression and secretion. Int J Cancer. 2013; 132:E1-10.

22. Avnet S, Di Pompo G, Lemma S, Salerno M, Perut F, Bonuccelli G, Granchi D, Zini N and Baldini N. V-ATPase is a candidate therapeutic target for Ewing sarcoma. Biochimica et biophysica acta. 2013; 1832:1105-1116.

23. Perut F, Avnet S, Fotia C, Baglio SR, Salerno M, Hosogi S, Kusuzaki K and Baldini N. V-ATPase as an effective therapeutic target for sarcomas. Exp Cell Res. 2014; 320:21-32.

24. Di Cristofori A, Ferrero S, Bertolini I, Gaudioso G, Russo MV, Berno V, Vanini M, Locatelli M, Zavanone M, Rampini P, Vaccari T, Caroli M and Vaira V. The vacuolar H+ ATPase is a novel therapeutic target for glioblastoma. Oncotarget. 2015; 6:17514-31.

25. Hamm R, Zeino M, Frewert S and Efferth T. Up-regulation of cholesterol associated genes as novel resistance mechanism in glioblastoma cells in response to archazolid B. Toxicology and applied pharmacology. 2014; 281:78-86.

26. Huss M and Wieczorek H. Inhibitors of V-ATPases: old and new players. J Exp Biol. 2009; 212(Pt 3):341-346.

27. Bockelmann S, Menche D, Rudolph S, Bender T, Grond S, von Zezschwitz P, Muench SP, Wieczorek H and Huss M. Archazolid A binds to the equatorial region of the c-ring of the vacuolar H+-ATPase. J Biol Chem. 2010; 285:38304-38314.

28. Huss M, Sasse F, Kunze B, Jansen R, Steinmetz H, Ingenhorst G, Zeeck A and Wieczorek H. Archazolid and apicularen: novel specific V-ATPase inhibitors. BMC biochemistry. 2005; 6:13.

29. Huss M, Vitavska O, Albertmelcher A, Bockelmann S, Nardmann C, Tabke K, Tiburcy F and Wieczorek H. Vacuolar H(+)-ATPases: intra- and intermolecular interactions. Eur J Cell Biol. 2011; 90:688-695.

30. Sasse F, Steinmetz H, Hofle G and Reichenbach H. Archazolids, new cytotoxic macrolactones from Archangium gephyra (Myxobacteria). Production, isolation, physico-chemical and biological properties. The Journal of antibiotics. 2003; 56:520-525.

31. Menche D, Hassfeld J, Li J and Rudolph S. Total synthesis of archazolid A. Journal of the American Chemical Society. 2007; 129:6100-6101.

32. Roethle PA, Chen IT and Trauner D. Total synthesis of (-)-archazolid B. Journal of the American Chemical Society. 2007; 129:8960-8961.

33. Rath S, Liebl J, Furst R, Vollmar AM and Zahler S. Regulation of endothelial signaling and migration by v-ATPase. Angiogenesis. 2014; 17:587-601.

34. von Schwarzenberg K, Lajtos T, Simon L, Muller R, Vereb G and Vollmar AM. V-ATPase inhibition overcomes trastuzumab resistance in breast cancer. Mol Oncol. 2014; 8:9-19.

35. Kobia F, Duchi S, Deflorian G and Vaccari T. Pharmacologic inhibition of vacuolar H+ ATPase reduces physiologic and oncogenic Notch signaling. Mol Oncol. 2014; 8:207-220.

36. Perez-Sayans M, Somoza-Martin JM, Barros-Angueira F, Rey JM and Garcia-Garcia A. V-ATPase inhibitors and implication in cancer treatment. Cancer Treat Rev. 2009; 35:707-713.

37. Yan Y, Denef N and Schupbach T. The vacuolar proton pump, V-ATPase, is required for notch signaling and endosomal trafficking in Drosophila. Dev Cell. 2009; 17:387-402.

38. Valapala M, Hose S, Gongora C, Dong L, Wawrousek EF, Samuel Zigler J, Jr. and Sinha D. Impaired endolysosomal function disrupts Notch signalling in optic nerve astrocytes. Nat Commun. 2013; 4:1629.

39. Terziyska N, Castro Alves C, Groiss V, Schneider K, Farkasova K, Ogris M, Wagner E, Ehrhardt H, Brentjens RJ, zur Stadt U, Horstmann M, Quintanilla-Martinez L and Jeremias I. *In vivo* imaging enables high resolution preclinical trials on patients‘ leukemia cells growing in mice. PLoS One. 2012; 7:e52798.

40. Vick B, Rothenberg M, Sandhofer N, Carlet M, Finkenzeller C, Krupka C, Grunert M, Trumpp A, Corbacioglu S, Ebinger M, Andre MC, Hiddemann W, Schneider S, Subklewe M, Metzeler KH, Spiekermann K, et al. An advanced preclinical mouse model for acute myeloid leukemia using patients‘ cells of various genetic subgroups and *in vivo* bioluminescence imaging. PLoS One. 2015; 10:e0120925.

41. Altieri DC. Survivin, cancer networks and pathway-directed drug discovery. Nat Rev Cancer. 2008; 8:61-70.

42. Park E, Gang EJ, Hsieh YT, Schaefer P, Chae S, Klemm L, Huantes S, Loh M, Conway EM, Kang ES, Hoe Koo H, Hofmann WK, Heisterkamp N, Pelus L, Keerthivasan G, Crispino J, et al. Targeting survivin overcomes drug resistance in acute lymphoblastic leukemia. Blood. 2011;

118:2191-2199.

43. Purroy N, Abrisqueta P, Carabia J, Carpio C, Calpe E, Palacio C, Castellvi J, Crespo M and Bosch F. Targeting the proliferative and chemoresistant compartment in chronic lymphocytic leukemia by inhibiting survivin protein. Leukemia. 2014; 28(10):1993-2004.
44. Schneider LS, von Schwarzenberg K, Lehr T, Ulrich M, Kubisch-Dohmen R, Liebl J, Trauner D, Menche D and Vollmar AM. Vacuolar-ATPase Inhibition Blocks Iron Metabolism to Mediate Therapeutic Effects in Breast Cancer. Cancer Res. 2015; 75:2863-2874.
45. Greijer AE and van der Wall E. The role of hypoxia inducible factor 1 (HIF-1) in hypoxia induced apoptosis. Journal of clinical pathology. 2004; 57:1009-1014.
46. Koshiji M and Huang LE. Dynamic balancing of the dual nature of HIF-1alpha for cell survival. Cell Cycle. 2004; 3:853-854.
47. Sermeus A and Michiels C. Reciprocal influence of the p53 and the hypoxic pathways. Cell death & disease. 2011; 2:e164.
48. Fridman JS and Lowe SW. Control of apoptosis by p53. Oncogene. 2003; 22:9030-9040.
49. Sennoune SR, Bermudez LE, Lees JC, Hirsch J, Filleur S and Martinez-Zaguilan R. Vacuolar H+-ATPase is down-regulated by the angiogenesis-inhibitory pigment epithelium-derived factor in metastatic prostate cancer cells. Cell Mol Biol (Noisy-le-grand). 2014; 60:45-52.
50. Hinton A, Sennoune SR, Bond S, Fang M, Reuveni M, Sahagian GG, Jay D, Martinez-Zaguilan R and Forgac M. Function of a subunit isoforms of the V-ATPase in pH homeostasis and *in vitro* invasion of MDA-MB231 human breast cancer cells. J Biol Chem. 2009; 284:16400-16408.
51. Fan SH, Wang YY, Lu J, Zheng YL, Wu DM, Zhang ZF, Shan Q, Hu B, Li MQ and Cheng W. CERS2 Suppresses Tumor Cell Invasion and Is Associated with Decreased V-ATPase and MMP-2/MMP-9 activities in Breast Cancer. J Cell Biochem. 2015; 116:502-13.
52. Graham RM, Thompson JW and Webster KA. Inhibition of the vacuolar ATPase induces Bnip3-dependent death of cancer cells and a reduction in tumor burden and metastasis. Oncotarget. 2014; 5:1162-1173.
53. Scherer O, Steinmetz H, Kaether C, Weinigel C, Barz D, Kleinert H, Menche D, Muller R, Pergola C and Werz O. Targeting V-ATPase in primary human monocytes by archazolid potently represses the classical secretion of cytokines due to accumulation at the endoplasmic reticulum. Biochem Pharmacol. 2014; 91:490-500.
54. De Milito A, Iessi E, Logozzi M, Lozupone F, Spada M, Marino ML, Federici C, Perdicchio M, Matarrese P, Lugini L, Nilsson A and Fais S. Proton pump inhibitors induce apoptosis of human B-cell tumors through a caspase-independent mechanism involving reactive oxygen species. Cancer Res. 2007; 67:5408-5417.
55. Sukhai MA, Prabha S, Hurren R, Rutledge AC, Lee AY, Sriskanthadevan S, Sun H, Wang X, Skrtic M, Seneviratne A, Cusimano M, Jhas B, Gronda M, MacLean N, Cho EE, Spagnuolo PA, et al. Lysosomal disruption preferentially targets acute myeloid leukemia cells and progenitors. J Clin Invest. 2013; 123:315-328.
56. Funayama K, Murai F, Shimane M, Nomura H and Asano S. Adhesion-induced drug resistance in leukemia stem cells. Pharmacology. 2010; 86:79-84.
57. O'Neil J, Grim J, Strack P, Rao S, Tibbitts D, Winter C, Hardwick J, Welcker M, Meijerink JP, Pieters R, Draetta G, Sears R, Clurman BE and Look AT. FBW7 mutations in leukemic cells mediate NOTCH pathway activation and resistance to gamma-secretase inhibitors. J Exp Med. 2007; 204:1813-1824.
58. Breit S, Stanulla M, Flohr T, Schrappe M, Ludwig WD, Tolle G, Happich M, Muckenthaler MU and Kulozik AE. Activating NOTCH1 mutations predict favorable early treatment response and long-term outcome in childhood precursor T-cell lymphoblastic leukemia. Blood. 2006; 108:1151-1157.
59. van Grotel M, Meijerink JP, Beverloo HB, Langerak AW, Buys-Gladdines JG, Schneider P, Poulsen TS, den Boer ML, Horstmann M, Kamps WA, Veerman AJ, van Wering ER, van Noesel MM and Pieters R. The outcome of molecular-cytogenetic subgroups in pediatric T-cell acute lymphoblastic leukemia: a retrospective study of patients treated according to DCOG or COALL protocols. Haematologica. 2006; 91:1212-1221.
60. Mansour MR, Sulis ML, Duke V, Foroni L, Jenkinson S, Koo K, Allen CG, Gale RE, Buck G, Richards S, Paietta E, Rowe JM, Tallman MS, Goldstone AH, Ferrando AA and Linch DC. Prognostic implications of NOTCH1 and FBXW7 mutations in adults with T-cell acute lymphoblastic leukemia treated on the MRC UKALLXII/ECOG E2993 protocol. J Clin Oncol. 2009; 27:4352-4356.
61. Carter BZ, Milella M, Altieri DC and Andreeff M. Cytokine-regulated expression of survivin in myeloid leukemia. Blood. 2001; 97:2784-2790.
62. Carter BZ, Qiu Y, Huang X, Diao L, Zhang N, Coombes KR, Mak DH, Konopleva M, Cortes J, Kantarjian HM, Mills GB, Andreeff M and Kornblau SM. Survivin is highly expressed in CD34(+)38(-) leukemic stem/progenitor cells and predicts poor clinical outcomes in AML. Blood. 2012; 120:173-180.
63. Fukuda S, Hoggatt J, Singh P, Abe M, Speth JM, Hu P, Conway EM, Nucifora G, Yamaguchi S and Pelus LM. Survivin modulates genes with divergent molecular functions and regulates proliferation of hematopoietic stem cells through Evi-1. Leukemia. 2015; 29:433-40.
64. Smolewski P and Robak T. Inhibitors of apoptosis proteins (IAPs) as potential molecular targets for therapy of hematological malignancies. Curr Mol Med. 2011; 11:633-649.
65. Glodkowska-Mrowka E, Solarska I, Mrowka P, Bajorek K, Niesiobedzka-Krezel J, Seferynska I, Borg K and Stoklosa

T. Differential expression of BIRC family genes in chronic myeloid leukaemia—BIRC3 and BIRC8 as potential new candidates to identify disease progression. Br J Haematol. 2014; 164:740-742.

66. Moore AS, Alonzo TA, Gerbing RB, Lange BJ, Heerema NA, Franklin J, Raimondi SC, Hirsch BA, Gamis AS and Meshinchi S. BIRC5 (survivin) splice variant expression correlates with refractory disease and poor outcome in pediatric acute myeloid leukemia: a report from the Children's Oncology Group. Pediatr Blood Cancer. 2014; 61:647-652.
67. Altieri DC. Targeting survivin in cancer. Cancer Lett. 2013; 332:225-228.
68. Raetz EA, Morrison D, Romanos-Sirakis E, Gaynon P, Sposto R, Bhojwani D, Bostrom BC, Brown P, Eckroth E, Cassar J, Malvar J, Buchbinder A and Carroll WL. A phase I study of EZN-3042, a novel survivin messenger ribonucleic acid (mRNA) antagonist, administered in combination with chemotherapy in children with relapsed acute lymphoblastic leukemia (ALL): a report from the therapeutic advances in childhood leukemia and lymphoma (TACL) consortium. J Pediatr Hematol Oncol. 2014; 36:458-463.
69. Chen J, Pise-Masison CA, Shih JH, Morris JC, Janik JE, Conlon KC, Keating A and Waldmann TA. Markedly additive antitumor activity with the combination of a selective survivin suppressant YM155 and alemtuzumab in adult T-cell leukemia. Blood. 2013; 121:2029-2037.
70. Andersen MH, Svane IM, Becker JC and Straten PT. The universal character of the tumor-associated antigen survivin. Clin Cancer Res. 2007; 13:5991-5994.
71. Altieri DC. Validating survivin as a cancer therapeutic target. Nat Rev Cancer. 2003; 3:46-54.
72. Bulycheva E, Rauner M, Medyouf H, Theurl I, Bornhauser M, Hofbauer LC and Platzbecker U. Myelodysplasia is in the niche-novel concepts and emerging therapies. Leukemia. 2015; 29:259-68.
73. Breccia M and Alimena G. Efficacy and safety of deferasirox in myelodysplastic syndromes. Ann Hematol. 2013; 92:863-870.
74. Nicoletti I, Migliorati G, Pagliacci MC, Grignani F and Riccardi C. A rapid and simple method for measuring thymocyte apoptosis by propidium iodide staining and flow cytometry. J Immunol Methods. 1991; 139:271-279.
75. Muscolini M, Cianfrocca R, Sajeva A, Mozzetti S, Ferrandina G, Costanzo A and Tuosto L. Trichostatin A up-regulates p73 and induces Bax-dependent apoptosis in cisplatin-resistant ovarian cancer cells. Mol Cancer Ther. 2008; 7:1410-1419.
76. Liebl J, Zhang S, Moser M, Agalarov Y, Demir CS, Hager B, Bibb JA, Adams RH, Kiefer F, Miura N, Petrova TV, Vollmar AM and Zahler S. Cdk5 controls lymphatic vessel development and function by phosphorylation of Foxc2. Nat Commun. 2015; 6:7274.

MDM2 antagonist nutlin-3a sensitizes tumors to V-ATPase inhibition

Lina S. Schneider[a], Melanie Ulrich[a], Thorsten Lehr[b], Dirk Menche[c], Rolf Müller[d], Angelika M. Vollmar[a], Karin von Schwarzenberg[a]

[a]Department of Pharmacy, Pharmaceutical Biology, Ludwig-Maximilians-University of Munich, Butenandtstrasse 5-13, 81377 Munich, Germany

[b]Clinical Pharmacy, Saarland University, Campus C2 2, 66123 Saarbrücken, Germany

[c]Kekulé Institute of Organic Chemistry and Biochemistry, University of Bonn, Gerhard-Domagk-Str. 1, 53121 Bonn, Germany

[d]Saarland University, Helmholtz Institute for Pharmaceutical Research Saarland, Helmholtz Centre for Infection Research and Department of Pharmaceutical Biotechnology, PO 151150, 66042 Saarbrücken, Germany

Corresponding author: Dr. Karin von Schwarzenberg, Department of Pharmacy, Butenandtstrasse 5-13, 81377 Munich, Germany, Phone: +49-89-2180-77165, Email: karin.von.schwarzenberg@cup.uni-muenchen.de

Conflict of interest: There is no conflict of interest.

Abbreviations: [1] vacuolar-type ATPase, [2] oxidative phosphorylation, [3] TP53-induced glycolysis and apoptosis regulator, [4] U87MG, [5] insulin-like growth factor-binding protein 3

ABSTRACT

Treating cancer is one of the big challenges of this century and it has become evident that single chemotherapeutic treatment is rarely effective. As tumors often carry multiple mutations using combination therapy which addresses different targets seems therefore more beneficial. One of the most frequently mutated genes in tumors is the tumor suppressor p53. A lot of work has been put in the development of p53 activators, which are now in clinical studies against diverse cancers. Recently, we could show that inhibition of V-ATPase, a multisubunit proton pump, by archazolid induces p53 protein levels in cancer cells. In this study, we provide evidence that the combination of archazolid with the p53 activator nutlin-3a is synergistically inducing cell death in different p53 wild type tumor cell lines. Mechanistically, this effect could presumably be attributed to reduction of glycolysis as TIGAR mRNA levels were increased and glucose uptake and Glut1 protein levels were reduced. In addition, combination treatment highly activated pro-apoptotic pathways including IGFBP3 and Bax inducing caspase-9 and PARP cleavage. Remarkably, combination of archazolid and nutlin-3a was more efficient in reducing tumor growth compared to single dose treatment in a U87MG mouse model *in vivo*. Hence, our findings suggest the combination of archazolid and nutlin-3a as a highly promising strategy for the treatment of p53 wild type tumors.

Keywords: cancer, therapy, p53, V-ATPase, nutlin-3a

1. INTRODUCTION

Cancer is a major health problem worldwide. It remains the second most common cause of death in the United States (Siegel et al., 2015). The development of tumors is a multistep process involving four to seven independent mutations in most cancers. Targeting only one pathway in this complex disease network is, in many cases, insufficient to combat cancer. Hence, in these cases, combination drugs with multiple targets might be necessary to gain optimal therapeutic benefit (Zimmermann et al., 2007).

Recently, our group introduced archazolid, a myxobacteria-derived vacuolar-type ATPase (V-ATPase)[1] inhibitor (Bockelmann et al., 2010; Huss et al., 2005; Menche et al., 2007; Sasse et al., 2003), as a promising new anti-cancer agent (Schneider et al., 2015; von Schwarzenberg et al., 2012; Wiedmann et al., 2012). V-ATPases are multisubunit proton pumps expressed on endolysosomal membranes of almost all eukaryotic cells. They are responsible for maintaining the cellular pH homeostasis and play an important role in the regulation of receptor-mediated recycling (Hinton et al., 2009). *In vitro* experiments with different cancer cells showed a high cytotoxic potential of archazolid (Schneider et al., 2015; von Schwarzenberg et al., 2012). Mechanistically, V-ATPase inhibition blocked the iron metabolism of cancer cells resulting in altered glucose metabolism and p53 stabilization. In mouse experiments we could show that archazolid treatment reduced the tumor burden, however it was not successful in abrogating tumor growth completely (Schneider et al., 2015). This matter asked for a rational and innovative combination strategy, to achieve a better therapeutic efficacy for archazolid. Based on our previously published finding that archazolid stabilizes p53, we decided to combine in this study archazolid with the small molecule p53 activator nutlin-3a, which inhibits binding of p53 and MDM2 (Vassilev et al., 2004).

The transcription factor p53 is one of the most studied tumor suppressors which plays a key role in maintaining genomic stability. In normal unstressed cells, p53 is expressed at a low level controlled by its negative regulators like MDM2. p53 gets activated in response to a variety of stress signals including DNA damage, hypoxia or activation of oncogenes (Brooks and Gu, 2006; Vousden and Prives, 2009). It is frequently mutated in human tumors and best known for regulating cell cycle arrest, senescence and apoptosis (Khoo et al., 2014).

Interestingly, in recent years, it has become obvious that p53 also plays a pivotal role in regulating tumor metabolism, which strongly contributes to its tumor suppressing abilities. It regulates glycolysis, pentose phosphate pathway, oxidative phosphorylation (OXPHOS)[2] and lipid metabolism and can counteract many of the metabolic alterations associated with cancer development. Repression of glycolysis and activation of OXPHOS are the major metabolic functions of p53 which lead to tumor growth inhibition (Berkers et al., 2013). p53 activation not only directly inhibits glucose receptor transcription (Schwartzenberg-Bar-Yoseph et al., 2004) but also leads to an upregulation of TP53-induced glycolysis and apoptosis regulator (TIGAR)[3], which inhibits glycolysis by decreasing fructose-6-bisphosphate concentration (Bensaad et al., 2006).

Our work unveils that combination of archazolid and nutlin-3a is highly efficient in inducing cell death *in vitro* and in reducing tumor growth *in vivo* in p53 positive tumors. This is mediated by counteracting the pro-glycolytic activities of archazolid leading to a decrease of glycolysis-related parameters which may contribute to the increased cell death induction. This work provides new insight in the role of V-ATPase in tumor metabolism and proposes targeting the metabolic changes with nutlin-3a as a promising way for cancer therapy.

2. MATERIAL AND METHODS

2.1 Cell lines and reagents

The mammary cancer cell line MCF7, the liver carcinoma cell line HepG2 and the cervical cancer cell line Hela were recently purchased from DSMZ (Braunschweig, Germany). The mammary cancer cell line MDA-MB-231 was obtained from Cell Line Service Eppelheim (Germany). The glioblastoma cell line U87MG (U87)[4] was a kind gift from Prof. Adrian L. Harris (Department of Oncology, Wheatherall Institute of Molecular Medicine, Oxford University). MCF7 cells were cultivated in RPMI 1620 complimented with 10% FCS, 1% nonessential amino acids, 1% pyruvate and 125µg/L insulin. HepG2 and MDA-MB-231 cells were grown in DMEM High Glucose containing 10% FCS, Hela and U87 cells in RPMI 1620 supplemented with 10% FCS. Archazolid was isolated by Prof. Dirk Menche (Kekulé-Institute of Organic Chemistry and Biochemistry, University of Bonn, Bonn, Germany). Nutlin-3a was purchased from Sigma Aldrich (Taufkirchen, Germany).

2.2 Immunocytochemistry

2 x 10^4 MCF7 cells were seeded onto µ-slides 8-well ibidiTreat (IBIDI, Martinsried, Germany) and were treated as indicated. Then, cells were fixed with 4% paraformaldehyde (PFA), permeabilized with 0.2% Triton X-100/PBS and blocked with 1% BSA/PBS containing 0.1% Triton X-100. Antibody against p53 (Cell Signaling Technology, Danvers, MA) and AlexaFluor 488-goat-antimouse (Invitrogen, Waltham, MA) were diluted in blocking solution. Nuclei were stained with Hoechst 33342® (Hoechst) (Sigma Aldrich).

2.3 Western blot

Western blot analysis was performed as described before (Schneider et al., 2015). Following antibodies were used: p53, pAkt Ser^{473}, Akt, Bid, caspase-9, PARP (Cell

Signaling Technology), Glut1 (Novus, Littleton, CO), IGFBP3, HRP goat-antimouse (Santa Cruz Biotechnology, Heidelberg, Germany), Rb (BD Bioscience, Heidelberg, Germany), Bcl-2 (Calbiochem, Darmstadt, Germany), AIF (Chemicon, Billerica, MA), actin (Millipore, Darmstadt, Germany) and HRP-goat-antirabbit (Bio-Rad, Munich, Germany).

2.4 qPCR

RNA extraction, cDNA synthesis and qPCR were performed as described before (Schneider et al., 2015). All designed primers were purchased from Metabion (Planegg, Germany).

2.5 Cell death analysis

Cell death was assessed as described elsewhere (Schneider et al., 2015).

2.6 Measurement of metabolic activity

CellTiter-Blue Assay (Promega, Mannheim, Germany) was performed according to the manufacturer`s protocol to quantify metabolic activity.

2.7 Measurement of glucose uptake, ATP levels, Bax activation

Quantifications were performed as reported previously (von Schwarzenberg et al., 2012).

2.8 *In vivo* mouse model

For in vivo studies, six-week old female BALB/cOlaHsd-Foxn1^{nu}/Foxn1^{+} mice (Harlan, Indianapolis, IN) were used. 5 x 10^6 U87MG cells were resuspended in PBS/matrigel (Corning, Wiesbaden, Germany) (1:1) and injected subcutaneously into the flank of each mouse. After formation of palpable tumors, mice were divided into groups and treated daily intraperitoneally with 0.2 mg/kg archazolid in 5% DMSO/10% solutol/PBS, 5 mg/kg nutlin-3a 5% DMSO/10% solutol/PBS, with both or solvent

respectively. Measurement of tumors was done every 2 to 3 days with a caliper using the formula a x $b^2/2$. Modeling was performed using the non-linear mixed effects modeling technique with the software NONMEM 7.3 (Simeoni et al., 2004). Nutlin-3a PK model was built based on literature data (Zhang et al., 2010). Tumor growth curves were normalized to control. Animal experiments were approved by the District Government of Upper Bavaria in accordance with the German animal welfare and institutional guidelines.

2.9 Statistical analysis

For all statistics GraphPad Prism was used. Error bars display SEM, except *in vivo* tumor growth curves which show SD. Synergism was calculated with the Bliss formula $v=x_{combination}/((x_A-x_B)-(x_A*x_B))$ with v>1 indicating synergism.

3. RESULTS

3.1 Combination of archazolid and nutlin-3a strongly induce p53

We could recently show that the V-ATPase inhibitor archazolid induces p53 protein expression in breast cancer cells (Schneider et al., 2015). To start with, Fig. 1A shows that while low dose archazolid had no effect on p53 protein level, a combination with nutlin-3a even raises p53 protein levels over the level of nutlin-3a alone. To more deeply investigate this phenomenon, we analyzed the translocation of p53 to the nucleus – a prerequisite for p53 to be activated. We found that p53 is mostly located in the cytoplasm of untreated cells whereas it partially translocates to the nucleus after high dose archazolid treatment as well as after nutlin-3a treatment. Interestingly, a combination of the two compounds led to an almost complete reduction of cytosolic p53 and showed only activated p53 in the nucleus (Fig. 1B). This increased activation is due to stabilization of the protein and not enhanced transcription as there is no elevated mRNA level after combined treatment with archazolid and nutlin-3a (Fig 1C). Taken together, these findings indicate that combination of archazolid and nutlin-3a might have an improved anti-tumor activity in wild type p53 cells compared to the two compounds alone.

3.2 Combination of archazolid and nutlin-3a induces synergistic cell death in cancer cells

To analyze weather the increased p53 activation by archazolid and nutlin-3a has an effect on cell death induction, we used different p53 wild type tumor cell lines and one breast cancer cell line with mutated p53 and treated them with single drugs and combination. Subsequent flow cytometry analysis showed for MCF7, Hela and HepG2 cells synergistic cell death induction after combination treatment and for the glioblastoma cell line U87 reduced metabolic activity (Fig. 2A). As expected,

combination treatment in MDA-MB-231 cells, which have mutated p53, did not show any effects (Fig.2B). These results suggest that the synergistic cell death induction depends on p53 activation.

3.3 Treatment with combination of archazolid and nutlin-3a reduces glycolysis

To find a molecular explanation for the synergistic effects of archazolid and nutlin-3a, we investigated the cellular glucose metabolism since p53 has effects on tumor metabolism (Madan et al., 2012; Matoba et al., 2006; Schwartzenberg-Bar-Yoseph et al., 2004). Firstly, mRNA expression levels of TIGAR were analyzed in MCF7 cells. TIGAR is a known target of p53 and reduces glycolysis by lowering levels of the glycolytic intermediate fructose 2,6-bisphosphate (Bensaad et al., 2006). Archazolid alone slightly downregulated TIGAR mRNA levels and nutlin-3a showed as expected a strong induction. Interestingly, combination of the two drugs led to a 14-fold induction of TIGAR which is even higher than nutlin-3a alone (Fig. 3A). A long this line, combination of archazolid and nutlin-3a showed reduced glucose uptake (Fig. 3B) and Glut1 protein levels in MCF7 cells (Fig. 3C), which is not the case for each drug alone. Furthermore, archazolid increases the mRNA level of aldolase c, a key enzyme in glycolysis, which was diminished by combination with nutlin-3a (Fig. 3D). Consistently, ATP levels were strongly reduced in MCF7 cells treated with combination of archazolid and nutlin-3a (Fig. 3E). These observations indicate that nutlin-3a counters the pro-glycolytic activities of archazolid.

3.4 Combination treatment targets apoptotic pathways

Next, we wanted to connect the inhibition of glycolysis, mediated by combination of archazolid and nutlin-3a, with the apoptosis-inducing properties. First, we analyzed the expression of the p53 target proteins insulin-like growth factor-binding protein 3 (IGFBP3)[5] and Rb. Both can inhibit glycolysis and Akt (Clem and Chesney, 2012; Elzi

et al., 2012; Lee et al., 2004) and can lead to apoptosis induction or growth arrest (Elzi et al., 2012; Fan and Steer, 1999; Lee et al., 2004). We could show that the combination of archazolid and nutlin-3a leads to a strong induction of IGFBP3 and dephosphorylation of Rb (Fig. 4A, B). This effect is accompanied by an inhibition of Akt phosphorylation (Fig. 4C). Interestingly, both drugs alone did not show an inhibitory effect on Akt. In addition, combination strongly increases active Bax levels (Fig. 4D), but had no effect on Bcl-2, Bid and AIF (Fig. 4E). Finally, cleavage of caspase-9 (Fig. 4F) and PARP (Fig. 4G) is induced, altogether suggesting activation of pro-apoptotic pathways.

3.5 Combination of archazolid and nutlin-3a reduces tumor growth *in vivo*

Finally, to prove that combination of archazolid and nutlin-3a is efficient in reducing tumor growth *in vivo* we performed a xenograft mouse model using U87MG cells. 28 female SCID mice were treated with archazolid 0.2mg/kg, nutlin-3a 5mg/kg or combination over 17 days and tumor burden was measured and normalized to control (Fig. 5A). Growth rate of tumors treated with combination was significantly reduced compared to control. Moreover, combination was most effective in reducing tumor volume (50.4%). Along this line, tumors treated with combination showed highest doubling times (Fig.5B). These data render combination of archazolid and nutlin-3a promising and attractive strategy for the treatment of p53 wild type tumors.

4. DISCUSSION

Our study suggests combination of the V-ATPase inhibitor archazolid with the p53 activator nutlin-3a as a promising and viable strategy for the treatment of p53 wild type tumors and reveals novel insights into archazolid's mode of action.

Cancer is a multigenic disease. The process of oncogenesis requires in most tumors four to seven mutations. As only a few single-target drugs are able to efficiently combat this disease, a change to multi-target therapeutics has occurred in recent years. Combination drugs can be more efficient in controlling complex diseases and can overcome drug resistance. For example, patients suffering from breast cancer benefit from a combination of trastuzumab, targeting ErbB2, with the anti-VEGF antibody Avastin®. Along this line, multi-target therapies with traditional chemotherapeutics are well established in the clinical treatment of cancers (Zimmermann et al., 2007).

In the last decade, a lot work was done to explore the anti-tumor activity of V-ATPase inhibitors. Various reports prove the cytotoxic activity of V-ATPase inhibitors such as bafilomycin, concanamycin and archazolid in diverse cancer cell lines *in vitro* (Koul et al., 2013; Nakashima, 2003; Ohta et al., 1998; Schneider et al., 2015; von Schwarzenberg et al., 2012; Wu et al., 2009). *In vivo* experiments revealed the anti-metastatic potential of archazolid (Wiedmann et al., 2012) and NiK-12192, a small molecule V-ATPase inhibitor (Supino et al., 2007). However, treatment of solid tumors with V-ATPase inhibitors showed only weak effects *in vivo*. Treatment of Capan-1 tumors with bafilomycin showed a reduction of tumor growth only in high doses and tumors over 300mm^3 (Ohta et al., 1998). Lim et al. reported that tumor growth inhibition by bafilomycin is more effective in larger HIF1α-positive tumors (Lim et al., 2006). Moreover, the high toxicity of V-ATPase inhibitors was thought to be prohibitive for clinical use (Drose and Altendorf, 1997). Nevertheless, inhibition of V-

ATPase was shown to overcome chemoresistance *in vitro* (Sasazawa et al., 2009; You et al., 2009) and trastuzumab resistance in *vivo* (von Schwarzenberg et al., 2014).

As our own recently published work showed only a moderate reduction of tumor burden *in vivo* after archazolid treatment, we now intended to improve this by a rational combination approach. There are several ways for multi-target therapies to achieve better therapeutic efficacy, one is to address different targets within the same pathway (Zimmermann et al., 2007). Since our study further revealed that archazolid interferes with the iron metabolism of cells finally resulting in disturbed glucose metabolism and p53 stabilization (Schneider et al., 2015), combination treatment within the p53 pathway seemed promising.

p53 was extensively studied in the last decades as it is the most frequently mutated gene in tumors. Nevertheless, about half of all human cancers carry no mutation in this gene. Therefore, a lot of work has been put in the development of p53 activators, which are now in clinical studies against diverse cancers. One very promising approach is to activate p53 through small molecule MDM2 antagonists. In order to restore p53 function, in cases where it is mutated, efforts have been made to identify drugs which stabilize p53 conformation by acting as p53 chaperones through binding to it. Moreover, gene therapy has been used to manipulate the p53 network (Khoo et al., 2014).

In search for compounds that are able to block the p53-MDM2 binding, thereby activating p53, Vassilev et al. identified a class of small molecules named nutlins. They could show that nutlin-3 was efficient in reducing tumor growth of SJSA-1 xenografts (Vassilev, 2004) and others revealed its antitumor activity in MHM, LnCap and 22Rv1 xenografts (Tovar et al., 2006). Moreover, efficient reduction of tumor growth was shown in combination studies. For example targeting MDM2 with

nutlin-3 showed superior *in vivo* efficacy in leukemia when combined with valproic acid, which inhibits histone deacetylases (McCormack et al., 2011). To address the p53 pathway at two different points, we combined in this study archazolid with nutlin-3a in different cancer cell lines. p53 wild type tumor cells showed synergistic cell death induction *in vitro* while p53 mutant cells showed no effect, suggesting a p53 dependent mechanism.

Despite regulating cell cycle arrest, senescence and apoptosis, p53 is known to act on metabolism of cells, which contributes to its tumor suppressing abilities (Berkers et al., 2013). Interestingly, V-ATPase function was also connected to tumor metabolism. Recently, we could show that archazolid has an impact on the glucose metabolism of cancer cells (Schneider et al., 2015). In addition, others demonstrated that V-ATPase acts as a metabolic sensor by playing a role in amino acid sensing via mTOR and by physical interaction with glycolytic enzymes (Maxson and Grinstein, 2014; Zoncu et al., 2011). Along this line, we found decreased ATP levels – indicating insufficient energy supply – by the combination therapy as well as reduced glucose uptake and receptor expression, which can lead to a lowered glycolytic flux. In addition, mRNA levels of the p53 target TIGAR, recently identified to decrease fructose-6-bisphosphate concentration, and thereby glycolysis (Bensaad et al., 2006), were 14-fold increased after combination treatment. This was accompanied by reduced levels of the glycolytic intermediate aldolase further proposing that the combination counteracts glycolysis.

Moreover, other proteins, which have been associated with p53, were influenced by the combination of archazolid and nutlin-3a. The protein level of the IGF-related tumor suppressor IGFBP3 (Buckbinder et al., 1995), which was shown to attenuate tumor growth in different studies (Alami et al., 2008; Butt et al., 2000; Silha et al., 2006; Williams et al., 2000), was strongly increased. This was accompanied by

reduced phosphorylation of Akt. Interestingly, a probable connection between IGFBP3 and the Akt pathway was described before (Alami et al., 2008). In addition, combination treatment influenced a further player in the p53 network as it strongly dephosphorylates and activates Rb. Rb is best known for leading to cell cycle arrest as it gets increasingly phosphorylated during G1 and is hypophosphorylated in resting cells (Giacinti and Giordano, 2006).

One of the most studied functions of p53 is its ability to induce apoptosis in response to a variety of stress signals. As a consequence, transcriptionally active p53 can simultaneously target distinct pathways in the apoptotic network. For example, it regulates the expression of pro-apoptotic members of the Bcl-2 family, such as Bax, Puma or Bid. As a result of the predominant emergence of pro-apoptotic proteins, caspase activation and apoptosis is induced (Fridman and Lowe, 2003). In this study, combination of archazolid and nutlin-3a results in a synergistic activation of the pro-apoptotic protein Bax and a subsequent cleaveage of caspase-3 and PARP. Although p53 can target the apoptotic signaling cascade at several points, apoptosis induction via Bax seems to be specific as we could find no effect on Bcl-2, Bid or AIF, which are also p53 target proteins.

Most importantly, the combination of nutlin-3a and archazolid not only showed an effect *in vitro* but also strongly reduced growth of a wild type p53 glioblastoma xenograft mouse model compared to each drug alone.

Taken together, targeting the p53 pathway at two distinct points with archazolid and nutlin-3a unveiled strong tumor-inhibiting capabilities *in vitro* and *in vivo* in p53 wild type tumor cells. Mechanistically, combination treatment affects several parts in the p53 network: it reduces glycolysis, activates Bax, induces IGFBP3, dephosphorylates Rb and finally induces apoptosis. These results suggest

combination of archazolid and nutlin-3a as a highly promising treatment for p53 wild type tumors and opens up new therapeutic options for V-ATPase inhibitors.

ACKNOWLEDGEMENTS

The excellent work of Anja Arner is acknowledged. This work was supported by the DFG grant FOR 1406 SCHW 1781/1-1. The glioblastoma cell line U87 was a kind gift from Prof. Adrian L. Harris (Department of Oncology, Wheatherall Institute of Molecular Medicine, Oxford University). Archazolid was isolated by Prof. Dirk Menche (Kekulé-Institute of Organic Chemistry and Biochemistry, University of Bonn, Bonn, Germany).

REFERENCES

Alami, N., Page, V., Yu, Q., Jerome, L., Paterson, J., Shiry, L., Leyland-Jones, B., 2008. Recombinant human insulin-like growth factor-binding protein 3 inhibits tumor growth and targets the Akt pathway in lung and colon cancer models. Growth Horm. IGF Res. 18, 487-496.

Bensaad, K., Tsuruta, A., Selak, M.A., Vidal, M.N.C., Nakano, K., Bartrons, R., Gottlieb, E., Vousden, K.H., 2006. TIGAR, a p53-Inducible Regulator of Glycolysis and Apoptosis. Cell 126, 107-120.

Berkers, Celia R., Maddocks, Oliver D.K., Cheung, Eric C., Mor, I., Vousden, Karen H., 2013. Metabolic Regulation by p53 Family Members. Cell Metab. 18, 617-633.

Bockelmann, S., Menche, D., Rudolph, S., Bender, T., Grond, S., von Zezschwitz, P., Muench, S.P., Wieczorek, H., Huss, M., 2010. Archazolid A Binds to the Equatorial Region of the c-Ring of the Vacuolar H+-ATPase. J. Biol. Chem. 285, 38304-38314.

Brooks, C.L., Gu, W., 2006. p53 Ubiquitination: Mdm2 and Beyond. Mol. Cell 21, 307-315.

Buckbinder, L., Talbott, R., Velasco-Miguel, S., Takenaka, I., Faha, B., Seizinger, B.R., Kley, N., 1995. Induction of the growth inhibitor IGF-binding protein 3 by p53. Nature 377, 646-649.

Butt, A.J., Firth, S.M., King, M.A., Baxter, R.C., 2000. Insulin-like growth factor-binding protein-3 modulates expression of Bax and Bcl-2 and potentiates p53-independent radiation-induced apoptosis in human breast cancer cells. J. Biol. Chem. 275, 39174-39181.

Clem, B.F., Chesney, J., 2012. Molecular Pathways: Regulation of Metabolism by RB. Clin. Cancer Res. 18, 6096-6100.

Drose, S., Altendorf, K., 1997. Bafilomycins and concanamycins as inhibitors of V-ATPases and P-ATPases. J. Exp. Biol. 200, 1-8.

Elzi, D.J., Lai, Y., Song, M., Hakala, K., Weintraub, S.T., Shiio, Y., 2012. Plasminogen activator inhibitor 1 - insulin-like growth factor binding protein 3 cascade regulates stress-induced senescence. Proc. Natl. Acad. Sci. U. S. A. 109, 12052-12057.

Fan, G., Steer, C.J., 1999. The role of retinoblastoma protein in apoptosis. Apoptosis 4, 21-29.

Fridman, J.S., Lowe, S.W., 2003. Control of apoptosis by p53. Oncogene 22, 9030-9040.

Giacinti, C., Giordano, A., 2006. RB and cell cycle progression. Oncogene 25, 5220-5227.

Hinton, A., Bond, S., Forgac, M., 2009. V-ATPase functions in normal and disease processes. Pflugers Arch. 457, 589-598.

Huss, M., Sasse, F., Kunze, B., Jansen, R., Steinmetz, H., Ingenhorst, G., Zeeck, A., Wieczorek, H., 2005. Archazolid and apicularen: novel specific V-ATPase inhibitors. BMC Biochem. 6, 13.

Khoo, K.H., Verma, C.S., Lane, D.P., 2014. Drugging the p53 pathway: understanding the route to clinical efficacy. Nat. Rev. Drug Discov. 13, 217-236.

Koul, H.K., Kiyoshima, T., Yoshida, H., Wada, H., Nagata, K., Fujiwara, H., Kihara, M., Hasegawa, K., Someya, H., Sakai, H., 2013. Chemoresistance to Concanamycin A1 in Human Oral Squamous Cell Carcinoma Is Attenuated by an HDAC Inhibitor Partly via Suppression of Bcl-2 Expression. PLoS One 8, e80998.

Lee, H.Y., Moon, H., Chun, K.H., Chang, Y.S., Hassan, K., Ji, L., Lotan, R., Khuri, F.R., Hong, W.K., 2004. Effects of Insulin-like Growth Factor Binding Protein-3 and

Farnesyltransferase Inhibitor SCH66336 on Akt Expression and Apoptosis in Non-Small-Cell Lung Cancer Cells. J. Natl. Cancer Inst. 96, 1536-1548.

Lim, J.H., Park, J.W., Kim, M.S., Park, S.K., Johnson, R.S., Chun, Y.S., 2006. Bafilomycin Induces the p21-Mediated Growth Inhibition of Cancer Cells under Hypoxic Conditions by Expressing Hypoxia-Inducible Factor-1 Mol. Pharmacol. 70, 1856-1865.

Madan, E., Gogna, R., Kuppusamy, P., Bhatt, M., Pati, U., Mahdi, A.A., 2012. TIGAR induces p53-mediated cell-cycle arrest by regulation of RB-E2F1 complex. Br. J. Cancer 107, 516-526.

Matoba, S., Kang, J.G., Patino, W.D., Wragg, A., Boehm, M., Gavrilova, O., Hurley, P.J., Bunz, F., Hwang, P.M., 2006. p53 regulates mitochondrial respiration. Science 312, 1650-1653.

Maxson, M.E., Grinstein, S., 2014. The vacuolar-type H+-ATPase at a glance - more than a proton pump. J. Cell Sci. 127, 4987-4993.

McCormack, E., Haaland, I., Venås, G., Forthun, R.B., Huseby, S., Gausdal, G., Knappskog, S., Micklem, D.R., Lorens, J.B., Bruserud, Ø., Gjertsen, B.T., 2011. Synergistic induction of p53 mediated apoptosis by valproic acid and nutlin-3 in acute myeloid leukemia. Leukemia 26, 910-917.

Menche, D., Hassfeld, J., Li, J., Rudolph, S., 2007. Total Synthesis of Archazolid A. J. Am. Chem. Soc. 129, 6100-6101.

Nakashima, S., 2003. Vacuolar H+-ATPase Inhibitor Induces Apoptosis via Lysosomal Dysfunction in the Human Gastric Cancer Cell Line MKN-1. J. Biochem. 134, 359-364.

Ohta, T., Arakawa, H., Futagami, F., Fushida, S., Kitagawa, H., Kayahara, M., Nagakawa, T., Miwa, K., Kurashima, K., Numata, M., Kitamura, Y., Terada, T.,

Ohkuma, S., 1998. Bafilomycin A1 induces apoptosis in the human pancreatic cancer cell line Capan-1. J. Pathol. 185, 324-330.

Sasazawa, Y., Futamura, Y., Tashiro, E., Imoto, M., 2009. Vacuolar H+-ATPase inhibitors overcome Bcl-xL-mediated chemoresistance through restoration of a caspase-independent apoptotic pathway. Cancer Sci. 100, 1460-1467.

Sasse, F., Steinmetz, H., Höfle, G., Reichenbach, H., 2003. Archazolids, New Cytotoxic Macrolactones from Archangium gephyra (Myxobacteria) Production, Isolation, Physico-chemical and Biological Properties. J. Antibiot. (Tokyo) 56, 520-525.

Schneider, L.S., von Schwarzenberg, K., Lehr, T., Ulrich, M., Kubisch-Dohmen, R., Liebl, J., Trauner, D., Menche, D., Vollmar, A.M., 2015. Vacuolar-ATPase Inhibition Blocks Iron Metabolism to Mediate Therapeutic Effects in Breast Cancer. Cancer Res. 75, 2863-2874.

Schwartzenberg-Bar-Yoseph, F., Armoni, M., Karnieli, E., 2004. The tumor suppressor p53 down-regulates glucose transporters GLUT1 and GLUT4 gene expression. Cancer Res. 64, 2627-2633.

Siegel, R.L., Miller, K.D., Jemal, A., 2015. Cancer statistics, 2015. CA Cancer J. Clin. 65, 5-29.

Silha, J.V., Sheppard, P.C., Mishra, S., Gui, Y., Schwartz, J., Dodd, J.G., Murphy, L.J., 2006. Insulin-Like Growth Factor (IGF) Binding Protein-3 Attenuates Prostate Tumor Growth by IGF-Dependent and IGF-Independent Mechanisms. Endocrinology 147, 2112-2121.

Simeoni, M., Magni, P., Cammia, C., De Nicolao, G., Croci, V., Pesenti, E., Germani, M., Poggesi, I., Rocchetti, M., 2004. Predictive pharmacokinetic-pharmacodynamic modeling of tumor growth kinetics in xenograft models after administration of anticancer agents. Cancer Res. 64, 1094-1101.

Supino, R., Petrangolini, G., Pratesi, G., Tortoreto, M., Favini, E., Bo, L.D., Casalini, P., Radaelli, E., Croce, A.C., Bottiroli, G., Misiano, P., Farina, C., Zunino, F., 2007. Antimetastatic Effect of a Small-Molecule Vacuolar H+-ATPase Inhibitor in in Vitro and in Vivo Preclinical Studies. J. Pharmacol. Exp. Ther. 324, 15-22.

Tovar, C., Rosinski, J., Filipovic, Z., Higgins, B., Kolinsky, K., Hilton, H., Zhao, X., Vu, B.T., Qing, W., Packman, K., Myklebost, O., Heimbrook, D.C., Vassilev, L.T., 2006. Small-molecule MDM2 antagonists reveal aberrant p53 signaling in cancer: Implications for therapy. Proc. Natl. Acad. Sci. U. S. A. 103, 1888-1893.

Vassilev, L.T., 2004. In Vivo Activation of the p53 Pathway by Small-Molecule Antagonists of MDM2. Science 303, 844-848.

Vassilev, L.T., Vu, B.T., Graves, B., Carvajal, D., Podlaski, F., Filipovic, Z., Kong, N., Kammlott, U., Lukacs, C., Klein, C., Fotouhi, N., Liu, E.A., 2004. In vivo activation of the p53 pathway by small-molecule antagonists of MDM2. Science 303, 844-848.

von Schwarzenberg, K., Lajtos, T., Simon, L., Müller, R., Vereb, G., Vollmar, A.M., 2014. V-ATPase inhibition overcomes trastuzumab resistance in breast cancer. Mol. Oncol. 8, 9-19.

von Schwarzenberg, K., Wiedmann, R.M., Oak, P., Schulz, S., Zischka, H., Wanner, G., Efferth, T., Trauner, D., Vollmar, A.M., 2012. Mode of Cell Death Induction by Pharmacological Vacuolar H+-ATPase (V-ATPase) Inhibition. J. Biol. Chem. 288, 1385-1396.

Vousden, K.H., Prives, C., 2009. Blinded by the Light: The Growing Complexity of p53. Cell 137, 413-431.

Wiedmann, R.M., von Schwarzenberg, K., Palamidessi, A., Schreiner, L., Kubisch, R., Liebl, J., Schempp, C., Trauner, D., Vereb, G., Zahler, S., Wagner, E., Muller, R., Scita, G., Vollmar, A.M., 2012. The V-ATPase-Inhibitor Archazolid Abrogates

Tumor Metastasis via Inhibition of Endocytic Activation of the Rho-GTPase Rac1. Cancer Res. 72, 5976-5987.

Williams, A.C., Collard, T.J., Perks, C.M., Newcomb, P., Moorghen, M., Holly, J.M., Paraskeva, C., 2000. Increased p53-dependent apoptosis by the insulin-like growth factor binding protein IGFBP-3 in human colonic adenoma-derived cells. Cancer Res. 60, 22-27.

Wu, Y.C., Wu, W.K.K., Li, Y., Yu, L., Li, Z.J., Wong, C.C.M., Li, H.T., Sung, J.J.Y., Cho, C.H., 2009. Inhibition of macroautophagy by bafilomycin A1 lowers proliferation and induces apoptosis in colon cancer cells. Biochem. Biophys. Res. Commun. 382, 451-456.

You, H., Jin, J., Shu, H., Yu, B., Milito, A.D., Lozupone, F., Deng, Y., Tang, N., Yao, G., Fais, S., Gu, J., Qin, W., 2009. Small interfering RNA targeting the subunit ATP6L of proton pump V-ATPase overcomes chemoresistance of breast cancer cells. Cancer Lett. 280, 110-119.

Zhang, F., Tagen, M., Throm, S., Mallari, J., Miller, L., Guy, R.K., Dyer, M.A., Williams, R.T., Roussel, M.F., Nemeth, K., Zhu, F., Zhang, J., Lu, M., Panetta, J.C., Boulos, N., Stewart, C.F., 2010. Whole-Body Physiologically Based Pharmacokinetic Model for Nutlin-3a in Mice after Intravenous and Oral Administration. Drug Metab. Dispos. 39, 15-21.

Zimmermann, G.R., Lehár, J., Keith, C.T., 2007. Multi-target therapeutics: when the whole is greater than the sum of the parts. Drug Discov. Today 12, 34-42.

Zoncu, R., Bar-Peled, L., Efeyan, A., Wang, S., Sancak, Y., Sabatini, D.M., 2011. mTORC1 Senses Lysosomal Amino Acids Through an Inside-Out Mechanism That Requires the Vacuolar H+-ATPase. Science 334, 678-683.

FIGURE LEGENDS

Fig.1: p53 translocates to the nucleus in archazolid- and nutlin-3a-treated MCF7 cells. (A) p53 protein levels were analyzed by western blot in MCF7 cells after 24 h of treatment. **(B)** p53 and nuclei were stained in permeabilzed MCF7 cells after 24 h of indicated treatment. Pictures of cells were taken with confocal microscopy. Scale bars, 10 µm. **(A, B)** Representative experiments out of three independent experiments are shown. **(C)** p53 mRNA levels were quantified by qPCR in MCF7 cells after 24 h of treatment. Bars are the SEM of three independent experiments performed in duplicate.

Fig.2: Archazolid and nutlin-3a synergistically induce cell death in p53 wild type tumor cells. (A, B) Cell death induction after archazolid and nutlin-3a treatment (48 h in MCF7, Hela and MDA-MB-231cells; 24 h in HepG2 cells) was assessed by flow cytometry (quantification of PI-permeable cells for MCF7, Hela and HepG2 cells; quantification of SubG1 for MDA-MB-231 cells). Metabolic activity of U87 cells was analyzed by Cell Titer Blue assay. Bars are the SEM of three independent experiments performed in triplicate. Synergism was calculated with the Bliss formula (values: 1,59 for MCF7; 2,45 for Hela; 2,43 for HepG2 and 1,25 for U87).

Fig.3: Reduced glycolysis in cells treated with archazolid and nutlin-3a. (A, D) qPCR analysis was performed in MCF7 cells to quantify TIGAR and aldolase c mRNA levels after 24 h of treatment. Bars are the SEM of three independent experiments performed in duplicate. **(B)** To assess glucose uptake, flow cytometry analysis was performed after 8 h of treatment in MCF7 cells. Therefore, cells were incubated with 100 µM 2-NBDG (2-[N-(7-Nitrobenz-2-Oxa-1,3-Diazol-4-yl)Amino]-2-Deoxy-D-Glucose) in HANKS buffer for 30 min at 37 °C. Synergism was calculated with the Bliss formula (value: 1,05). **(C)** Western blot analysis was performed in

MCF7 cells after 48 h of treatment to detect Glut1 protein levels. One representative experiment out of three independent experiments is shown. **(E)** ATP levels were determined by Cell Titer Glow assay. Therefore, MCF7 cells were treated with archazolid and nutlin-3a for 24 h, subsequently incubated with CTG and analyzed with a luminometer. Synergism was calculated with the Bliss formula (value: 1,32). **(B, E)** Bars are the SEM of three independent experiments performed in triplicate.

Fig.4: Combination treatment targets apoptotic pathways including IGFBP3 and Bax. (A-C, E-G) MCF7 cells were treated for 24 h and western blot analysis was performed to detect IGFBP3, Rb (48 h), pAkt, Akt, Bcl-2, Bid, AIF, caspase-9, PARP (48 h), tubulin and actin protein levels. Representative experiments out of three independent experiments are shown. **(D)** Flow cytometry analysis was used to quantify active Bax levels after 24 h of archazolid and nutlin-3a treatment in MCF7 cells. Bars are the SEM of three independent experiments performed in triplicate. Synergism was calculated with the Bliss formula (value: 3,13).

Fig.5: Combination of archazolid and nutlin-3a efficiently reduces tumor growth of U87 cancer cells *in vivo*. (A) U87 tumor cells were subcutaneously injected into the flanks of 28 SCID mice (co: n=6; arch: n=7; nutlin-3a: n=7; combination: n=8). Mice were treated daily intraperitoneally with 0.2 mg/kg archazolid, 5 mg/kg nutlin-3a, both or equal amounts of solvent. Tumor growth curves are normalized to control. Bars display SD. **(B)** Growth rate, reduction and doubling time were calculated from data in Fig. 5A. Growth rate was calculated based on control growth rate. Reduction is in relation to control.

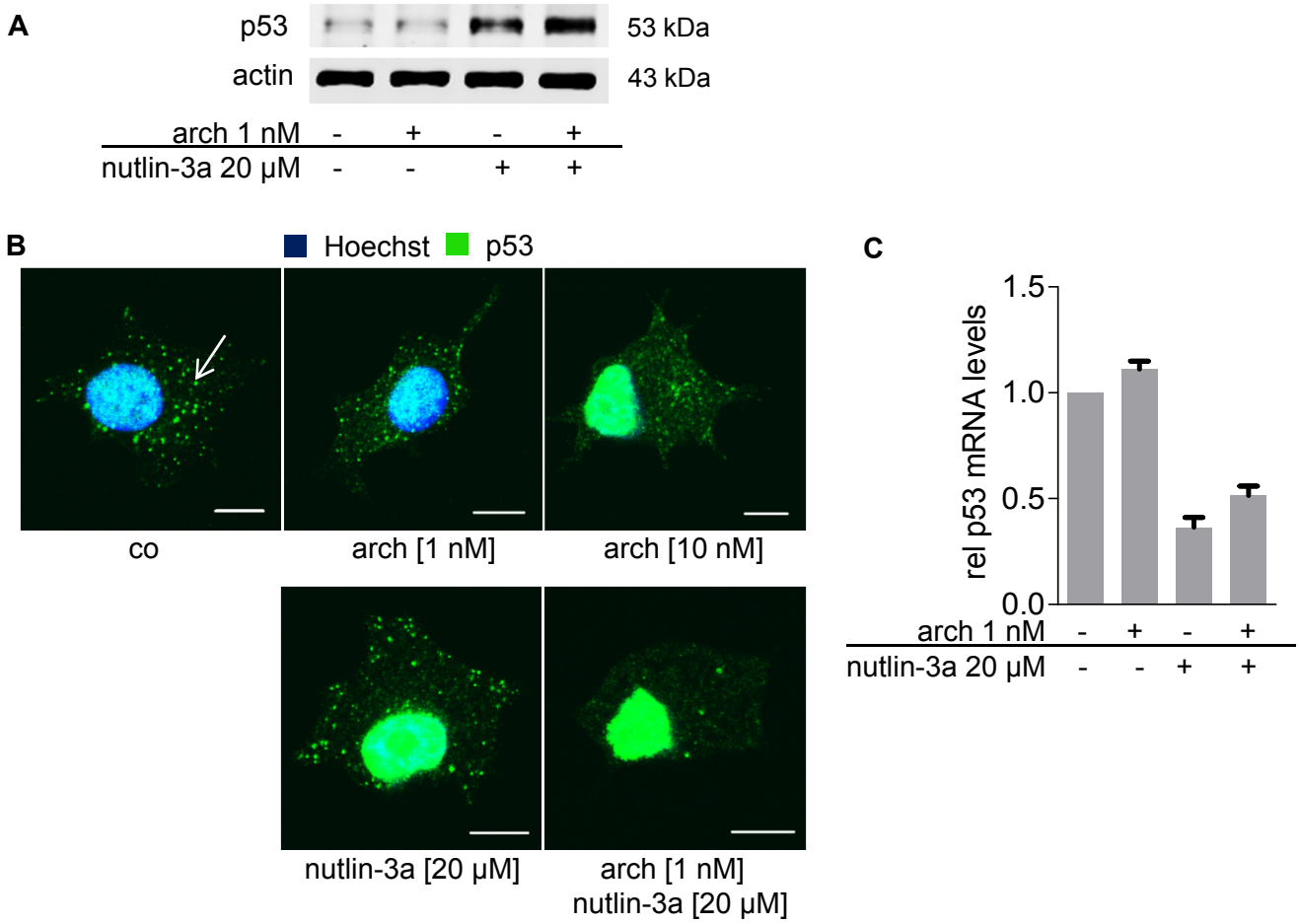
A
p53
53 kDa
actin
43 kDa
arch 1 nM - + - +
nutlin-3a 20 µM - - + +
B
Hoechst
p53
co
arch [1 nM]
arch [10 nM]
nutlin-3a [20 µM]
arch [1 nM]
nutlin-3a [20 µM]
C
rel p53 mRNA levels
1.5
1.0
0.5
0.0
arch 1 nM - + - +
nutlin-3a 20 µM - - + +

Figure 1

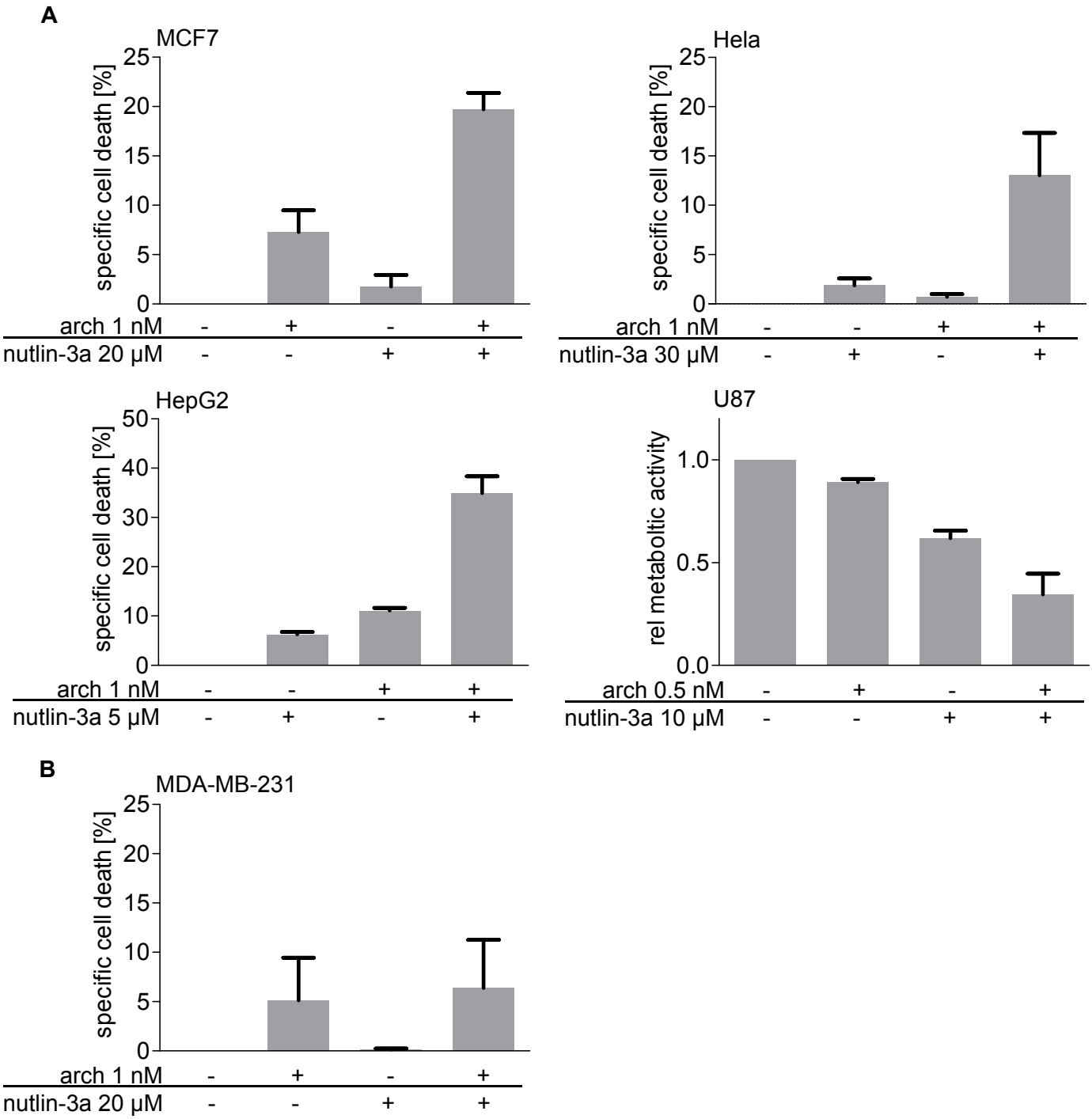
A
MCF7
specific cell death [%]
25
20
15
10
5
0
arch 1 nM - + - +
nutlin-3a 20 µM - - + +
Hela
specific cell death [%]
arch 1 nM - - + +
nutlin-3a 30 µM - + - +
HepG2
specific cell death [%]
50
40
30
20
10
0
arch 1 nM - - + +
nutlin-3a 5 µM - + - +
U87
rel metaboltic activity
1.0
0.5
0.0
arch 0.5 nM - + - +
nutlin-3a 10 µM - - + +
B
MDA-MB-231
specific cell death [%]
arch 1 nM - + - +
nutlin-3a 20 µM - - + +

Figure 2

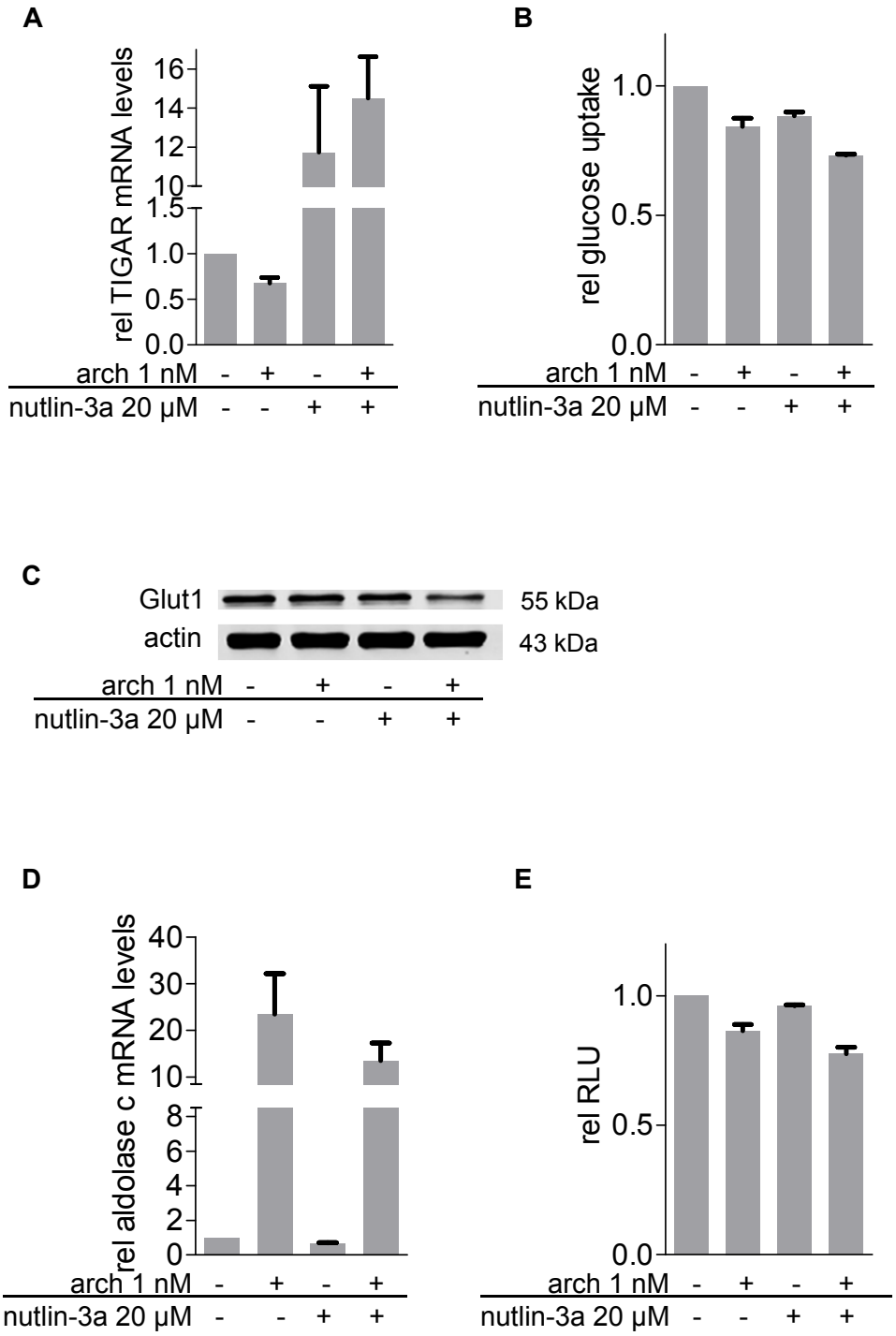
A
rel TIGAR mRNA levels
16
14
12
10
1.5
1.0
0.5
0.0
arch 1 nM - + - +
nutlin-3a 20 µM - - + +
B
rel glucose uptake
1.0
0.5
0.0
arch 1 nM - + - +
nutlin-3a 20 µM - - + +
C
Glut1
actin
55 kDa
43 kDa
arch 1 nM - + - +
nutlin-3a 20 µM - - + +
D
rel aldolase c mRNA levels
40
30
20
10
8
6
4
2
0
arch 1 nM - + - +
nutlin-3a 20 µM - - + +
E
rel RLU
1.0
0.5
0.0
arch 1 nM - + - +
nutlin-3a 20 µM - - + +

Figure 3

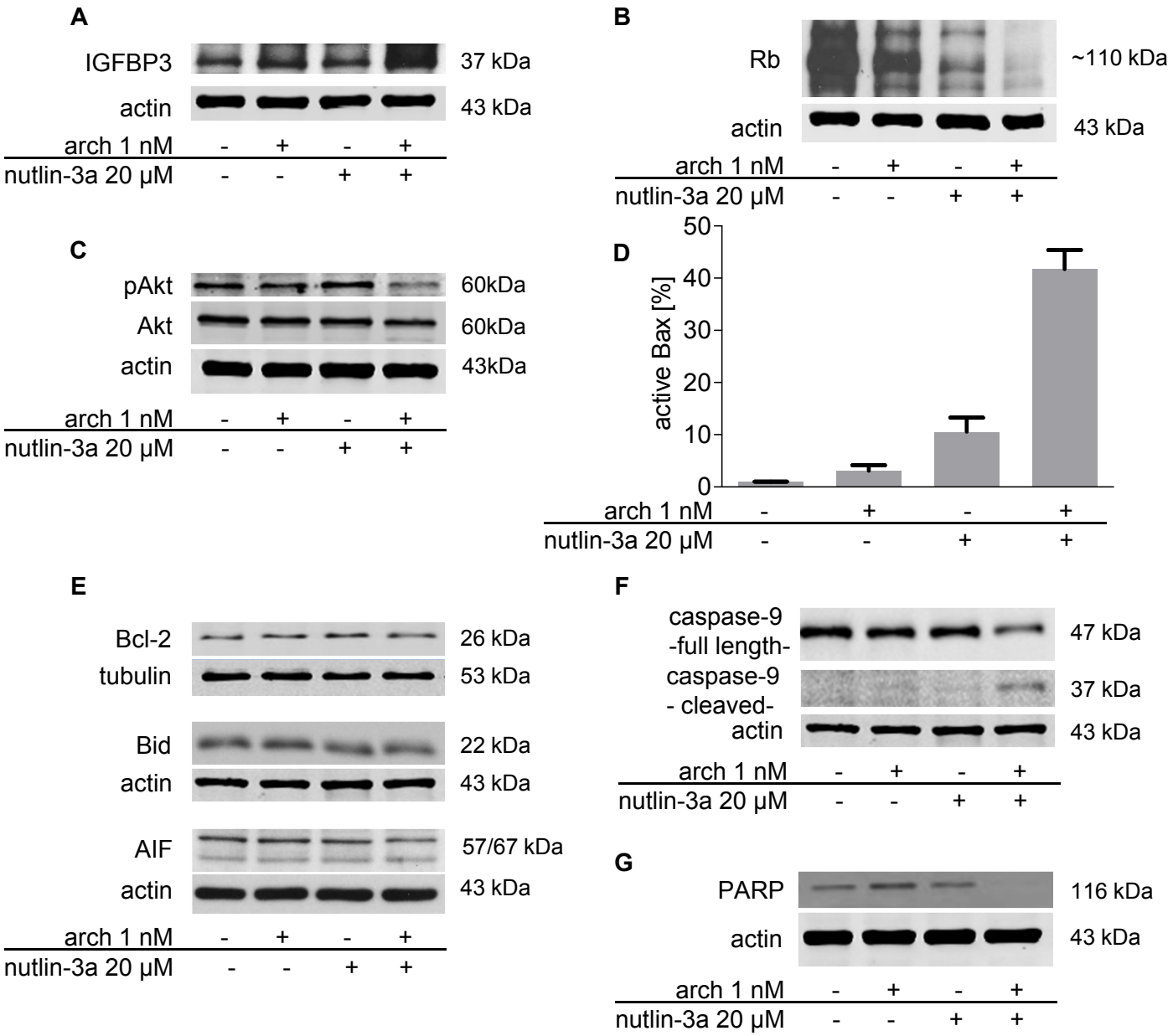
A
IGFBP3
37 kDa
actin
43 kDa
arch 1 nM - + - +
nutlin-3a 20 µM - - + +
B
Rb
~110 kDa
actin
43 kDa
arch 1 nM - + - +
nutlin-3a 20 µM - - + +
C
pAkt
60kDa
Akt
60kDa
actin
43kDa
arch 1 nM - + - +
nutlin-3a 20 µM - - + +
D
active Bax [%]
50
40
30
20
10
0
arch 1 nM - + - +
nutlin-3a 20 µM - - + +
E
Bcl-2
26 kDa
tubulin
53 kDa
Bid
22 kDa
actin
43 kDa
AIF
57/67 kDa
actin
43 kDa
arch 1 nM - + - +
nutlin-3a 20 µM - - + +
F
caspase-9
-full length-
47 kDa
caspase-9
- cleaved-
37 kDa
actin
43 kDa
arch 1 nM - + - +
nutlin-3a 20 µM - - + +
G
PARP
116 kDa
actin
43 kDa
arch 1 nM - + - +
nutlin-3a 20 µM - - + +

Figure 4

A

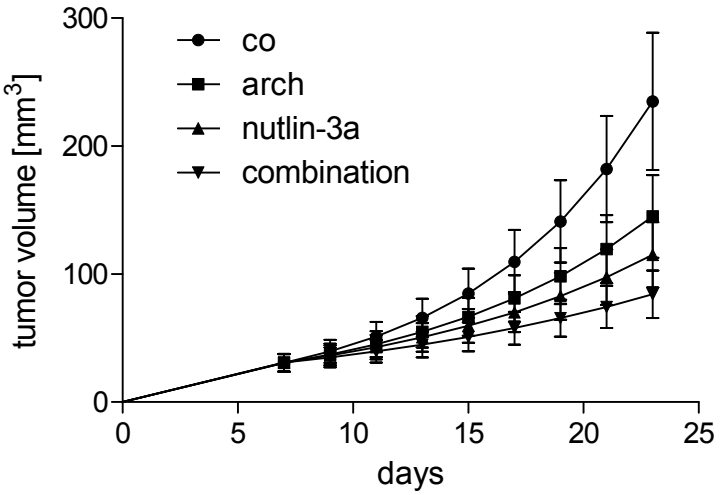

B

Groups	Growth rate [h^{-1}]	Reduction [%]	Doubling Time [h]
control	0.0053	0	131
arch	0.0040	23.6	171
nutlin-3a	0.0034	35.2	202
combination	0.0026	50.4	264

Figure 5

Two-pore channel function is crucial for migration of invasive cancer cells

Lina S. Schneider[1‡], Christian Grimm[2‡], Yu-Kai Chao[2], Anna Watermann[1], Melanie Ulrich[1], Doris Mayr[3], Christian Wahl-Schott[2], Martin Biel[2*], Angelika M. Vollmar[1*]

[1]Department of Pharmacy, Pharmaceutical Biology, Ludwig-Maximilians-University of Munich, Butenandtstrasse 5-13, 81377 Munich, Germany

[2]Department of Pharmacy, Center for Drug Research and Center for Integrated Protein Science Munich (CIPSM), Ludwig-Maximilians-University of Munich, Butenandtstrasse 5-13, 81377 Munich, Germany

[3]Pathological Institute, Ludwig-Maximilians-University of Munich, Thalkirchner Strasse 36, 80337 Munich, Germany

[‡]These authors contributed equally to this work

***Corresponding authors:** Prof. Dr. Martin Biel, Phone: +49-89-2180-77328, Email: martin.biel@cup.uni-muenchen.de; Prof. Dr. Angelika M. Vollmar, Phone: +49-89-2180-77172, Email: angelika.vollmar@cup.uni-muenchen.de

Running title: Role for TPCs in cancer cell migration

ABSTRACT

Metastasis is the main cause of cancer-related deaths. Hence, there is an urgent need to find new therapies. In this study, we introduce a promising new target for the treatment of invasive cancers. Inhibition of two-pore channels (TPCs), recently identified NAADP- and $PI(3,5)P_2$-sensitive Ca^{2+}-permeable cation channels in the endolysosomal system of cells, abrogated migration of metastatic cancer cells *in vitro*. Remarkably, tetrandrine, lately discovered to inhibit TPCs, showed *in vivo* efficacy reducing lung metastasis of mammary mouse cancer cells. As a molecular explanation, we found that disrupting TPC function halted β1-integrin trafficking, leading to accumulation in EEA1-positive vesicles. This is suggested to be due to alterations in Ca^{2+} signaling since pH was not affected. As a consequence, invasive cancer cells are no longer able to form leading edges, which is substantially required for adequate migration. Our study links TPCs to fundamental processes in cancer cell migration proposing that they are promising novel targets for the treatment of metastatic cancers.

INTRODUCTION

Metastasis is the major cause of cancer-related deaths. The formation of secondary, metastatic growth includes proliferation and extensive vascularization of the primary tumor, detachment and invasion of tumor cells, circulation of single tumor cells, arrest in distant sites, extravasation and finally proliferation within the organ (Fidler, 2003). Extensive studies in the last decades contributed to a better understanding of these processes. However, still about 90% of cancer-associated mortality is due to metastasis. Therefore, new strategies to prevent metastasis are urgently needed (Chaffer & Weinberg, 2011; Fidler, 2003).

To successfully colonize secondary sites, cancer cells gained the ability to migrate (Chaffer & Weinberg, 2011; Hood & Cheresh, 2002). A crucial step in migration is the binding to ligands of the extracellular matrix (ECM), which is mediated by integrins. These cell surface receptors display a diverse family of glycoproteins consisting of 18 α-subunits and 8 β-subunits. Besides mediating cell attachment to the ECM, integrins are linked to the cytoskeleton through the formation of clusters with actin-associated proteins such as vinculin. Furthermore, ligation of integrins induces a network of intracellular signaling pathways including the activation of focal adhesion kinase (FAK) and Src, altogether regulating cell migration (Hood & Cheresh, 2002).

In order to fulfill the function as migration-promoting receptors, integrins have to be trafficked to the front of the cell for assembly of focal adhesions. These adhesions act as traction sites for the movement and are afterwards disassembled at the rear of the cell, for detachment. Hence, integrins need to be dynamically turned over, which is achieved by endocytic trafficking (Maritzen et al, 2015; Ridley, 2003). After endocytosis, integrins are carried to early endosomes where sorting into recycling and degradative pathways takes place. Under normal conditions, the larger

portion recycles back to the plasma membrane. Disturbing this process can alter the composition of focal adhesions, thereby influencing cell migration (Maritzen et al, 2015).

There is increasing evidence that two-pore channels (TPCs) are key players in the regulation of endocytic transport (Brailoiu et al, 2009; Calcraft et al, 2009; Zong et al, 2009). It has been postulated that inhibiting these channels alters Ca^{2+} signaling during endolysosomal fusion events resulting in defects in vesicle trafficking (Grimm et al, 2014; Ruas et al, 2010; Ruas et al, 2014). TPCs are assigned to the superfamily of voltage-gated ion channels (Calcraft et al, 2009). There are two different TPC subtypes present in primates, TPC1 and TPC2. TPC1 is primarily expressed on endosomal membranes while TPC2 dominates on lysosomal membranes (Calcraft et al, 2009; Rietdorf et al, 2011; Ruas et al, 2010). Activation of these channels is presumably triggered by the second messenger nicotinic acid adenine dinucleotide phosphate (NAADP) and by phosphatidylinositol 3,5-bisphosphate ($PI(3,5)P_2$) (Calcraft et al, 2009; Jha et al, 2014; Schieder et al, 2010; Wang et al, 2012). Distinct experiments suggested TPCs as Ca^{2+}-permeable channels indicating that TPCs might be involved in Ca^{2+} release from endo- and lysosomal stores (Calcraft et al, 2009; Grimm et al, 2014; Ruas et al, 2015; Schieder et al, 2010; Zong et al, 2009).

This work unveils that TPCs play a crucial role in the formation of metastasis as silencing TPC1 and TPC2 reduced the adhesion and migration of invasive tumor cells *in vitro*. Similar results were achieved with Ned-19, an antagonist of NAADP (Naylor et al, 2009), and tetrandrine, recently shown to inhibit TPC1 and TPC2 (Sakurai et al, 2015). Remarkably, the latter showed efficacy in a metastatic *in vivo* model. Inhibition of TPCs led to the accumulation of integrins in endocytic vesicles

and to impaired formation of leading edges indicating that TPCs are significantly involved in integrin recycling.

RESULTS

TPCs in cancer cells

TPCs have been described in different cell types (Favia et al, 2014; Grimm et al, 2014; Sakurai et al, 2015), however not in cancer cells so far. TPC2 mRNA is distinctly expressed in T24 (bladder cancer), Jurkat (leukemia) and HUH7 (HCC) cells (Fig. 1A). mRNA levels of TPC1 were particularly high in T24 and HUH7 cells (Fig. 1B). Tumor tissue sections of HCC patients showed a highly positive staining for TPC2 (Fig. 1C). Together, these data suggest the presence of TPCs in cancer cells. To verify TPC functionality in T24 cancer cells, we isolated lysosomes and performed endolysosomal patch-clamp experiments. The applied whole-endolysosmal patch-clamp method is illustrated in Fig. 1D. $PI(3,5)P_2$-elicited currents were strongly reduced after applying tetrandrine (Fig. 1E, F), recently shown to inhibit TPC1 and TPC2 (Sakurai et al, 2015).

TPCs affect cancer cell migration and adhesion

Previous studies in TPC2-deficient MEF cells showed defects in the endolysosmal degradation pathway (Grimm et al, 2014; Ruas et al, 2014). As alterations in this pathway through inhibition of another endolysosome-associated protein, the vacuolar ATPase (V-ATPase), have been described to reduce the ability of invasive cancer cells to migrate (Wiedmann et al, 2012), we hypothesized that TPCs affect cancer cell migration. Silencing TPC1 and TPC2 by siRNA in T24 cells resulted in significantly reduced migration through pores in Boyden chamber assays (Fig. 2A). Knockdown efficiency is shown in Fig. 2B. Moreover, these cells showed diminished adhesion after 1 h of seeding (Fig. 2C). To get more information about the migratory defect, movement of silenced cells exposed to a diffusive gradient of FCS (0 to 10%) was analyzed. Figure 2 D shows control cells moving clearly towards the highest

FCS concentrations whereas knockdown cells displayed reduced directional migration, which is expressed as pValue in the Rayleigh test. Not only directed migration but also cell mobility seems to be affected as velocity was significantly reduced in silenced cells. Thus, TPC1 and TPC2 seem to play a pivotal role in two major steps of metastasis formation: adhesion and migration.

Pharmacological inhibition of TPC1 and TPC2 reduces cancer cell migration

To further investigate the potential of TPCs as novel targets for cancer therapy, two pharmacological inhibitors of TPC1 and TPC2 were used. The NAADP antagonist Ned-19 (Naylor et al, 2009) showed significant reduction of migration through pores in T24 and HUH7 cells (Fig. 3A). Along this line, treatment with tetrandrine abrogated migration in Boyden chambers in T24, HUH7 and 4T1 cells (Fig. 3B). Importantly, Ned-19 and tetrandrine had no effect on cell survival in all tested concentrations and at all tested time points (Fig. 3C). These results strengthen our finding that TPC1 and TPC2 are required for migration of cancer cells.

Accumulation of enlarged acidic vesicles after Ned-19 treatment

As TPC1 and TPC2 are located in the endolysosomal system (Calcraft et al, 2009; Rietdorf et al, 2011; Ruas et al, 2010) of cells, investigating this process after inhibition of TPCs seemed mandatory. Firstly, membranes of cells were stained with PKH26 fluorescent dye and subsequently allowed to recycle. As Figure 4A indicates, cells treated with Ned-19 accumulated up to 3-fold enlarged vesicles compared to control cells indicating that general recycling was impaired after TPC inhibition. Staining with Lysotracker Red DND-99 showed that the accumulated enlarged vesicles are acidic compartments. This experiment further indicates that acidification of endocytic vesicles was not affected after Ned-19 treatment (Fig. 4B). However, alterations in calcium homeostasis may disturb trafficking of endosomes to

lysosomes (Grimm et al, 2014; Lu et al, 2013; Ruas et al, 2010). To this end, cytosolic calcium levels were measured with fura-2AM in cancer cells during TPC inhibition. Calcium release out of lysosomes was stimulated by nigericin. In contrast to control, tetrandrine-treated cells displayed no increase in cytosolic calcium levels (Fig. 4C), suggesting disturbed calcium homeostasis as possible cause of impaired recycling.

Disturbed β1-integrin recycling through inhibition of TPCs

Integrins feature prominently in cancer cell adhesion and migration. Under normal conditions these transmembrane receptors get rapidly recycled through the endolysosomal system (Maritzen et al, 2015). Since inhibition of TPCs hampered endocytosis, we checked whether recycling of β1-integrin is hindered as well. An internalization assay of β1-integrin in T24 cells showed a 3-fold enlargement of β1-integrin positive vesicles after Ned-19 treatment compared to control (Fig. 5A). Moreover, staining of β1-integrin-positive vesicles with EEA1 and LAMP3 displayed a higher overlap of β1-integrin vesicles with EEA1, indicating an accumulation in early endosomes rather than lysosomes (Fig. 5B). In summary, these findings illustrate that β1-integrin recycling is disturbed after TPC inhibition.

Polarization and protrusion of the cell are essential for accurate cell migration. Protrusions in the direction of migration are stabilized through integrins linked to the actin cytoskeleton. Therefore, integrins have to be recycled to the leading edges of migrating cells (Maritzen et al, 2015; Ridley, 2003). To explore the ability to form leading edges, scratch assays were performed. Under these conditions, Ned-19 inhibited the formation of wound-directed, β1-integrin-, pSrc-, pFAK- and vinculin-positive polarized lamellipodia (Fig. 6A). These findings can be easily accounted for by disturbed β1-integrin trafficking to the front of the cell. Consistently, total protein

levels of β1-integrin, FAK, pFAK, Src and pSrc were not significantly altered after Ned-19 treatment (Fig. 6B), further corroborating an effect on β1-integrin recycling.

Reduced formation of lung metastasis *in vivo* by pharmacological TPC inhibition

To extend the relevance of TPC inhibition on chemotactic migration and invasion, we investigated whether tetrandrine was effective in abrogating cancer cell dissemination in a mouse model. The 4T1-Luc syngeneic metastatic mouse mammary cancer model was used for this purpose (Aslakson & Miller, 1992; Tao et al, 2008; Yang et al, 2004). 4T1-Luc cells are expressing a luciferase reporter which enables for live imaging. After intravenous injection, 4T1-Luc cells disseminate to distant organs homing preferably to lungs. Along this line, control animals showed easily detectable lung metastasis after five days of 4T1-Luc cell injection. Remarkably, pretreatment with tetrandrine significantly diminished formation of lung metastasis (Fig. 7). These findings further support the hypothesis that targeting TPCs might be a very promising and viable strategy for metastatic cancer therapy.

DISCUSSION

This study designates TPCs as promising targets for the treatment of invasive cancers. Disruption of TPC function abrogates cancer cell migration *in vitro* and *in vivo*, resulting from disturbed integrin trafficking in the endolysosomal system.

TPCs are Ca^{2+}-permeable voltage-gated channels located in the membrane of endosomes and lysosomes (Calcraft et al, 2009; Grimm et al, 2014; Rietdorf et al, 2011; Ruas et al, 2010; Ruas et al, 2015; Schieder et al, 2010; Zong et al, 2009). In recent years, evidence has accumulated that TPCs are substantially implicated in the regulation of endolysosomal trafficking. Thus, a lack of TPC2 in mouse embryonic fibroblasts resulted in an accumulation of LDL and EGF/EGFR in intracellular vesicles (Grimm et al, 2014) and led to delayed PDGFRβ degradation, which requires trafficking to lysosomes (Ruas et al, 2014). Overexpression of TPCs retained cholera toxin within endolysosomes, which is normally delivered to the Golgi, and enlarged lysosomes dramatically (Ruas et al, 2010). Disrupting TPC function also reduced Ebola virus trafficking through endosomal vesicles, preventing infection (Sakurai et al, 2015). Consistently, we observed an accumulation of integrins in early endosomes after TPC inhibition in invasive cancer cells. Alterations in Ca^{2+} signaling are widely accepted to lead to impaired trafficking and fusion of endocytic vesicles (Grimm et al, 2014; Ruas et al, 2010). This hypothesis is further supported by the finding that Ca^{2+} chelators, BAPTA and EGTA-AM, are able to inhibit fusion of late endosomes and lysosomes (Pryor et al, 2000). In this context, it is interesting to note that another Ca^{2+}-permeable endolysosomal channel, TRPML1, has been proposed to be required for fusion between late endosomes and lysosomes in *Drosophila* (Wong et al, 2012). In humans, loss or mutation of this channel leads to the lysosomal storage disorder mucolipidosis type IV (Bargal et al, 2000; Chen et al, 2014; Slaugenhaupt et al, 1999), further supporting the importance of Ca^{2+} signaling.

When looking at general endocytic trafficking and receptor recycling, another protein located in the endolysosmal membrane of cells comes into focus, the V-ATPase. V-ATPases are multiunit proton pumps, which actively transport protons from the cytoplasm into intracellular compartments thereby regulating its pH (Forgac, 2007). In several reports, it has been observed that altering pH by inhibition of V-ATPase results in impaired trafficking and recycling of signaling molecules. Hence, disturbed V-ATPase function led to the accumulation of Notch in the endolysosomal system (Kobia et al, 2014) and of cholesterol in intracellular compartments (Kozik et al, 2012). In cancer cells, inhibition of V-ATPase affected EGF receptor (Wiedmann et al, 2012) and transferrin receptor internalization, the latter resulting in apoptosis (Schneider et al, 2015).

Taken together, targeting the endolysosmal system either by TPC or V-ATPase inhibition can apparently both impair adequate endocytic trafficking. As it is quite evident for V-ATPase inhibition that this is due to altered pH, there is still an ongoing discussion regarding TPCs. As mentioned above, impaired Ca^{2+} signaling may be one reason, however it has also been postulated that alkalinizing of the lysosomal pH is responsible for the inhibition of autophagosomal-lysosomal fusion (Lu et al, 2013). In our study, we observed an accumulation of enlarged acidic vesicles after TPC inhibition, hence, no alkalinizing of pH. However, we found that tetrandrine completely halted intracellular Ca^{2+} release evoked by nigericin, suggesting that acute block of endolysosomal Ca^{2+} signaling might explain the observed trafficking defects. Other recent publications have also found no evidence for changes in endolysosomal pH under basal conditions in TPC-deficient cells (Cang et al, 2013; Grimm et al, 2014; Ruas et al, 2014).

Regardless of what the main cause of this impairment is, inhibition of TPC function led to a clear accumulation of β1-integrins in early endosomes. Integrins link

the cell to the ECM enabling adhesion and migration (Huttenlocher & Horwitz, 2011). To migrate, the cell must be polarized meaning that different molecular processes occur at the front and back of a moving cell (Ridley, 2003). Therefore, several proteins are trafficked towards the front of the cell. For example, growth factor receptors and chemokine receptors are recycled to specific sites of the leading edge to mediate pro-migratory signals. Importantly, adhesive contacts are regulated by the recycling and degradation of integrins (Maritzen et al, 2015). Hence, the turnover of integrins is crucial for migration. We could observe in our studies, in addition to an accumulation of β1-integrin in enlarged vesicles, reduced β1-integrin localization at the leading edge of migrating cells after TPC inhibition. These findings suggest that disrupted TPC function alters β1-integrin trafficking, resulting in reduced adhesion to ECM and insufficient polarization of the cell.

Besides mediating adhesion to ECM, integrins are also essential for cell migration as they regulate pro-migratory signaling pathways. Thus, integrin ligation induces clustering, resulting in the activation of FAK. Active FAK recruits Src family kinases to focal adhesions, altogether promoting cell migration and invasion. In addition, focal contacts contain different actin-associated proteins such as vinculin which links integrin to the cytoskeleton (Hood & Cheresh, 2002). In our study, inhibition of TPC function clearly diminished the accumulation of integrin, pFAK, pSrc and vinculin at the leading edge of migrating cells. This suggests that adequate β1-integrin trafficking is crucial for the initiation of pro-migratory mechanisms.

To fulfill these functions, integrins form heterodimeric receptors. Pairing of α and β subunits decides for the specific binding of certain matrix ligands. Previous investigations on the β1-integrin subunit revealed a central role in adhesion, extravasation and migration in T24 cancer cells (Heyder et al, 2005). Moreover, reports show that β1-integrin and FAK signaling is implicated in the initial proliferation

of cancer cells disseminated into the lungs (Shibue & Weinberg, 2009). Our own experiments are consistent with these notions. Further research over the last several years led to the development of integrin targeted therapeutics, which are now tested in clinical studies against cancer and other diseases (Hood & Cheresh, 2002). The monoclonal antibody *Volociximab* is the first α5β1 integrin antagonist in clinical trials against metastatic clear cell renal cell carcinoma, metastatic melanoma, non-small cell lung cancer and peritoneal cancer among others (Almokadem & Belani, 2012; Millard et al, 2011). In addition, several therapeutic antibodies targeting αvβ3 integrin are under development or in clinical phases as anti-tumor agents such as *Vitaxin* and *CNTO 95* (Millard et al, 2011). Taken together, targeting integrins is a highly promising and viable strategy for the treatment of metastatic cancers.

Taken together, our study reveals a potential novel role for TPCs in the formation of metastasis. Impaired TPC function reduced adhesion and migration of cancer cells *in vitro* and diminished formation of metastasis *in vivo*. Most likely this is due to disturbed trafficking of integrins, known to act pro-migratory. Here we link TPCs to fundamental processes in cancer cell migration, rendering them new and attractive targets for the treatment of invasive carcinomas.

MATERIAL AND METHODS

Cell lines and Reagents

The cancer cell line T24 was obtained from Dr. B. Mayer (Surgical Clinic, LMU, Munich, Germany) and authenticated by the DSMZ, HUH7 were purchased from Japanese Collection of Research Bioresources and 4T1-Luc (4T1) from PerkinElmer. T24 cells were grown in McCoy's, HUH7 cells in DMEM High Glucose and 4T1 cells in RPMI-1640 medium. All media were supplemented with 10% FCS. *trans*-Ned-19 (Ned-19) was purchased from Tocris® Bioscience, tetrandrine from Santa Cruz Biotechnology.

qRT-PCR

qRT-PCR of TPC1 and TPC2 was performed as described previously (Schneider et al, 2015). Following primers were used: TPC2 fw 5'-GTA CCC CTC TTG TGT GGA CG-3', rv 5'-GGC CCT GAC AGT GAC AAC TT-3'; TPC1 fw 5'-GGA GCC CTT CTA TTT CAT CGT-3', rv 5'-CGG TAG CGC TCC TTC AAC T-3';

Whole-endolysosomal patch clamp

Whole-endolysosomal patch-clamp recordings were performed by modified conventional patch-clamp. T24 cells were treated with 1 µM vacuolin-1 at least 4 h. Currents were recorded using an EPC-10 patch-clamp amplifier and PatchMaster acquisition software (HEKA, Lambrecht/Pfalz, Germany). Data were digitized at 40 kHz and filtered at 2.8 kHz. Recording pipettes had a resistance of 8-10 MΩ. Liquid junction potential was corrected. Pipette solution (corresponding to luminal endolysosomal solution) contained 140 mM NaMSA, 5 mM KMSA, 2 mM CaMSA, 1 mM $CaCl_2$, 10 mM HEPES and 10 mM MES, pH 4.6. Bath solution (corresponding to cytosolic solution) contained 140 mM KMSA, 5 mM KOH, 4 mM NaCl, 0.39 mM $CaCl_2$, 1 mM EGTA, and 10 mM HEPES, pH 7.2. $PI(3,5)P_2$ was used in a water-

soluble diC8 form (A.G. Scientific). All compounds including $PI(3,5)P_2$ were prepared as high-concentration stock solutions, added to the bath solutions to match the final concentration indicated. pH of bath solution and pipette solution were adjusted with KOH and MSA, respectively. All recordings were obtained at 21-23 °C and were analyzed using PatchMaster and Origin 6.1 (OriginLab, Northampton, MA) software.

Tissue staining

2 µm tissue sections were used. Antigen retrieval was done with Target Retrieval Solution from Dako and sections were heated for 30 min in the microwave. Blocking of endogenous peroxidase was done in 7.5% hydrogen peroxide for 10 min. Anti-TPC2 (atlas antibodies, diluted 1:60) was applied as primary antibody for 1 h at RT. For antibody detection, ImmPress™ reagent anti-rabbit Ig was utilized according to the manual and DAB+ for 3 min at RT was used as a chromogen. Slides were counterstained with hematoxylin for 20 sec and finally embedded in mounting medium and covered with glass coverslips.

Cell transfection

$2x10^5$ T24 cells were transfected using the ScreenFect® A Transfection Kit (Genaxxon bioscience). TPC1 and TPC2 were silenced using siRNA from Santa Cruz Biotechnology. Non-targeting siRNA was used as a control.

Boyden chamber assay

$1x10^5$ treated or silenced cells were placed on top of the Transwell® chamber (Corning) in media without FCS. 24-well plate was filled with medium with 10% FCS. Transwell® chambers were placed in it and incubated for 16 h. Migrated cells were fixed and stained with crystal violet/methanol. The top of the Transwell® chamber was cleaned and pictures were taken. Migrated cells were counted with Image J (National Institutes of Health).

Adhesion assay

$5x10^4$ silenced T24 cells were seeded onto µ-slides 8-well ibidiTreat and allowed to attach for 1 h. Subsequently, cells were fixed with 4% paraformaldehyde (PFA) and stained with rhodamine-phalloidin (Molecular Probes®) and Hoechst 33342® (Hoechst) (Sigma) for 30 min. Cells were mounted with FluorSave™ Reagent mounting medium (Merck) and analyzed with a Zeiss LSM 510 Meta confocal microscope (Jena).

Chemotaxis

$6x10^4$ T24 cells were seeded on µ-Slide Chemotaxis^{3D} (IBIDI) and allowed to attach for 3 h. Chemotaxis experiment (20 h) was performed as described before (Wiedmann et al, 2012). Cell tracking was performed with Image J plugin Manual tracking (Fabrice Cordelières, Institut Curie, Orsay). 30 cells were tracked per experiment. Data analysis was done with Chemotaxis and Migration Tool (IBIDI). Rayleigh test was used to describe uniformity of distribution of cell endpoints. With $p>0.05$ uniformity is rejected (Zengel et al, 2011).

Measurement of cell death

Flow cytometry analysis was performed as described before (Schneider et al, 2015). Specific cell death was calculated as follows: specific cell death = [(x – Co) / (100 – Co)] x 100

Membrane staining

$2x10^4$ HUH7 cells were seeded onto µ-slides 8-well ibidiTreat. For membrane labeling, the PKH 26 red fluorescent cell linker mini kit was used (Sigma). After treatment, cells were incubated with the dye according to the manufacturer's instructions for 2 min. After removal, cells were incubated with pure FCS for 1 min followed by an incubation of 2 h in medium. Cells were then fixed with PFA and

stained with Hoechst for 10 min. Washed cells were mounted in FluorSave™ Reagent mounting medium and cells were analyzed by confocal microscopy.

Lysotracker staining

$2x10^4$ T24 cells were seeded onto µ-slides 8-well ibidiTreat and stimulated. Thereafter, cells were incubated for 30 min with 1 µM Lysotracker® Red DND-99 (Molecular Probes®) and Hoechst in PBS. After removal, pictures were taken immediately with a Zeiss LSM 510 Meta confocal microscope.

Measurement of intracellular calcium

Calcium measurement was performed as described before (Grimm et al, 2014). Briefly, $3x10^4$ T24 cells were seeded onto µ-slides 8-well ibidiTreat and were stimulated the next day. Then, cells were loaded with 4 µM fura-2AM (Invitrogen) for 1 h in a standard bath solution (see ref.). After that, cells were washed with 2 mM EGTA for 30 min. Cells were imaged in the presence of 2 mM EGTA. An Axiovert200 microscope (Zeiss), IMAGO-QE and Polychrome V (TILL Photonics GmbH) were used for measurement.

β1-integrin internalization

$1x10^4$ T24 cells were seeded onto µ-slides 8-well ibidiTreat and stimulated. Cells were starved for 90 min and stained with β1-integrin (TS2/16) (Santa Cruz) in cold 0.01% BSA/DMEM without FCS for 45 min at 4 °C. Washed cells were incubated with 0.01% BSA/DMEM with FCS for 1 h at 37 °C. Next, 1 µM phorbol 12-myristat 13-acetat (Merck) in 0.01% BSA/ DMEM with FCS was added for 30 min at 37 °C. After washing and fixing cells with PFA, 0.1% Triton-X100 was added. AlexaFlour 488-goat-antimouse (Molecular Probes®) and Hoechst were used for 1 h to stain cells. Washed cells were embedded in FluorSave™ Reagent mounting medium and analyzed by confocal microscopy.

Immunocytochemistry

$1x10^4$ T24 cells were seeded onto µ-slides 8-well ibidiTreat (IBIDI). Treated and PFA fixed cells were permeabilized with 0.2% Triton X-100/PBS. Hereafter, unspecific binding sites were blocked with 1% BSA/PBS containing 0.1% Triton X-100. Antibodies were diluted in blocking solution. Used antibodies are given below: β1-integrin (TS2/16), EEA1, LAMP3 (Santa Cruz). Nuclei were stained with Hoechst. Cells were embedded in FluorSave™ Reagent mounting medium and analyzed by confocal microscopy.

Staining of migrating cells

A confluent T24 cell layer was scratched with a pipette tip, after treatment. Cells were allowed to migrate for 5 h and subsequently fixed with PFA. Samples were stained as described in section immunocytochemistry. Antibodies given below were used: β1-integrin (TS2/16), vinculin (Santa Cruz), $pFAK^{Sr732}$, $pSrc^{pY418}$ (Invitrogen), AlexaFluor 680-goat-antirabbit and AlexaFluor 643-goat-antimouse (Molecular Probes®). Rhodamine-phalloidin was used to stain actin, Hoechst for nuclei.

Western blot

Western blot was performed as described before (Schneider et al, 2015). Following antibodies were used: β1-integrin (TS2/16), FAK (Santa Cruz), $pFAK^{Sr732}$, $pSrc^{pY418}$ (Molecular Probes®), Src (L4A1) (Cell Signalling), actin (Millipore), HRP-goat-antirabbit (Bio-Rad) and HRP-goat-antimouse (Santa Cruz).

***In vivo* mouse model**

4T1-Luc cells were pretreated with 10 µM tetrandrine or DMSO for 24 h. Female BALB/cOlaHsd mice (Harlan) were inoculated with $1x10^5$ 4T1-Luc cells via the tail vein. After five days, imaging of the mice was performed using the IVIS Lumina system with Living Image software 4.4 (Caliper Life Sciences) 15 min after

intraperitoneal injection of 6 mg Na-luciferin (PerkinElmer). The total signal per defined region of interest was calculated as photons/second/cm^2 (total flux/area). Animal experiments were approved by the District Government of Upper Bavaria in accordance with the German animal welfare and institutional guidelines.

Statistical analysis

GraphPad Prism Software was used for all statistical analysis. In some experiments data were normalized to control or as indicated.

ACKNOWLEDGEMENTS

This work was supported, in part, by funding of the German Research Foundation (SFB/TRR152 TP04 to C.G., TP06 to C.W.-S., and TP12 to M.B., FOR1406 to AMV).

CONFLICT OF INTEREST

The authors declare no conflict of interest.

THE PAPER EXPLAINED

PROBLEM: Cancer is a leading cause of death worldwide. Most cancer-related deaths are due to metastasis. To colonize distant sites, cancer cells are highly dependent on their ability to migrate. Disrupting this process is thought to be a promising approach for new anti-cancer drugs.

RESULTS: Here we show that function of recently identified Ca^{2+}-permeable endolysosomal two pore channels (TPCs) is crucial for cancer cell motility. Pharmacological inhibition of these channels abrogated migration of invasive cancer cells *in vitro* and *in vivo*. Moreover, we provide evidence for the underlying molecular mechanisms as integrin recycling was disturbed.

IMPACT: Our study suggests TPCs as promising new targets for the treatment of metastatic cancers.

REFERENCES

Almokadem S, Belani CP (2012) Volociximab in cancer. *Expert Opin Biol Ther* 12**:** 251–257

Aslakson CJ, Miller FR (1992) Selective events in the metastatic process defined by analysis of the sequential dissemination of subpopulations of a mouse mammary tumor. *Cancer Res* 52**:** 1399–1405

Bargal R, Avidan N, Ben-Asher E, Olender Z, Zeigler M, Frumkin A, Raas-Rothschild A, Glusman G, Lancet D, Bach G (2000) Identification of the gene causing mucolipidosis type IV. *Nat Genet* 26**:** 118–123

Brailoiu E, Churamani D, Cai X, Schrlau MG, Brailoiu GC, Gao X, Hooper R, Boulware MJ, Dun NJ, Marchant JS et al (2009) Essential requirement for two-pore channel 1 in NAADP-mediated calcium signaling. *J Cell Biol* 186**:** 201–209

Calcraft PJ, Ruas M, Pan Z, Cheng X, Arredouani A, Hao X, Tang J, Rietdorf K, Teboul L, Chuang K-T et al (2009) NAADP mobilizes calcium from acidic organelles through two-pore channels. *Nature* 459**:** 596–600

Cang C, Zhou Y, Navarro B, Seo Y-j, Aranda K, Shi L, Battaglia-Hsu S, Nissim I, Clapham David E, Ren D (2013) mTOR Regulates Lysosomal ATP-Sensitive Two-Pore Na+ Channels to Adapt to Metabolic State. *Cell* 152**:** 778–790

Chaffer CL, Weinberg RA (2011) A Perspective on Cancer Cell Metastasis. *Science* 331**:** 1559–1564

Chen C-C, Keller M, Hess M, Schiffmann R, Urban N, Wolfgardt A, Schaefer M, Bracher F, Biel M, Wahl-Schott C et al (2014) A small molecule restores function to

TRPML1 mutant isoforms responsible for mucolipidosis type IV. *Nat Commun* 5**:** 4681

Favia A, Desideri M, Gambara G, D'Alessio A, Ruas M, Esposito B, Del Bufalo D, Parrington J, Ziparo E, Palombi F et al (2014) VEGF-induced neoangiogenesis is mediated by NAADP and two-pore channel-2-dependent Ca2+ signaling. *Proc Natl Acad Sci USA* 111**:** E4706–E4715

Fidler IJ (2003) Timeline: The pathogenesis of cancer metastasis: the 'seed and soil' hypothesis revisited. *Nat Rev Cancer* 3**:** 453–458

Forgac M (2007) Vacuolar ATPases: rotary proton pumps in physiology and pathophysiology. *Nat Rev Mol Cell Biol* 8**:** 917–929

Grimm C, Holdt LM, Chen C-C, Hassan S, Müller C, Jörs S, Cuny H, Kissing S, Schröder B, Butz E et al (2014) High susceptibility to fatty liver disease in two-pore channel 2-deficient mice. *Nat Commun* 5**:** 4699

Heyder C, Gloria-Maercker E, Hatzmann W, Niggemann B, Zänker KS, Dittmar T (2005) Role of the β1-integrin subunit in the adhesion, extravasation and migration of T24 human bladder carcinoma cells. *Clin Exp Metastasis* 22**:** 99–106

Hood JD, Cheresh DA (2002) Role of Integrins in Cell Invasion and Migration. *Nat Rev Cancer* 2**:** 91–100

Huttenlocher A, Horwitz AR (2011) Integrins in Cell Migration. *Cold Spring Harb Perspect Biol* 3**:** a005074–a005074

Jha A, Ahuja M, Patel S, Brailoiu E, Muallem S (2014) Convergent regulation of the lysosomal two-pore channel-2 by Mg2+, NAADP, PI(3,5)P2 and multiple protein kinases. *EMBO J* 33**:** 501–511

Kobia F, Duchi S, Deflorian G, Vaccari T (2014) Pharmacologic inhibition of vacuolar H+ ATPase reduces physiologic and oncogenic Notch signaling. *Mol Oncol* 8**:** 207–220

Kozik P, Hodson NA, Sahlender DA, Simecek N, Soromani C, Wu J, Collinson LM, Robinson MS (2012) A human genome-wide screen for regulators of clathrin-coated vesicle formation reveals an unexpected role for the V-ATPase. *Nat Cell Biol* 15**:** 50–60

Lu Y, Hao BX, Graeff R, Wong CWM, Wu WT, Yue J (2013) Two Pore Channel 2 (TPC2) Inhibits Autophagosomal-Lysosomal Fusion by Alkalinizing Lysosomal pH. *J Biol Chem* 288**:** 24247–24263

Maritzen T, Schachtner H, Legler DF (2015) On the move: endocytic trafficking in cell migration. *Cell Mol Life Sci* 72**:** 2119–2134

Millard M, Odde S, Neamati N (2011) Integrin targeted therapeutics. *Theranostics* 1**:** 154–188

Naylor E, Arredouani A, Vasudevan SR, Lewis AM, Parkesh R, Mizote A, Rosen D, Thomas JM, Izumi M, Ganesan A et al (2009) Identification of a chemical probe for NAADP by virtual screening. *Nat Chem Biol* 5**:** 220–226

Pryor PR, Mullock BM, Bright NA, Gray SR, Luzio JP (2000) The role of intraorganellar Ca(2+) in late endosome-lysosome heterotypic fusion and in the reformation of lysosomes from hybrid organelles. *J Cell Biol* 149**:** 1053–1062

Ridley AJ (2003) Cell Migration: Integrating Signals from Front to Back. *Science* 302**:** 1704–1709

Rietdorf K, Funnell TM, Ruas M, Heinemann J, Parrington J, Galione A (2011) Two-pore Channels Form Homo- and Heterodimers. *J Biol Chem* 286**:** 37058–37062

Ruas M, Rietdorf K, Arredouani A, Davis LC, Lloyd-Evans E, Koegel H, Funnell TM, Morgan AJ, Ward JA, Watanabe K et al (2010) Purified TPC Isoforms Form NAADP Receptors with Distinct Roles for Ca2+ Signaling and Endolysosomal Trafficking. *Curr Biol* 20**:** 703–709

Ruas M, Chuang KT, Davis LC, Al-Douri A, Tynan PW, Tunn R, Teboul L, Galione A, Parrington J (2014) TPC1 Has Two Variant Isoforms, and Their Removal Has Different Effects on Endo-Lysosomal Functions Compared to Loss of TPC2. *Mol Cell Biol* 34**:** 3981–3992

Ruas M, Davis LC, Chen CC, Morgan AJ, Chuang KT, Walseth TF, Grimm C, Garnham C, Powell T, Platt N et al (2015) Expression of Ca2+-permeable two-pore channels rescues NAADP signalling in TPC-deficient cells. *EMBO J* 34**:** 1743–1758

Sakurai Y, Kolokoltsov AA, Chen CC, Tidwell MW, Bauta WE, Klugbauer N, Grimm C, Wahl-Schott C, Biel M, Davey RA (2015) Two-pore channels control Ebola virus host cell entry and are drug targets for disease treatment. *Science* 347**:** 995–998

Schieder M, Rotzer K, Bruggemann A, Biel M, Wahl-Schott CA (2010) Characterization of Two-pore Channel 2 (TPCN2)-mediated Ca2+ Currents in Isolated Lysosomes. *J Biol Chem* 285**:** 21219–21222

Schneider LS, von Schwarzenberg K, Lehr T, Ulrich M, Kubisch-Dohmen R, Liebl J, Trauner D, Menche D, Vollmar AM (2015) Vacuolar-ATPase Inhibition Blocks Iron Metabolism to Mediate Therapeutic Effects in Breast Cancer. *Cancer Res* 75**:** 2863–2874

Shibue T, Weinberg RA (2009) Integrin 1-focal adhesion kinase signaling directs the proliferation of metastatic cancer cells disseminated in the lungs. *Proc Natl Acad Sci USA* 106**:** 10290–10295

Slaugenhaupt SA, Acierno Jr JS, Helbling LA, Bove C, Goldin E, Bach G, Schiffmann R, Gusella JF (1999) Mapping of the Mucolipidosis Type IV Gene to Chromosome 19p and Definition of Founder Haplotypes. *Am J Hum Genet* 65**:** 773–778

Tao K, Fang M, Alroy J, Sahagian GG (2008) Imagable 4T1 model for the study of late stage breast cancer. *BMC Cancer* 8**:** 228

Wang X, Zhang X, Dong X-p, Samie M, Li X, Cheng X, Goschka A, Shen D, Zhou Y, Harlow J et al (2012) TPC Proteins Are Phosphoinositide- Activated Sodium-Selective Ion Channels in Endosomes and Lysosomes. *Cell* 151**:** 372–383

Wiedmann RM, von Schwarzenberg K, Palamidessi A, Schreiner L, Kubisch R, Liebl J, Schempp C, Trauner D, Vereb G, Zahler S et al (2012) The V-ATPase-Inhibitor Archazolid Abrogates Tumor Metastasis via Inhibition of Endocytic Activation of the Rho-GTPase Rac1. *Cancer Res* 72**:** 5976–5987

Wong C-O, Li R, Montell C, Venkatachalam K (2012) Drosophila TRPML Is Required for TORC1 Activation. *Curr Biol* 22**:** 1616–1621

Yang J, Mani SA, Donaher JL, Ramaswamy S, Itzykson RA, Come C, Savagner P, Gitelman I, Richardson A, Weinberg RA (2004) Twist, a Master Regulator of Morphogenesis, Plays an Essential Role in Tumor Metastasis. *Cell* 117**:** 927–939

Zengel P, Nguyen-Hoang A, Schildhammer C, Zantl R, Kahl V, Horn E (2011) µ-Slide Chemotaxis: A new chamber for long-term chemotaxis studies. *BMC Cell Biol* 12**:** 21

Zong X, Schieder M, Cuny H, Fenske S, Gruner C, Rötzer K, Griesbeck O, Harz H, Biel M, Wahl-Schott C (2009) The two-pore channel TPCN2 mediates NAADP-dependent Ca2+-release from lysosomal stores. *Pfluegers Arch/Eur J Physiol* 458**:** 891–899

FIGURE LEGENDS

Fig.1: TPCs in cancer cells. (A, B) mRNA levels of TPC2 and TPC1 in different cancer cell lines was assessed by qRT-PCR using the SYBR Green PCR Master Mix. Expression level of MDA-MB-231 cells was set 1. Bars are the SEM of three independent experiments performed in duplet. **(C)** Human liver sections (HCC and surrounding tissue) were stained with an antibody against TPC2. Counterstaining was done with hematoxylin. One representative specimen is shown. **(D)** Cartoon illustrating whole-endolysosomal patch clamp method. **(E)** Representative current-voltage relation recorded from a vacuolin-enlarged endolysosomal vesicle manually isolated from cultured T24 cells. Shown are the effect of 1 µM $PI(3,5)P_2$, and the blocking effect of 500 nM tetrandrine. **(F)** Population data for current amplitudes at -100 mV obtained from experiments as shown in A; p*<0.05, Student's *t*-test, data are shown as mean ±SEM.

Fig.2: Silencing of TPC1 and TPC2 leads to reduced migration and adhesion in cancer cells. For all experiments T24 cells were silenced with siRNA against TPC1 and TPC2 for 72 h. **(A)** siRNA-treated cells were allowed to migrate in Transwell® chambers for 16 h. **(B)** qPCR analysis of TPC1 and TPC2 mRNA levels were assessed with the SYBR Green PCR Master Mix. Bars are the SEM of three independent experiments performed in duplet. **(C)** After silencing, cells were allowed to adhere for 1 h, fixed and stained (rhodamine-phalloidin, Hoechst). Cells were analyzed by confocal microscopy. Scale bars, 150 µm. **(A, C)** Bars are the SEM of three independent experiments, p*<0.05 (One-way ANOVA, Dunnett's multiple comparison test). **(D)** Movement of silenced T24 cells along a FCS gradient was monitored (20 h) by live cell imaging and analyzed for directed migration (pValue)

and velocity (Image-J, IBIDI software). Dashed line indicates p=0.05. Bars are the SEM of three independent experiments, p*<0.05 (t-test).

Fig.3: Ned-19 and tetrandrine inhibit cancer cell migration. (A, B) T24, HUH7 and 4T1 cells were pretreated with Ned-19 and tetrandrine for 8 h (*T24*: 250 µM Ned-19, 15 µM Tet; *HUH7*: 150 µM Ned-19, 2,5 µM Tet; *4T1*: 10 µM Tet). Cells were allowed to migrate in Transwell® chambers for 16 h in the presence of the inhibitor. Bars are the SEM of three independent experiments, p*<0.05 (t-test). **(C)** Cell death was assessed after 24 h of treatment with inhibitors used in **A** and **B** by flow cytometry analysis. Means of three independent experiments performed in triplicate ±SEM is displayed.

Fig.4: Inhibition of TPCs disrupts endocytic recycling presumably through disturbed Ca^{2+} signaling. (A) Membranes were stained with PKH 26 red in HUH7 cells after 24 h of Ned-19 (150 µM) treatment. Cells were allowed to recycle again for 2 h. Fixed cells were analyzed by confocal microscopy. **(B)** Ned-19-treated T24 cells (250 µM, 24 h) were stained with Lysotracker® Red DND-99 and analyzed by confocal microscopy. **(A, B)** Nuclei were stained with Hoechst (blue). Vesicles were analyzed with Image J. Bars are the SEM of three independent experiments, p*<0.05 (t-test). Scale bars, 20µm. **(C)** Intracellular calcium levels were measured with fura-2AM in T24 cells. Cells were pretreated with 15 µM tetrandrine (5 h) and loaded with fura-2AM. Calcium imaging was performed in Ca^{2+}-free EGTA buffer. Nigericin was used to release Ca^{2+} from the endolysosomal system. One representative experiment is shown. Bars are the SEM of five independent experiments (with 9-16 cells, each), p*<0.05 (t-test).

Fig.5: β1-integrin recycling is hindered after TPC inhibition. (A) Internalized β1-integrin was stained in T24 cells after 24 h of Ned-19 treatment (250 µM). Scale bars,

20 µm (upper pictures) and 10 µm (lower pictures). **(B)** Ned-19-treated T24 cells (250 µM, 24 h) were stained for β1-integrin, EEA1, LAMP3 and nuclei with Hoechst (blue). Scale bars, 10 µm. **(A, B)** Pictures of cells were taken with confocal microscopy. **(A)** Vesicles were analyzed with Image J. Bars are the SEM of three independent experiments, p*<0.05 (t-test).

Fig.6: TPC function is required for formation of leading edges. (A) T24 cells were scratched and let migrate for 5 h after a pretreatment with 250 µM Ned-19 for 16 h. Fixed cells were stained for actin, β1-integrin, pSrc, pFAK and vinculin. One representative picture out of three independent experiments is shown. Scale bars, 20 µm. **(B)** Total protein amounts of β1-integrin, pSrc, Src, pFAK and FAK were detected by western blot analysis in T24 cells after treatment with 250 µM Ned-19 for 24 h. One representative blot is shown. Quantification was done with Image J. Bars are the SEM of three independent experiments.

Fig.7: Inhibition of TPC function in 4T1-Luc cells reduces the formation of lung metastasis *in vivo*. $1x10^5$ 4T1-Luc cells, pretreated with 10 µM tetrandrine or respectively DMSO, were injected intravenously into BALB/cOlaHsd mice. On day five after cell inoculation bioluminescence signals were measured by imaging the mice ventrodorsal. The total signal per defined region of interest was calculated as photons/second/cm^2 (total flux/area). Bars are the SEM, p*<0.05 (t-test).

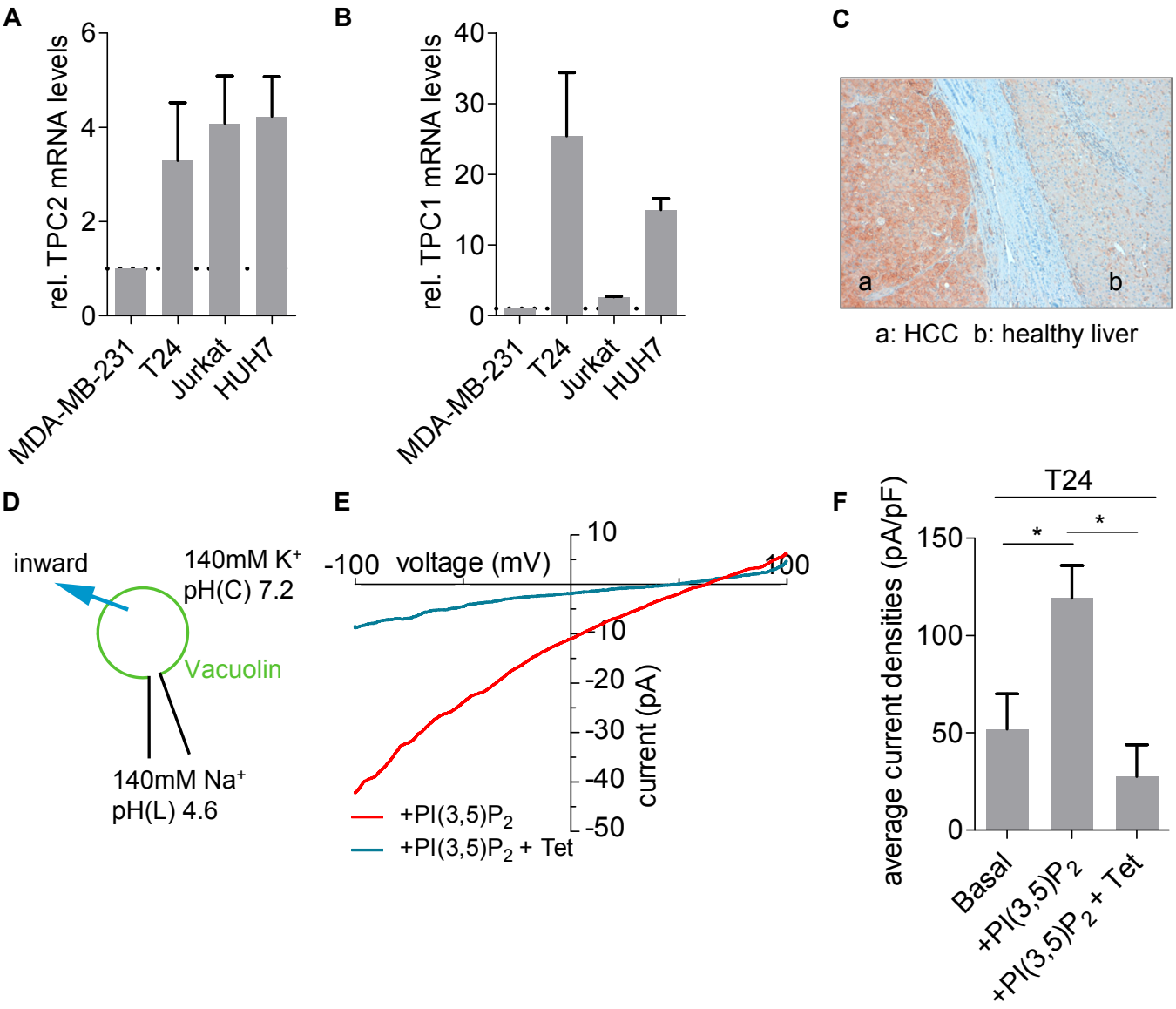
A
rel. TPC2 mRNA levels
0
2
4
6
MDA-MB-231
T24
Jurkat
HUH7
B
rel. TPC1 mRNA levels
0
10
20
30
40
MDA-MB-231
T24
Jurkat
HUH7
C
a
b
a: HCC b: healthy liver
D
inward
140mM K+
pH(C) 7.2
Vacuolin
140mM Na+
pH(L) 4.6
E
-100 voltage (mV) 100
10
-10
-20
-30
-40
-50
current (pA)
+PI(3,5)P2
+PI(3,5)P2 + Tet
F
T24
*
*
average current densities (pA/pF)
0
50
100
150
Basal
+PI(3,5)P2
+PI(3,5)P2 + Tet

Figure 1

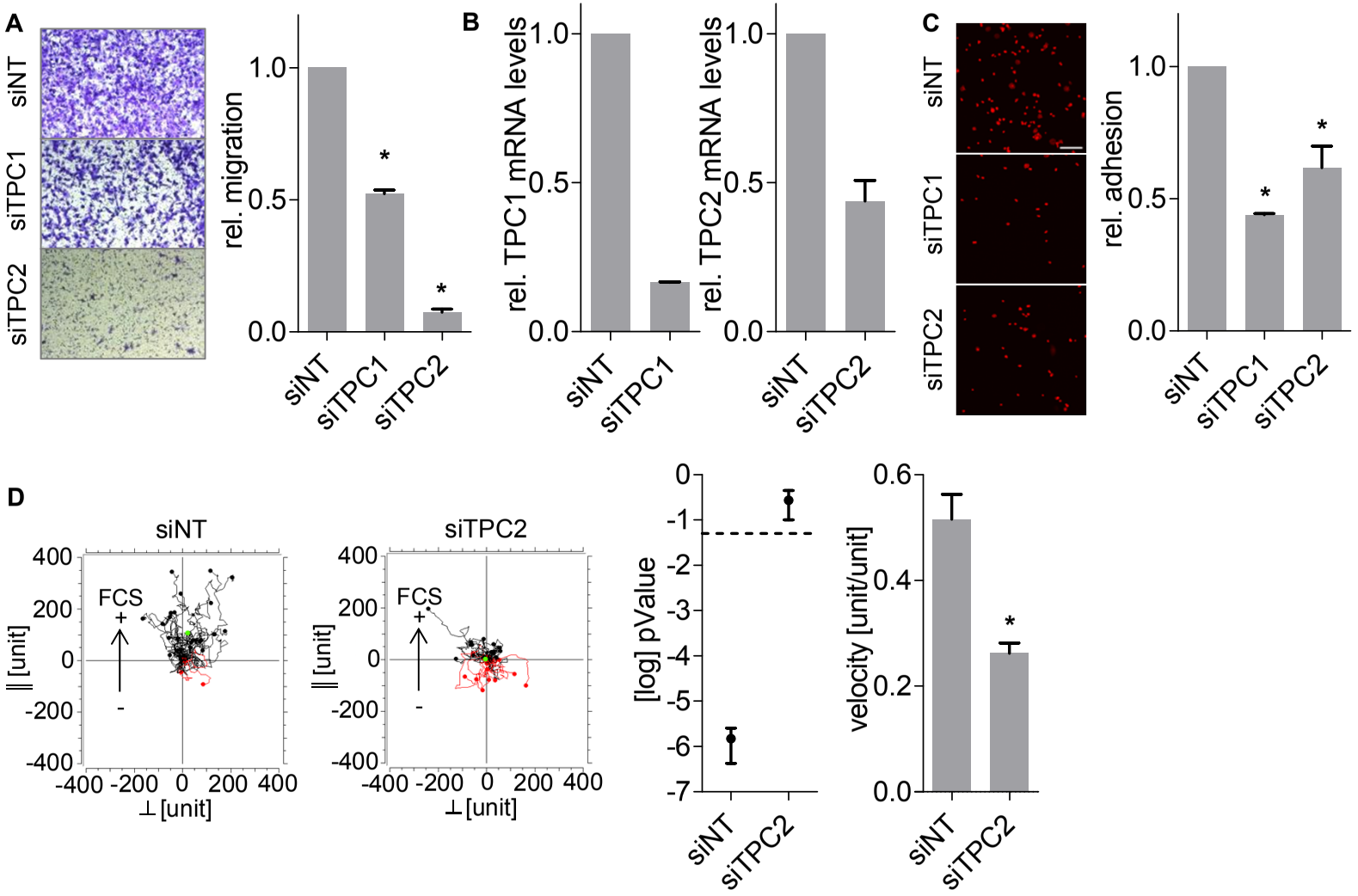
A
siNT
siTPC1
siTPC2
rel. migration
1.0
0.5
0.0
*
*
siNT
siTPC1
siTPC2
B
rel. TPC1 mRNA levels
1.0
0.5
0.0
siNT
siTPC1
rel. TPC2 mRNA levels
1.0
0.5
0.0
siNT
siTPC2
C
siNT
siTPC1
siTPC2
rel. adhesion
1.0
0.5
0.0
*
*
siNT
siTPC1
siTPC2
D
siNT
siTPC2
FCS
+
-
400
200
0
-200
-400
-400 -200 0 200 400
∥ [unit]
⊥ [unit]
[log] pValue
0
-1
-2
-3
-4
-5
-6
-7
siNT
siTPC2
velocity [unit/unit]
0.6
0.4
0.2
0.0
*
siNT
siTPC2

Figure 2

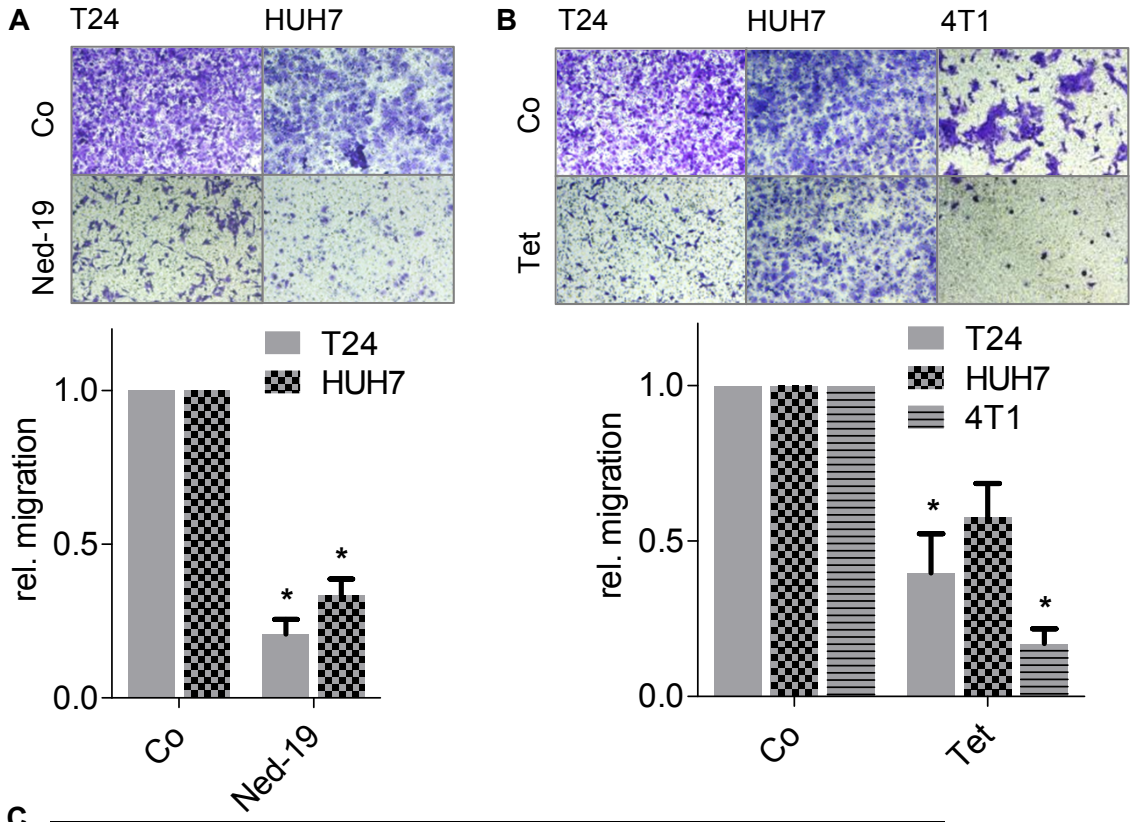

C

Spec. cell death [%]	T24	HUH7	4T1
Ned-19	-0.57 ± 1.66	3.37 ± 0.53	
Tet	1.61± 3.91	2.82 ± 0.89	2.36 ± 0.91

Figure 3

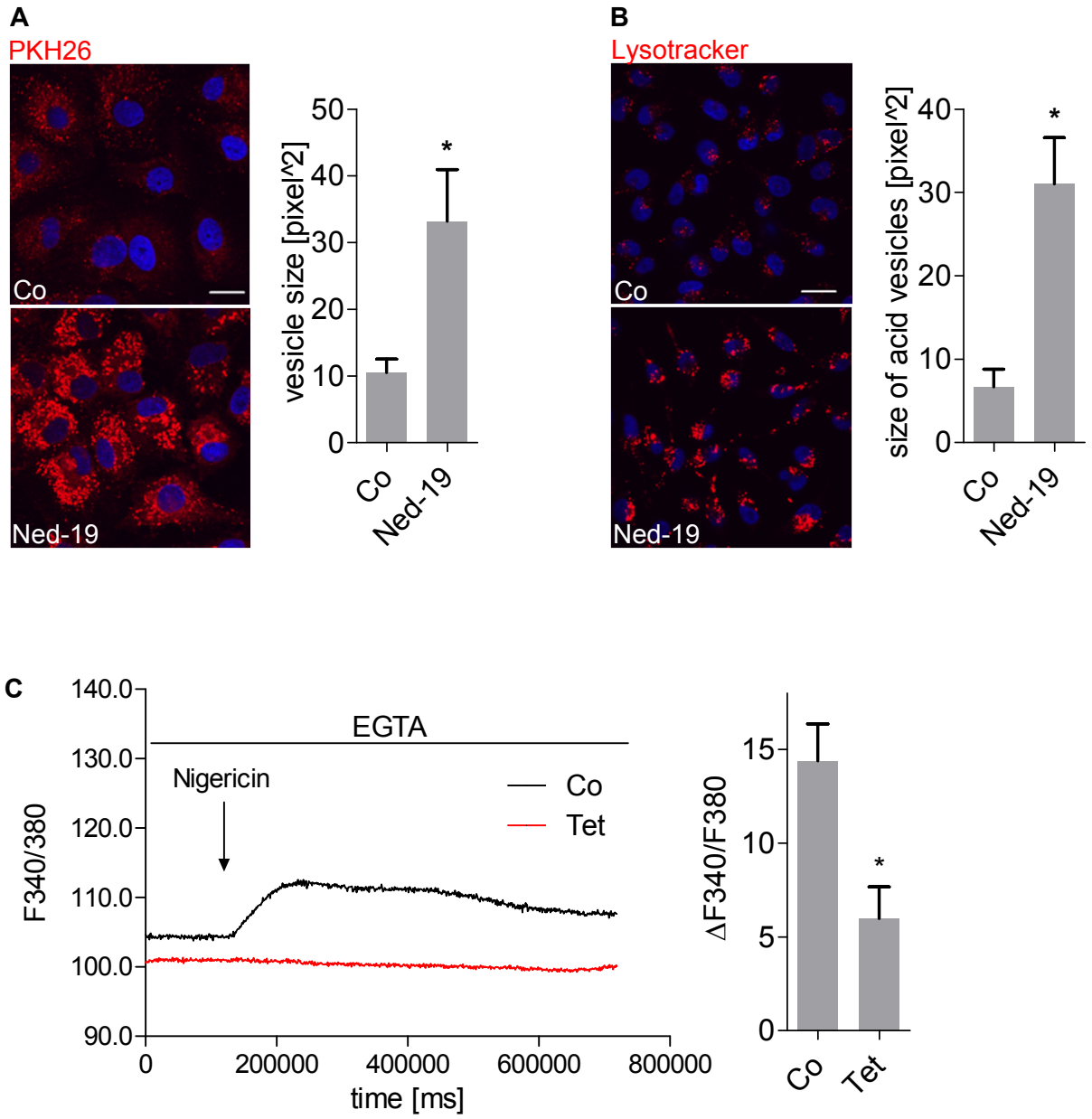
A
PKH26
Co
Ned-19
vesicle size [pixel^2]
50
40
30
20
10
0
*
Co
Ned-19
B
Lysotracker
Co
Ned-19
size of acid vesicles [pixel^2]
40
30
20
10
0
*
Co
Ned-19
C
EGTA
Nigericin
Co
Tet
F340/380
140.0
130.0
120.0
110.0
100.0
90.0
0
200000
400000
600000
800000
time [ms]
ΔF340/F380
15
10
5
0
*
Co
Tet

Figure 4

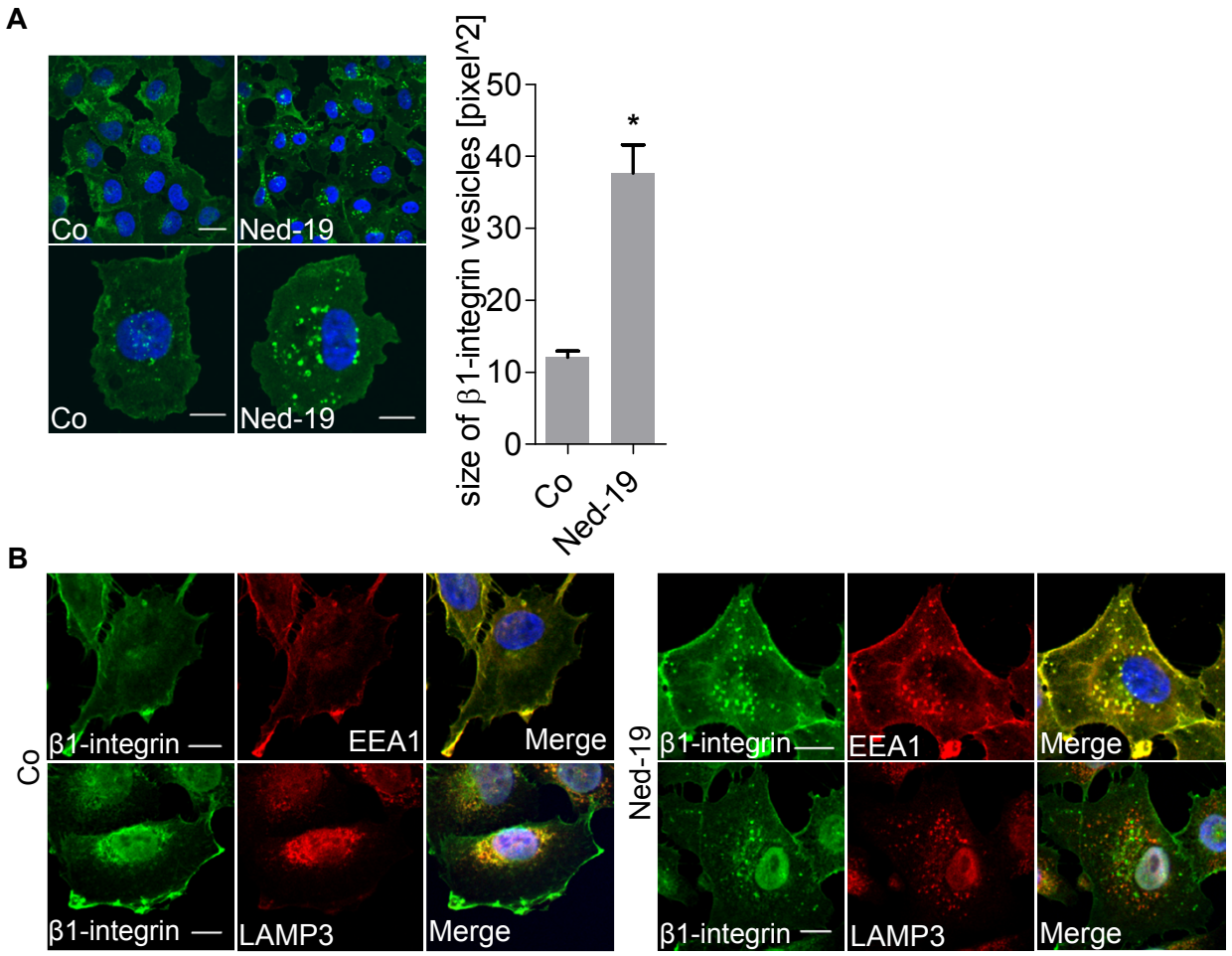
A
Co
Ned-19
Co
Ned-19
size of β1-integrin vesicles [pixel^2]
50
40
30
20
10
0
*
Co
Ned-19
B
Co
β1-integrin
EEA1
Merge
β1-integrin
LAMP3
Merge
Ned-19
β1-integrin
EEA1
Merge
β1-integrin
LAMP3
Merge

Figure 5

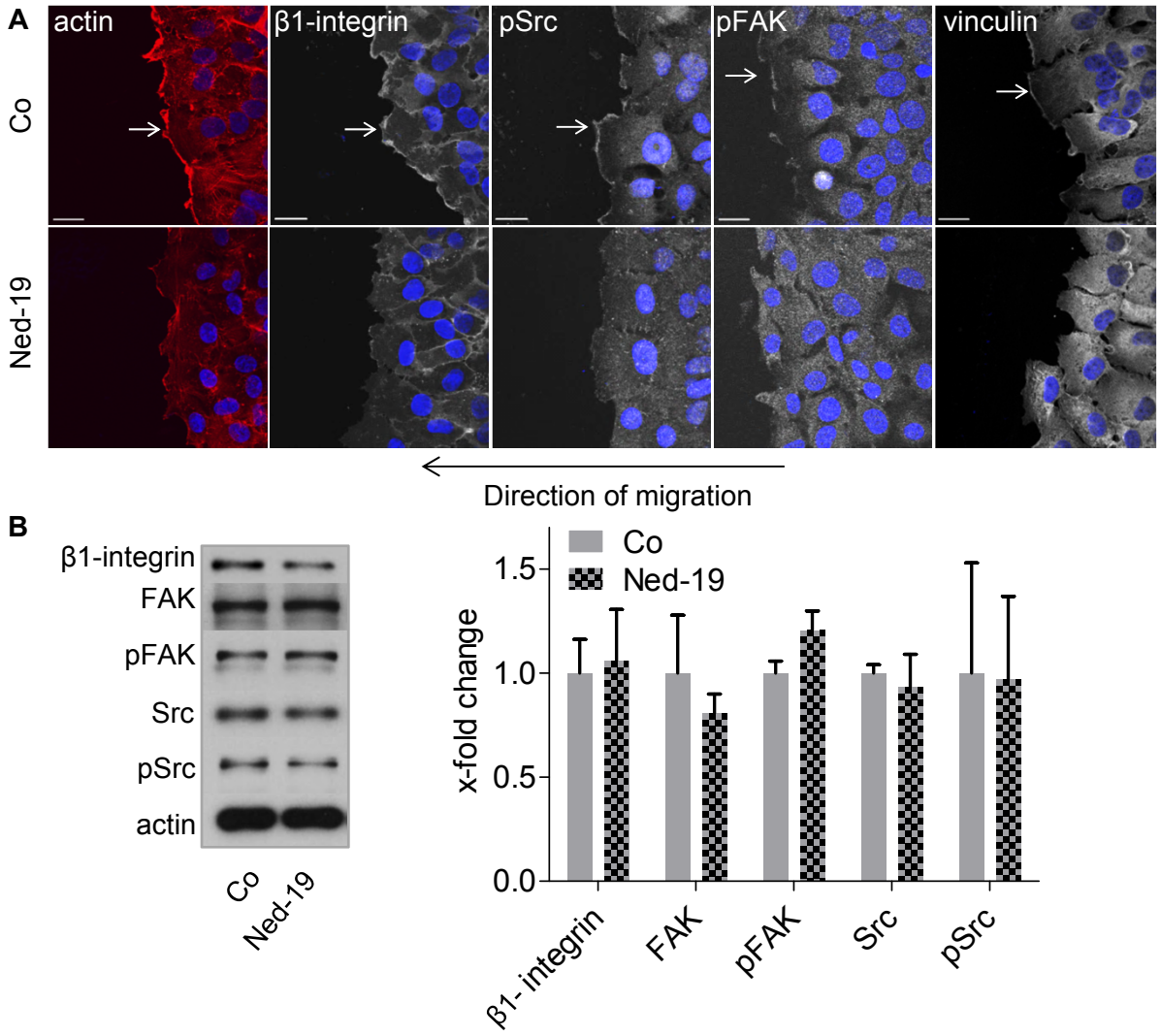
A
actin
β1-integrin
pSrc
pFAK
vinculin
Co
Ned-19
Direction of migration
B
β1-integrin
FAK
pFAK
Src
pSrc
actin
Co
Ned-19
Co
Ned-19
x-fold change
1.5
1.0
0.5
0.0
β1- integrin
FAK
pFAK
Src
pSrc

Figure 6

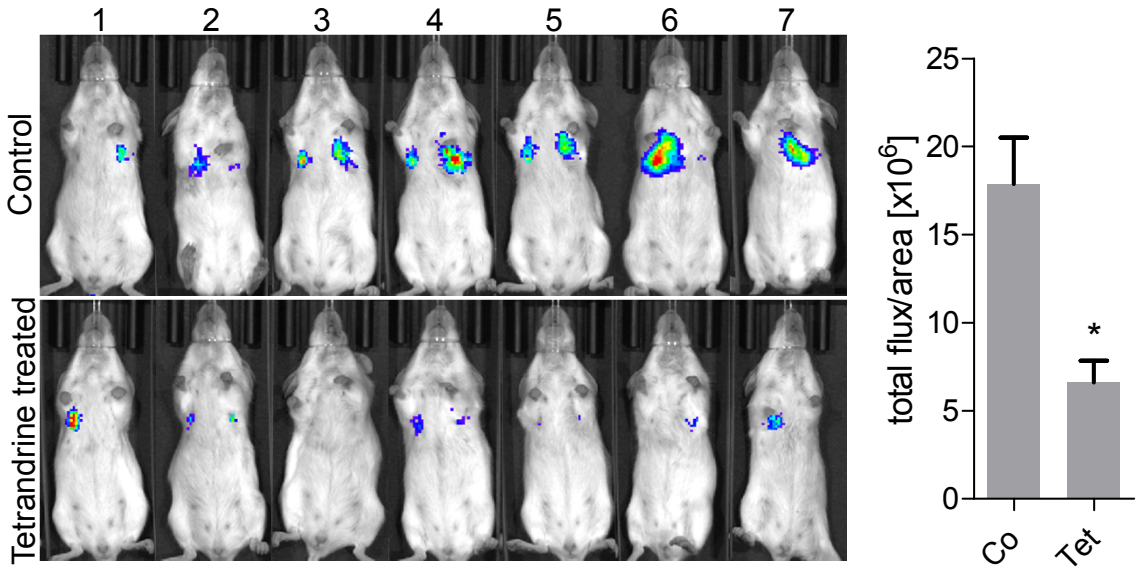
1
2
3
4
5
6
7
Control
Tetrandrine treated
25
20
15
10
5
0
total flux/area [x10^6]
*
Co
Tet

Figure 7